Journal of Statistical Physics, Vol. 55, Nos. 5/6, 1989

Surface Properties of Finite Classical Coulomb Systems: Debye–Hückel Approximation and Computer Simulations

Ph. Choquard,[1] B . Piller,[1] R. Rentsch,[1] and P. Vieillefosse[2]

Received December 25, 1988

We report analytical and numerical studies of surface correlations in finite, homogeneously polarizable, classical Coulomb systems placed in an insulating or conducting environment. Their purpose is to understand the phenomenological, shape-dependent laws of electrostatics, from the point of view of statistical mechanics; we focus on the knowledge of the dielectric susceptibility of the system, a quantity proportional to the equilibrium fluctuation of the system's instantaneous polarization per unit volume. This goal has been achieved for a system in a conducting state. The picture is that the shape-dependent part of the susceptibilities results from the action of unbounded observables (the second moments of the instantaneous polarization of the system) on long-range surface correlations and that the relations of electrostatics are verified by means of shape-dependent thermodynamic limits. This picture is supported (i) by exact solutions and asymptotic analysis of the Debye–Hückel approximation of multicomponent plasmas in disks and spheres with insulating and conducting environment and also in ellipses in a vacuum, and (ii) by computer simulations of a one-component plasma in a disk with different environments, notably a conducting environment with permeable and impermeable wall. These observations have revealed for the first time the reason why the susceptibility of a conducting disk in a conductor with impermeable walls diverges linearly with the radius of the disk: this is due to the occurrence of long-range radial correlations in the conductor. These findings are quantitatively interpreted in terms of a novel "canonical" Debye–Hückel approximation as contrasted to the ordinary "grand canonical" version. Lastly a fresh look at the problem of the surface

[1] Institut de Physique Théorique, École Polytechnique Fédérale de Lausanne, PHB-Ecublens, CH-1015 Lausanne, Switzerland.

[2] Laboratoire de Physique Théorique des Liquides, Université Pierre et Marie Curie, Paris Cédex 05, France.

0022-4715/89/0600-1185$06.00/0

correlations of a conductor in a vacuum, which places the observer close to the surface of the conductor but in the vacuum, is presented and applied to the disk, the ellipse, the cylinder, the sphere, and the wedge.

KEY WORDS: Phenomenological electrostatics; shape-dependent effects; dielectric susceptibility; surface correlations; Debye–Hückel approximation; grand ensemble computer simulation.

1. INTRODUCTION

This paper is a contribution to the theory of the size and shape dependence of the dielectric susceptibility of finite, homogeneously polarizable, classical Coulomb systems surrounded by a medium of arbitrary dielectric constant. Contact with the laws of electrostatics is achieved through a systematic study of surface correlations in model systems.

The original motivation of this work was the lack of understanding, from the point of view of statistical mechanics, of the phenomenological laws of electrostatics which govern the relations connecting the dielectric constant ε of a macroscopic piece of a homogeneously polarizable system, its susceptibility tensor, the depolarization tensor associated with its shape, and the dielectric constant of the surrounding medium.

This gap has now been filled when the system is in a conducting state. The overall picture is (1) that the shape-dependent part of the susceptibilities results from the action of unbounded observables (the second moments of the instantaneous polarization of the system) on long-range surface correlations, both angular and radial, and (2) that the relations of electrostatics are verified by means of shape-dependent thermodynamic limits, a crucial and novel prescription in the field.

In a certain sense, the results presented here and in two previous papers (refs. 1 and 2, henceforth referred to as I and II, respectively) constitute a missing piece in the series of work dealing with the screening properties of infinite and semi-infinite Coulomb systems as recently reviewed by Martin.[3] More work needs to be done if the system is in a dielectric state, if it can undergo phase transitions such as dielectric–plasma or para–ferroelectric ones, and, of course, if it is not classical. More work needs also to be done on the theory of image forces.

The first exact results on the size and shape dependence of the dielectric susceptibility of a classical conductor appeared in ref. 1. Direct calculation of the susceptibility of a two-dimensional one-component plasma (OCP) in a disk for the particular value of the coupling constant $q^2/k_B T = 2$, for which the model is exactly solvable, produced the value $\pi^{-1}[1-(\pi N/2)^{-1/2}+2N^{-1}+O(N^{-3/2})]$, which is π^{-1} in the thermo-

dynamic limit as required by the Clausius–Mossotti relation, but which is twice as large as the value given by the second-moment Stillinger–Lovett sum rule. Why $\pi^{-1} = (2\pi)^{-1} + (2\pi)^{-1}$ is a question addressed to in the second paper.[2] There it was shown that, for the same solvable model again, the susceptibility consisted of a bulk part $= (2\pi)^{-1}$ and of a surface part. To study the latter, the concept of partial second moment was introduced and it was shown that the surface contribution followed a very long-range law in π^{-2} $\arcsin(r/2R)$, originally suggested by computer simulations, and which saturates to $(2\pi)^{-1}$ at the disk diameter. The origin of this law was that, for two particles close to the edge of the disk, the pair correlation function decayed with the inverse square of their distance, a typical dipole–dipole interaction due to the asymmetric screening of the charges when they are close to the edge of the domain. Computer simulations of a two-component Coulomb system in a disk and at high temperature confirmed the generality of the "arc sine" law followed by the partial susceptibility of this system.

So far we have been dealing with systems surrounded by the vacuum, i.e., $\varepsilon' = 1$.

At this stage, a series of questions emerged naturally, namely: What about the Clausius–Mossotti relation, which says that the susceptibility of a disk-shaped conductor surrounded by an insulator of dielectric constant ε' is, in the thermodynamic limit, given by $\pi/2 + \varepsilon'\pi/2$? What about the size dependence of this law? What about the origin of its divergence if the surrounding medium is a conductor, i.e., $\varepsilon' = \infty$? What about other shapes, such as elliptic ones? What about three-dimensional systems? These are the questions addressed in this paper.

The problem of providing answers to these questions is that there is no solvable model of finite Coulomb systems of given size and shape and subjected to image forces resulting from the presence of a surrounding medium with arbitrary dielectric constant. For that reason, we have (1) had recourse to the linear Debye–Hückel approximation, which had already, and successfully, been applied to the investigation of surface correlations of semi-infinite systems (ref. 4, p. 55) for $\varepsilon' = 1$, and (2) conducted a series of computer experiments with the OCP on a disk in different environments to guide us and to enable confrontation with the results of the Debye–Hückel theory.

The paper is constructed as follows.

In Section 2, we review the laws of electrostatics which relate the dielectric constant ε of a homogeneously polarizable system to its polarization fluctuation (PF) susceptibility, its depolarization tensor, and the dielectric constant ε' of the surrounding medium. We observe in particular that it is only with Neumann boundary conditions ($\varepsilon' = 0$) that the PF

susceptibility tensor of a finite conductor converges toward the isotropic Stillinger–Lovett (SL) value and this for all admissible shapes. In this section, we introduce also a distinction between $\chi(\mathrm{PF})$ and the second moment susceptibility $\chi(\mathrm{SM})$, which coincide only when the perfect screening sum rule is satisfied. If not, as illustrated by three examples at the end of this section, one has to introduce an excess susceptibility $\Delta\chi$ produced by charge fluctuations.

In Section 3, we present the Debye–Hückel (DH) approximation for finite systems in an ε' environment and we discuss its application to the disk and to the sphere. We find that the DH approximation is capable of reproducing in the thermodynamic limit the predictions of electrostatics summarized in Section 2. Through the splitting of $\chi(\mathrm{P(F)} = \chi(\mathrm{SM}) + \Delta\chi$, we learn about the size dependence of these contributions and which one of them diverges in the case of a metallic environment. We show that, owing to imperfect screening or to charge fluctuations as known in grand canonical ensemble theories, $\Delta\chi$ diverges linearly with the radius of the system, whereas $\chi(\mathrm{SM})$ saturates toward the SL value. This value is not relevant here since the susceptibility must diverge in the thermodynamic limit. The same result has been obtained for a disk-shaped subdomain of a finite or infinite OCP at the particular coupling constant $e^2\beta = 2$: $\chi(\mathrm{PF})$ is dominated by a diverging $\Delta\chi$ due to charge fluctuations and $\chi(\mathrm{SM}) = 1/2\pi$. Why does $\chi(\mathrm{SM})$ diverge in a canonical ensemble theory in which the perfect screening sum rule is satisfied? This is, according to Martin's recent review (ref. 3, Section IIIG.1), an open question. It is dealt with in Section 6.

In Section 4, we analyze the surface correlation functions of the DH approximation for a disk and for a sphere. We find that, as the first term of an asymptotic expansion, the surface correlations decay with the inverse square of the *chord* of the disk. For the sphere, we find a surface correlation decaying with the inverse cube of the chord plus an angular-independent contribution proportional to the inverse cube of the radius R. In three dimensions, this result does not fit with a rigorous upper bound established by Federbush and Kennedy (ref. 5, pp. 368–369), which is that the surface correlation function decays with the inverse cube of the *arc*. We comment on this at the end of Section 5.2.

Section 5 is devoted to the detailed algebraic calculations of the SM, excess, and PF susceptibility of the disk and of the sphere on the basis of the expansion given in Section 3, in which the results are summarized. It is also mentioned that the susceptibilities calculated from the surface correlation functions give exactly the same results as those obtained directly from expectation value of the first three terms of the expansions. We find in particular that the three-dimensional analog of the long-range

$\pi^{-2}\arcsin(r/2R)$ law for the partial susceptibility of a disk is given by $(4\pi)^{-1}[(r/2R)+(r/2R)^4]$, which produces again the exact surface contribution $1/2\pi$ at $r=2R$.

In Section 6, we take up the difficult and so far unsolved problem of the divergence of the SM susceptibility for a conductor in a conductor with impermeable walls, i.e., Dirichlet boundary conditions for the bare Coulomb interaction but preservation of the charge neutrality sum rule. The key finding, suggested by the computer experiments reported in Section 7, is that on the edge of the disk the canonical truncated pair correlation function possesses an angular-independent component proportional to the inverse radius of the disk, and that the latter decays exponentially toward the interior. In the Appendix B, we show that the truncated radial pair distribution function possesses a depression of amplitude R^{-1} close to the diameter of the disk and that the second moment of this function is proportional to the disk radius. In this Appendix, we propose a three-dimensional version of this feature, which is an R^{-2} amplitude of the corresponding function. At the end of Section 6, we discuss also the cross-over of the surface susceptibility from an ε' to an R behavior, which occurs at $\varepsilon'/\kappa R \approx 1$ (κ^{-1} being the Debye length), as suspected.

In Section 7, we present some results obtained by Monte Carlo simulations of an OCP on a disk. We consider the case where the system is surrounded by vacuum, by a dielectric environment, and by a conductor. Besides the usual canonical ensemble simulations, we perform some runs in a grand ensemble, where not only are fluctuations of neutral pairs allowed, as in the traditional grand ensemble simulations of Coulomb systems, but so are charge fluctuations. The usually arbitrary scale length L which occurs in the logarithmic potential affects, in the grand ensemble simulation, the physical properties of the system, except if $\varepsilon'=\infty$. This is shown to be so, since the metallic boundary conditions are the only boundary conditions compatible with the hypothesis of the grand ensemble. The polarization fluctuations of the OCP are very similar in both ensembles, and their size dependence is in good agreement with the DH theory at a coupling constant Γ as high as 0.5. However, the correlation functions are different in the two ensembles for a metallic environment represented by Dirichlet boundary conditions. Whereas they vanish at large distance in the grand ensemble, they manifest a depression at a distance close to the diameter of the disk in the canonical ensemble. The entire profile of the radial pair distribution function is remarkably well reproduced by the canonical DH approximation developed in Appendix B.

Anisotropic shapes are studied in Sections 8 and 9. In Section 8, the particular case of an elliptic geometry is considered. The solution of the DH equation exhibits again a slow decay of the correlation functions along

the wall. The new result is that the strength of the correlations in regions of high curvature is increased. This feature is reminiscent of the "needle effect" known in electrostatics and provides an intuitive explanation to the problem of the shape-dependent susceptibilities in terms of correlation functions.

A fresh look at the problem of the surface correlations of a conductor in a vacuum is proposed in Section 9. The idea is to approach the problem of the surface correlation of a conductor in the vacuum from outside, i.e., from a point source located at a point close to the boundary of the system but exterior to it. An intuitive description of the situation is presented, and proved in Appendix D for the disk, that, for sufficiently smooth shapes (i.e., of curvature larger than the Debye length), the surface correlation of the conductor is given by the bigradient of the exterior Coulomb kernel satisfying Dirichlet boundary conditions. This proposal is applied to the disk, to the ellipse, to the sphere, and to the cylinder, and reproduces exactly the results known for these smooth shapes. Then it is applied to the problem of a three-dimensional wedge which possesses a singular shape and here, for an opening angle $2\pi - \theta$, it predicts an algebraic decay $\sim |z - z'|^{-(1+2\pi/\theta)}$. This result does not fit with a conjecture, based on the Carnie and Chan sum rule and published in ref. 6, which says that the decay should behaves as $1/[|z - z'| \log^2(\kappa |z - z'|)]$. We comment on this at the end of Section 9.5.

Appendix A deals with the question of the semi-infinite plane limit of the DH kernel for the disk. The contents of Appendices B, C, and D are reported in the summary of Sections 7–9.

2. DIELECTRIC CONSTANTS AND SUSCEPTIBILITIES

In this section, we generalize the relations (2.1)–(2.11) of II to the case where the systems considered are surrounded by a medium of dielectric constant ε', we analyze some important consequences of these generalizations for the plasma state in particular, and we generalize the relations (2.24)–(2.27) of II to the cases where the perfect screening sum rule is not satisfied. This can happen in finite systems.

The presence of a dielectricum surrounding the systems confined in their domain Λ modifies their Hamiltonians in two ways: (i) through the kernel of the interaction potential, which conveys the effects of the image charges, but which we do not discuss further here (cf. Section 7), and (ii) through the coupling of their instantaneous polarization $\mathscr{P}$ with the external field E_0, which occurs via the field E_a acting in Λ. This field is linearly related to the applied field with coefficients which depend upon ε' and upon the size-invariant but shape-dependent depolarization tensor T_Λ defined by Eq. (2.7) of II. Considering for simplicity but without loss of generality a

coordinate system in which T_Λ is diagonal and consequently the susceptibility tensor as well, Eq. (2.1) of II becomes, for each component of the corresponding vectors,

$$\mathscr{P} = \chi_\Lambda^{\varepsilon'} E_a \tag{2.1}$$

with

$$E_a = \frac{\varepsilon' E_0}{\varepsilon' + (1-\varepsilon') T_\Lambda} \tag{2.2}$$

according to the laws of electrostatics (ref. 7, pp. 59–86; ref. 8, pp. 237–248). Another modification affects the depolarization field E_1. Whereas Eqs. (2.2)–(2.5) of II are left unchanged by ε', Eq. (2.6) becomes for each component again[7]

$$E_1 = -\frac{(\varepsilon - \varepsilon')\, s_v T_\Lambda \mathscr{P}}{\varepsilon'(\varepsilon - 1)} \tag{2.3}$$

Together with Eqs. (2.3)–(2.5) of II, the present Eqs. (2.1)–(2.3) constitute a set of six linear homogeneous equations for each component of the fields E_0, E_a, E_1, E, and D and of the mean polarization $\mathscr{P}$. Nontrivial solutions of these sets imply the vanishing of the associated determinants. This yields the compatibility relations:

$$\varepsilon = \frac{\varepsilon' + (1-\varepsilon') T_\Lambda + \varepsilon' s_v (1 - T_\Lambda) \chi_\Lambda^{\varepsilon'}}{\varepsilon' + (1-\varepsilon') T_\Lambda - s_v T_\Lambda \chi_\Lambda^{\varepsilon'}} \tag{2.4}$$

The synthetic form of Eq. (2.4) is apparently new. Clearly, Eq. (2.11) of II is recovered for $\varepsilon' = 1$. Strictly speaking, macroscopic electrostatics demands that on the rhs of Eq. (2.4), the thermodynamic limit of $\chi_\Lambda^{\varepsilon'}$ be taken. We shall nevertheless use the above equation as a definition of $\varepsilon(|\Lambda|)$ in order to examine its size dependence, notably for conductors.

We proceed with a detailed analysis of interesting special cases of Eq. (2.4) in taking care of undetermined limiting ratios on its rhs. To do so, we distinguish (i) $\varepsilon' = \infty$ and 0 from $0 < \varepsilon' < \infty$ and (ii) regular from singular shapes of Λ. We define the latter as follows: A regular (singular) shape is such that all (one at least of) the components of $T_\Lambda \in]0, 1[$ ($=0$ or $=1$), their sum being of course equal to 1. In this sense ellipses and ellipsoids have regular shapes, since $0 < T_{ii} < 1$ ($i = 1, \ldots, v$), while strips, slabs, and cylinders have singular shapes, since their depolarization tensors are given by (1, 0), (1, 0, 0), and (1/2, 1/2, 0) respectively.

(A) $\varepsilon' = \infty$. In this case, the interaction kernel satisfies Dirichlet

boundary conditions, the surrounding medium is a conductor, and Eq. (2.4) becomes

$$\varepsilon = \frac{(1-T_\Lambda)(1+s_v\chi_\Lambda^\infty)}{1-T_\Lambda} = 1 + s_v\chi_\Lambda^\infty; \qquad T_\Lambda \neq 1 \tag{2.5}$$

(B) $\varepsilon' = 0$. Here the interaction kernel satisfies Neumann conditions on $\partial\Lambda$, which, although unphysical, will nevertheless prove very important in what follows, and Eq. (2.4) becomes

$$\varepsilon = \frac{T_\Lambda}{(1-s_v\chi_\Lambda^0)T_\Lambda} = \frac{1}{1-s_v\chi_\Lambda^0}; \qquad T_\Lambda \neq 0 \tag{2.6}$$

(C) $T_\Lambda = 0$. The corresponding component of the susceptibility tensor is its transverse component $\chi_{||}^{\varepsilon'}$ and Eq. (2.4) becomes in this case

$$\varepsilon = \varepsilon'(1+s_v\chi_{||}^{\varepsilon'})/\varepsilon' = 1 + s_v\chi_{||}^{\varepsilon'}; \qquad \varepsilon' > 0 \tag{2.7}$$

(D) $T_\Lambda = 1$. The corresponding component of χ_Λ is its normal component $\chi_\perp$ and we get

$$\varepsilon = 1/(1-s_v\chi_\perp^{\varepsilon'}); \qquad \varepsilon' < \infty \tag{2.8}$$

We are left with the singular cases $T_\Lambda = 1$, $\varepsilon' = \infty$ and $T_\Lambda = 0$, $\varepsilon' = 0$ so far undetermined. For the operational reason that the dielectric constant of the medium surrounding a system has to be chosen before the thermodynamic limit of the system is taken, we propose to extend Eq. (2.5) to the limit $T_\Lambda \to 1$ and Eq. (2.6) to the limit $T_\Lambda \to 0$.

(E) $\varepsilon = \infty$. The system considered is a conductor. Of particular interest are the critical values reached by the components of χ_Λ in this state. Setting the denominator of Eq. (2.4) equal to zero results in

$$\chi_\Lambda^{P;\varepsilon'} = \frac{1}{s_v} + \frac{\varepsilon'(1-T_\Lambda)}{s_v T_\Lambda} \tag{2.9}$$

This relation is valid without further precautions for regular shapes and $0 \leqslant \varepsilon' \leqslant \infty$ and for singular shapes and $0 < \varepsilon' < \infty$. According to the sequence of limits proposed above, we have also

$$\text{th lim}\, \chi_\Lambda^{P;\infty} = \infty \tag{2.10}$$

and

$$\text{th lim}\, \chi_\Lambda^{P;0} = 1/s_v \tag{2.11}$$

for all shapes.

For the singular shapes ($T_\Lambda = 1$ and 0, respectively) we have in particular

$$\chi_\perp^P = 1/s_v; \qquad \varepsilon' < \infty \tag{2.12a}$$

$$\chi_\perp^P = \infty; \qquad \varepsilon' = \infty \tag{2.12b}$$

and

$$\chi_{||}^P = \infty; \qquad \varepsilon' > 0 \tag{2.13a}$$

$$\chi_{||}^P = 1/s_v; \qquad \varepsilon' = 0 \tag{2.13b}$$

Equation (2.11) is particularly interesting. Indeed, its rhs is immediately identified as the Stillinger–Lovett value of the bulk susceptibility of an infinite conductor. The lhs of Eq. (2.11) tells us that it is with and only with Neumann boundary conditions that the susceptibility of a finite conductor converges to the SL value and this for all shapes compatible with the requirement that the system be homogeneously polarizable. In fact, these boundary conditions minimize the surface effects and, although unphysical, may be of practical interest, notably in computer experiments.

Let us consider next the susceptibilities. In II we considered only the case where the SM and PF susceptibilities are identical. This occurs whenever the excess charge density $\int_\Lambda S(x, y)\, dy = 0$. This is called the *perfect screening or monopole sum rule*. It is always satisfied if the system is treated in a canonical ensemble theory. For reasons to become clear later, we wish to relax this condition. Then, the excess charge density will induce an excess susceptibility.

Using again the identity

$$x_i y_i = -\frac{(y_i - x_i)^2}{2} + \frac{x_i^2 + y_i^2}{2}$$

and generalizing in an obvious way the notation of I and II, we have

$$\chi_{ii;\Lambda}^{\varepsilon'}(\mathrm{PF}) = \chi_{ii;\Lambda}^{\varepsilon'}(\mathrm{SM}) + \Delta\chi_{ii;\Lambda}^{\varepsilon'} \tag{2.14}$$

with

$$\chi_{ii;\Lambda}^{\varepsilon'}(\mathrm{PF}) = \frac{\beta}{|\Lambda|} \int_\Lambda x_i y_i S_\Lambda^{\varepsilon'}\, d^\nu x\, d^\nu y \tag{2.15}$$

$$\chi_{ii;\Lambda}^{\varepsilon'}(\mathrm{SM}) = -\frac{\beta}{2|\Lambda|} \int_\Lambda (y_i - x_i)^2\, S_\Lambda^{\varepsilon'}(x, y)\, d^\nu x\, d^\nu y \tag{2.16}$$

and

$$\Delta\chi_{ii;\Lambda}^{\varepsilon'} = \frac{\beta}{2|\Lambda|}\int_{\Lambda}(x_i^2 + y_i^2)\, S_{\Lambda}^{\varepsilon'}(x, y)\, d^{\nu}x\, d^{\nu}y \tag{2.17}$$

where we recall that

$$S_{\Lambda}^{\varepsilon'}(x, y) = \sum_{\alpha} q_{\alpha}^2 \rho_{\alpha;\Lambda;\varepsilon'}(x)\, \delta(x-y) + \sum_{\alpha;\,\beta} q_{\alpha} q_{\beta} \rho_{\alpha\beta;\Lambda;\varepsilon'}^{T}(x, y) \tag{2.18}$$

is the charge–charge correlation function.

In the following sections we shall meet the violation of the monopole sum rule on three occasions: (i) when the grand canonical ensemble is used with $\varepsilon' = \infty$, (ii) when the polarization fluctuations are investigated in a permeable subdomain of a finite or infinite system, and (iii) when the correlation functions of finite systems are described in the framework of approximate schemes like the Debye–Hückel (DH) mean field theory, with the exception of a few particular boundary conditions.

3. DEBYE–HÜCKEL APPROXIMATION AND SUM RULES

In the absence of exactly solvable models of multicomponents classical Coulomb systems with image charges we have recourse to the linearized DH approximation, which has already been successfully applied to the study of the long-range transverse pair correlation function near the surface of semi-infinite conductors filling a half-space[4] or a cylinder.[9] However, whereas infinite or semi-infinite systems are necessarily neutral, finite systems can bear finite charges which spread over their walls. This feature introduces a new parameter into the theory and it is an interesting property of the DH approximation that it can mimic this situation.

This approximation is defined as follows: Let ρ_{α} and q_{α} be the number density and the particle charge of the species α. A unique mean Debye wave number κ occurs, defined through $\kappa^2 = \beta s_{\nu} \sum_{\alpha} q_{\alpha}^2 \rho_{\alpha}$. We define also $\rho = \sum_{\alpha} \rho_{\alpha}$ and $\Gamma = \beta \sum_{\alpha} q_{\alpha}^2 \rho_{\alpha} \rho^{-1}$ in such a way that $\kappa^2 = s_{\nu} \Gamma \rho$. In the DH approximation the one-particle densities $\rho_{\alpha;\Lambda}^{\varepsilon'}(x)$ are to be taken constant and equal to ρ_{α} for $x \in \Lambda$ and zero otherwise. The truncated two-particle correlation functions are approximated by their high-temperature and asymptotic form:

$$\rho_{\alpha\beta;\Lambda;\varepsilon'}^{T}(x, y) = -\beta q_{\alpha} q_{\beta} \rho_{\alpha} \rho_{\beta} G_{\Lambda}^{\varepsilon'}(x, y) \tag{3.1}$$

where $G_{\Lambda}^{\varepsilon'}(x, y)$ is the DH kernel discussed below and $\beta = (K_{\mathrm{B}} T)^{-1}$.

In this approximation the charge–charge correlation function $S^{\varepsilon}_{\Lambda}(x, y)$ becomes

$$S^{\varepsilon'}_{\Lambda}(x, y) = \frac{\Gamma\rho}{\beta}\left[\delta(x-y) - \Gamma\rho G^{\varepsilon'}_{\Lambda}(x, y)\right] \tag{3.2}$$

and the DH kernel satisfies the self-consistent equation

$$-\Delta_x G^{\varepsilon'}_{\Lambda}(x, y) = \Xi_{\Lambda}(x)\frac{s_v\beta}{\Gamma\rho} S^{\varepsilon'}_{\Lambda}(x, y) \tag{3.3}$$

where Ξ_{Λ} is the characteristic function of the domain Λ and y is a point source in Λ. For $x \in \Lambda$ we shall speak of $G^{\varepsilon'}_{\Lambda;\text{in}}(x, y)$ and for $x \notin \Lambda$, where the rhs of Eq. (3.3) vanishes, we shall speak of $G^{\varepsilon'}_{\Lambda;\text{out}}(x, y)$. We note here that whereas the effective interactions as well as the correlation functions are usually defined for x and $y \in \Lambda$, the DH kernel, like the Coulomb kernel, can be defined for both x and $y \notin \Lambda$, a situation considered in Section 9. The boundary conditions satisfied by the inner and outer kernels are discussed below. It is convenient to introduce here the dimensionless charge density:

$$p^{\varepsilon'}_{\Lambda}(y) = \frac{\beta}{\Gamma\rho}\int_{\Lambda} d^{\nu}x\, S^{\varepsilon'}_{\Lambda}(x, y) \tag{3.4}$$

In terms of the above functions, the PF, SM, and excess susceptibilities read as follows:

$$\chi^{\varepsilon'}_{ii;\Lambda}(\text{PF}) = \frac{\Gamma\rho}{|\Lambda|}\int_{\Lambda} x_i y_i\left[\delta(x-y) - \Gamma\rho G^{\varepsilon'}_{\Lambda}(x, y)\right] d^{\nu}x\, d^{\nu}y \tag{3.5}$$

$$\chi^{\varepsilon'}_{ii;\Lambda}(\text{SM}) = \frac{\Gamma^2\rho^2}{2|\Lambda|}\int_{\Lambda} (x_i - y_i)^2\, G^{\varepsilon'}_{\Lambda}(x, y)\, d^{\nu}x\, d^{\nu}y \tag{3.6}$$

and

$$\Delta\chi^{\varepsilon'}_{ii;\Lambda} = \frac{\Gamma\rho}{|\Lambda|}\int_{\Lambda} y_i^2\, p^{\varepsilon'}_{\Lambda}(y)\, d^{\nu}y \tag{3.7}$$

In the next section the DH kernel is constructed explicitely for circular and spherical domains of radius R by means of expansions in terms of Bessel functions of the second kind for $G^{\varepsilon'}_{\Lambda;\text{in}}(x, y)$ and harmonic functions for $G^{\varepsilon'}_{\Lambda,\text{out}}(x, y)$ with coefficients satisfying the following boundary conditions: continuity of the inner and outer parts of $G^{\varepsilon'}_{\Lambda;\text{in}}(x, y)$ and $G^{\varepsilon'}_{\Lambda;\text{out}}(x, y)$ and continuity of the normal derivative of $G^{\varepsilon'}_{\Lambda;\text{in}}(x, y)$ and ε' times the normal derivative of $G^{\varepsilon'}_{\Lambda;\text{out}}(x, y)$, for x or y on $\partial\Lambda$. The coefficients of the

angular-independent part of these expansions depend upon a parameter L/R through the amplitude of the surface Coulomb potential $\ln(L/R) \equiv \xi_D$ for the disk and through $(L-R)/R \equiv \xi_S$ for the sphere. As to the boundary conditions, they can be understood if we write $G^{\varepsilon'}_{\Lambda;\text{in}}(x, y)$ in integral form. In the DH approximation, the effective interaction between two particles $q_\alpha q_\beta G^{\varepsilon'}_{\Lambda;\text{in}}(x, y)$ is determined by the *Ornstein–Zernicke equation*, in which the direct correlation function is approximated by $-\beta$ times the bare Coulomb interaction $q_\alpha q_\beta C^{\varepsilon'}_{\Lambda}(x, y)$, where $C^{\varepsilon'}_{\Lambda}(x, y)$ is the Coulomb kernel, which satisfies the standard boundary conditions on $\partial\Lambda$ because the dielectric constant ε' of the surrounding medium is generally $\neq 1$ [cf. Eq. (7.1), for example]. It is than easy to show that the boundary conditions satisfied by the DH kernel derive from the following integral equation:

$$G^{\varepsilon'}_{\Lambda}(x, y) = C^{\varepsilon'}_{\Lambda}(x, y) + \frac{\kappa^2}{s_\nu} \int_\Lambda d^\nu z \, C^{\varepsilon'}_{\Lambda}(x, z) \, G^{\varepsilon'}_{\Lambda}(z, y) \tag{3.8}$$

Considering again circular or spherical systems, it can be shown that, for the solution of Eq. (3.8) to be everywhere regular, $L/R \geqslant 1$. It transpires from the integral equation (3.8) that the excess density $p^{\varepsilon'}_{\Lambda}(y)$ will depend upon ξ_D and ξ_S, and consequently the monopole sum rule, the excess, and SM susceptibilities as well, whereas $\chi(\text{PF})$ does not. We can show now how the charge Q_{in} of a finite DH system is related to the amplitude of the surface potential of the associated Coulomb kernel. Integration of Eq. (5.30) (written in units of the Debye length) over Λ yields indeed for large disks or spheres

$$\begin{aligned} Q_{\text{in}} = \int_\Lambda p^{\varepsilon'}_{\Lambda}(|y|)\, d^\nu y &= \int_\Lambda \varepsilon' \left(\frac{Z}{|y|}\right)^{\bar{0}} \frac{I_{\bar{0}}(|y|)}{\lambda_\Lambda z I_{\bar{1}}(Z) - \varepsilon' I_{\bar{0}}(Z)}\, d^\nu y \\ &\approx \varepsilon'(\varepsilon' + \lambda_\Lambda Z)^{-1} \, |\partial\Lambda| \end{aligned} \tag{3.9}$$

where $\bar{n} = n + (\nu - 2)/2$, $\lambda_\Lambda > 0$ with $\lambda_\Lambda = \xi_D$ for $\nu = 2$, $\lambda_\Lambda = \xi_S + 1$ for $\nu = 3$, $0 < \varepsilon' < \infty$, and where $|\partial\Lambda| = 2\pi Z$ for $\nu = 2$ and $4\pi Z^2$ for $\nu = 3$. This relation indicates clearly that the excess charge associated with the DH approximation is controlled by the parameter λ_Λ, and how.

Another quantity of interest is the polarization charge which may occur at the surface of the domains. With $|y|$, the modulus of y, and ω designating the angular variables, the surface charge density is given by

$$\sigma(Z, |y|, \omega) = \frac{1}{s_\nu} \left(\frac{\partial G^{\varepsilon'}_{\Lambda;\text{in}}}{\partial |x|} - \frac{\partial G^{\varepsilon'}_{\Lambda;\text{out}}}{\partial |x|} \right)_{|x| = Z} \tag{3.10}$$

and the polarization charge by

$$P_{\Lambda}^{\varepsilon'}(Z, |y|) = Z^{\nu-1} \int \sigma(Z, |y|, \omega)\, d\omega$$

$$= (1-\varepsilon') \left(\frac{Z}{|y|}\right)^{\bar{0}} \frac{I_{\bar{0}}(|y|)}{\lambda_{\Lambda} z I_{\bar{1}}(Z) + \varepsilon' I_{\bar{0}}(Z)} \tag{3.11}$$

It follows that

$$p_{\Lambda}^{\varepsilon'}(Z, |y|) + P_{\Lambda}^{\varepsilon'}(Z, |y|) = \left(\frac{Z}{|y|}\right)^{\bar{0}} \frac{I_{\bar{0}}(|y|)}{\lambda_{\Lambda} Z I_{\bar{1}}(Z) + \varepsilon' I_{\bar{0}}(Z)} \tag{3.12}$$

This charge density is concentrated in a thin surface layer. The total excess charge Q will thus be proportional to the surface $|\partial\Lambda|$ of Λ. Integration of Eq. (3.12) over y results in

$$Q = \int_{\Lambda} d^{\nu}y \, [p_{\Lambda}^{\varepsilon'}(Z, |y|) + P_{\Lambda}^{\varepsilon'}(Z, |y|)] \approx (\varepsilon' + \lambda_{\Lambda} Z)^{-1} \, |\partial\Lambda| \tag{3.13}$$

for large Z.

We notice that for regular values of the reference potentials λ_{Λ} $(0 < \lambda_{\Lambda} < \infty)$ and for a given Z the Neumann boundary condition $\varepsilon' = 0$ produces the ordinary charge neutrality of the inner part:

$$p_{\Lambda}^{0}(\lambda_{\Lambda}, Z, |y|) = 0 \tag{3.14}$$

(for continuity reasons we extend this result to the case $\lambda_{\Lambda} \to 0$, assuming that ε' is equal to zero *a priori*), whereas the Dirichlet boundary condition $\varepsilon' = \infty$ produces the neutrality of the inner part plus polarization charge:

$$p_{\Lambda}^{\infty}(\lambda_{\Lambda}, Z, |y|) + P_{\Lambda}^{\infty}(\lambda_{\Lambda}, Z, |y|) = 0 \tag{3.15}$$

We observe next that for the singular value $\lambda_{\Lambda} = 0$

$$p_{\Lambda}^{\varepsilon'}(0, Z, |y|) = \left(\frac{Z}{|y|}\right)^{\bar{0}} \frac{I_{\bar{0}}(|y|)}{I_{\bar{0}}(Z)}; \qquad \varepsilon' > 0 \tag{3.16}$$

and that for $\lambda_{\Lambda} = \infty$

$$p_{\Lambda}^{\varepsilon'}(\infty, Z, |y|) = 0; \qquad \varepsilon' < \infty \tag{3.17}$$

In summary we observe that if we set *a priori* $\varepsilon' = 0$ or $\lambda_{\Lambda} = \infty$, the DH approximation satisfies the monopole sum rule. Thus, in these two cases, it mimics the properties of a canonical ensemble. In *all other*

cases, the DH approximation mimics the properties of a grand canonical ensemble.

In order to give an idea of the consequences of the DH approximation applied to finite systems notably due to the violation of the monopole sum rule, we give a summary, limited to the susceptibilities, of the results established for the disk ($\nu=2$) and for the sphere ($\nu=3$) in the following three sections. These results give the ε' and size dependence of the susceptibilities, including the "grand canonical" case $\lambda_A \to \infty$, $\varepsilon' \to \infty$, with $\lambda_A/\varepsilon' \to 0$.

Section 6 will be devoted to the study of the "canonical" case (i.e., $\varepsilon' \to \infty$, $\lambda_A \to \infty$, with $\varepsilon'/\lambda_A \to 0$) with the purpose of understanding the origin of the divergence of the PF susceptibility.

From Sections 3–5 we gather the following results:

(A) $\varepsilon'=0$, all λ_A. In this case we have

$$\chi^0_{11;A}(\mathrm{PF}) = \frac{1}{2\pi(\nu-1)} + O(Z^{-1}) \tag{3.18a}$$

$$\Delta\chi^0_{11;A} = 0 \tag{3.18b}$$

$$\chi^0_{11;A}(\mathrm{SM}) = \chi^0_{11;A}(\mathrm{PF}) \tag{3.18c}$$

As expected from Eq. (2.9), the PF susceptibility produces the SL value. The saturation is reached with the inverse radius, in contrast with the case of the OCP on a sphere at $\Gamma=2$, for which we found in Eq. (7.8) of II a saturation inversely proportional to the surface of the sphere.

(B) $\varepsilon'=\infty$, all λ_A. Here we find

$$\chi^\infty_{11;A}(\mathrm{PF}) = \frac{Z}{2\pi(\nu-1)} - \frac{\nu+1}{4\pi(\nu-1)} + O(Z^{-1}) \tag{3.19a}$$

$$\Delta\chi^\infty_{11;A} = \frac{Z}{2\pi(\nu-1)} - \frac{\nu+3}{4\pi(\nu-1)} + O(Z^{-1}) \tag{3.19b}$$

$$\chi^\infty_{11;A}(\mathrm{SM}) = \frac{1}{2\pi(\nu-1)} + O(Z^{-1}) \tag{3.19c}$$

The divergence of the PF susceptibility and consequently that of ε according to Eq. (2.5) goes linearly with the radius of the ν-dimensional sphere. It is not due to the SM susceptibility, which produces the SL value, but to the second moment of the imperfectly screening point source.

(C) $0<\varepsilon'<\infty$, $\lambda_A>0$. In these cases, the results are

$$\chi^{\varepsilon'}_{11;A}(\mathrm{PF})=\frac{1}{2\pi(\nu-1)}+\frac{\varepsilon'}{2\pi}+O(Z^{-1}) \tag{3.20a}$$

$$\Delta\chi^{\varepsilon'}_{11;A}=\frac{\varepsilon'}{2\pi}\left[\frac{1}{\lambda_A(\nu-1)}+O\left(\frac{1}{\lambda_A Z}\right)\right] \tag{3.20b}$$

$$\chi^{\varepsilon'}_{11;A}(\mathrm{SM})=\frac{1}{2\pi(\nu-1)}+\frac{\varepsilon'}{2\pi}\left[1-\frac{1}{\lambda_A(\nu-1)}+O\left(\frac{1}{\lambda_A Z}\right)\right]+O(Z^{-1}) \tag{3.20c}$$

The ε' contribution to the PF susceptibility will turn out to result from long-range surface correlations, as shown in Sections 4.1 and 4.2.

Notice that Eq. (3.20a) reproduces exactly the results expected from Eq. (2.9).

(D) $0<\varepsilon'<\infty$, $\lambda_A=0$. Here we find

$$\chi^{\varepsilon'}_{11;A}(\mathrm{PF})=\frac{1}{2\pi(\nu-1)}+\frac{\varepsilon'}{2\pi}+O(Z^{-1}) \tag{3.21a}$$

$$\Delta\chi^{\varepsilon'}_{11;A}=\Delta\chi^{\infty}_{11;A}=\frac{Z}{2\pi(\nu-1)}-\frac{\nu+3}{4\pi(\nu-1)}+O(Z^{-1}) \tag{3.21b}$$

$$\chi^{\varepsilon'}_{11;A}(\mathrm{SM})=-\frac{Z}{2\pi(\nu-1)}+\frac{\nu+3}{4\pi(\nu-1)}+\frac{1}{2\pi(\nu-1)}+\frac{\varepsilon'}{2\pi}+O(Z^{-1}) \tag{3.21c}$$

We notice that the PF susceptibility given by Eq. (3.21a) equals that given by Eq. (3.20a), i.e., is independent of λ_A, as expected. We notice, furthermore, that the excess susceptibility given by Eq. (3.21b) is equal to that given by Eq. (3.19b). This property will be explain in Section 5.2. We remark lastly that while in case B the divergence of $\Delta\chi^{\varepsilon'}_{11;A}$ entails that of $\chi^{\varepsilon'}_{11;A}(\mathrm{PF})$, this is no longer true in D, since the divergence of $\Delta\chi^{\varepsilon'}_{11;A}$ is compensated by that of $\chi^{\varepsilon'}_{11;A}(\mathrm{SM})$.

The main conclusion to be drawn from these results is that, for a spherical geometry at least, the DH approximation applied to finite systems is capable of reproducing in the thermodynamic limit the predictions of classical electrostatics.

In Section 8 it will be proved that this property still holds for an elliptic geometry.

4. DH KERNEL AND LONG-RANGE SURFACE BEHAVIOR: DISK AND SPHERE

In this section we solve Eq. (3.3) in order to obtain the DH kernel explicitly, both for the disk and the sphere. We then analyze their long-

range surface behavior. This is presented in Section 4.1 for the disk and Section 4.2 for the sphere.

4.1. The Disk

The solution to Eq. (3.3) which obeys the continuity conditions on the surface of the disk is given as an expansion in Bessel functions of the second kind and order n ($n \in N$) with respect to the norms $|x|$ of x and $|y|$ of y. The solution for the interior of the domain is a sum of two contributions:

$$G^{\varepsilon'}_{D;\text{in}}(x, y) = G^{1}_{D;\text{in}}(x, y) + G^{2;\varepsilon'}_{D;\text{in}}(x, y) \tag{4.1}$$

The first contribution corresponds to the familiar DH solution $K_0(\kappa|x-y|)$ for an infinite system, we take here as restricted to the disk. It is independent of ε' and can be expanded in the following way (ref. 10, p. 126):

$$G^{1}_{D;\text{in}}(x, y) = K_0(\kappa|x-y|) = \sum_{n \geqslant 0} \mu_n I_n(s_<) K_n(s_>) \cos n\theta; \qquad s_0, s < Z; \quad n \in N \tag{4.2}$$

where R is the radius of the disk, θ is the angle between x and y, $s_0 = \kappa|y|$, $s = \kappa|x|$, $Z = \kappa R$, $s_< = \min(s_0, s)$, and $s_> = \max(s_0, s)$. Here μ_n denotes the Neumann factor, which is defined by

$$\mu_n = 1 \quad \text{for } n = 0; \qquad \mu_n = 2 \quad \text{for } n \neq 0 \tag{4.3}$$

The second contribution is due to the presence of the boundary and hence depends upon ε'. Moreover, it is regular at $|x| = |y| = 0$ and can be written as

$$G^{2;\varepsilon'}_{D;\text{in}}(x, y) = -\sum_{n \geqslant 0} \mu_n C^{n}_{D;\text{in}} I_n(s_0) I_n(s) \cos n\theta; \qquad s_0, s < Z; \quad n \in N \tag{4.4}$$

where the coefficients $C^{n}_{D;\text{in}}$ are obtained with the help of the continuity conditions and the minus sign is introduced for convenience.

Proceeding with the general solution of Eq. (3.3), we have for the outer region

$$G^{\varepsilon'}_{D;\text{out}}(x, y) = \sum_{n \geqslant 0} \mu_n C^{n}_{D;\text{out}} I_n(s_0) F_n(s) \cos n\theta; \qquad s_0 < Z < s; \quad n \in N \tag{4.5}$$

where the $C^{n}_{D;\text{out}}$ are also coefficients depending upon the continuity conditions and where

$$F_n(s) = \ln\left(\frac{\kappa L}{s}\right) = \ln\left(\frac{L}{R}\right) + \ln\left(\frac{Z}{s}\right) = \xi_D + \ln\left(\frac{Z}{s}\right) \qquad \text{if} \quad n = 0$$

and

$$F_n(s) = s^{-n} \qquad \text{if} \quad n \neq 0 \tag{4.6}$$

A straightforward calculation of the coefficients $C^n_{D;\text{in}}$ and $C^n_{D;\text{out}}$ gives

$$C^n_{D;\text{in}} = \frac{\varepsilon' K_n(Z) F_n'(Z) - K_n'(Z) F_n(Z)}{\varepsilon' I_n(Z) F_n'(Z) - I_n'(Z) F_n(Z)}; \qquad n \geqslant 0 \tag{4.7}$$

and

$$C^n_{D;\text{out}} = [-Z(\varepsilon' I_n(Z) F_n'(Z) - I_n'(Z) F_n(Z))]^{-1}; \qquad n \geqslant 0 \tag{4.8}$$

where the prime denotes the normal derivative.

At this point it is convenient to split $C^n_{D;\text{in}}$ into an ε'-independent part (Neumann part $C^{n;0}_{D;\text{in}}$) and an ε'-dependent part ($C^{n;\Delta}_{D;\text{in}}$), the latter giving rise to long-range surface correlations, as shown below. Thus, with

$$C^n_{D;\text{in}} = C^{n;0}_{D;\text{in}} + (C^n_{D;\text{in}} - C^{n;0}_{D;\text{in}}) = C^{n;0}_{D;\text{in}} + C^{n;\Delta}_{D;\text{in}} \tag{4.9}$$

Eq. (4.7) becomes

$$C^n_{D;\text{in}} = \frac{K_n'(Z)}{I_n'(Z)} + \frac{\varepsilon' \hat{n}}{Z^2} \left[I_n'^2(Z) + \frac{\varepsilon' \hat{n}}{Z} I_n(Z) I_n'(Z) \right]^{-1}; \qquad n \geqslant 0, \quad \varepsilon' \geqslant 0 \tag{4.10}$$

where $\hat{n}$ is defined as

$$\hat{n} = \xi_D^{-1} = \left(\ln \frac{L}{R} \right)^{-1} \quad \text{if} \quad n = 0; \qquad \hat{n} = n \quad \text{if} \quad n \neq 0 \tag{4.11}$$

From Eq. (4.10) it follows that $G^{\varepsilon'}_{D;\text{in}}(x, y)$ can now be written as

$$\begin{aligned} G^{\varepsilon'}_{D;\text{in}}(x, y) &= G^1_{D;\text{in}}(x, y) + G^{2;0}_{D;\text{in}}(x, y) + G^{2;\Delta}_{D;\text{in}}(x, y) \\ &= \sum_{n \geqslant 0} \mu_n I_n(s_<) K_n(s_>) \cos n\theta \\ &\quad - \sum_{n \geqslant 0} \mu_n \frac{K_n'(Z)}{I_n'(Z)} I_n(s_0) I_n(s) \cos n\theta \\ &\quad - \frac{\varepsilon'}{Z^2} \sum_{n \geqslant 0} \mu_n \left(\frac{I_n(s_0) I_n(s)}{I_n'^2(Z) + (\varepsilon' \hat{n}/Z) I_n(Z) I_n'(Z)} \right) \hat{n} \cos n\theta \end{aligned} \tag{4.12}$$

We proceed now with the analysis of the long-range surface behavior of the ε'-dependent term of Eq. (4.12), namely when both $Z - s_0$ and $Z - s$ are close to zero and Z is large.

This analysis is done using the following asymptotic representations for the Bessel functions of the second kind and order $\alpha \in R$ (ref. 10, p. 122–123):

$$I_\alpha(u) = (2\pi u)^{-1/2} \exp(u) \left[\sum_{k=0}^{n} (-1)^k (\alpha; k)(2u)^{-k} + O(|u|^{-n-1}) \right]$$
$$(|\arg u| \leqslant \pi/2 - \delta) \tag{4.13}$$

and

$$K_\alpha(u) = \left(\frac{\pi}{2u}\right)^{1/2} \exp(-u) \left[\sum_{k=0}^{n} (\alpha; k)(2u)^{-k} + O(|u|^{-n-1}) \right]$$
$$(|\arg u| \leqslant \pi - \delta) \tag{4.14}$$

where δ is an arbitrarily small positive number and where $(\alpha; k)$ is defined by

$$(\alpha; k) = \frac{(4\alpha^2 - 1)(4\alpha^2 - 3^2) \cdots [4\alpha^2 - (2k-1)^2]}{2^{2k} k!}$$

with

$$(\alpha; 0) = 1 \tag{4.15}$$

With the idea to extract from the ε'-dependent part of Eq. (4.12) the dominant contributions in (ε'/Z), $(1/\xi_D Z)$ and n/Z, and using the result

$$\sum_{n \geqslant 0} \mu_n \hat{n} \cos n\theta \cong \frac{1}{\xi_D} - \frac{1}{2 \sin^2(\theta/2)}; \qquad \xi_D \gg \frac{\varepsilon'}{Z} \tag{4.16}$$

we find, for $\xi_D > 0$ and $0 < \varepsilon' < \infty$,

$$G_{D;\text{in}}^{2;\Delta} \underset{Z \to \infty}{\cong} -\frac{\varepsilon'}{Z} \left(\frac{1}{Z\xi_D} - \frac{1}{2Z \sin^2(\theta/2)} \right) \exp(-2Z) \exp(s_0 + s)[1 + O(Z^{-1})]$$
$$= \left(\frac{2\varepsilon'}{[2Z \sin(\theta/2)]^2} - \frac{\varepsilon'}{Z^2 \xi_D} \right) \exp(-2Z) \exp(s_0 + s)[1 + O(Z^{-1})] \tag{4.17}$$

Notice that $2Z \sin(\theta/2)$ represents the length of the chord which separates two points on the surface of the disk and that in the semi-infinite wall limit ($Z \to \infty$, $\theta \to 0$, $Z\theta = y$) together with the canonical limit $\xi_D \to \infty$ we recover the polynomial decay behavior ($\approx \varepsilon'/y^2$) along the wall

described by Jancovici [ref. 11, Eq. (2.6)]. More generally, we show in Appendix A how the DH kernel of the disk given by Eq. (4.12) goes over to the kernel of the semi-infinite plane given by Jancovici for $\varepsilon' = 1$ (ref. 4, p. 55). We also point out that, as expected, Eq. (4.17) vanishes for $\varepsilon' = 0$.

4.2. The Sphere

Just as in the two-dimensional disk case, the solution $G^{\varepsilon'}_{S;\text{in}}(x, y)$ of Eq. (3.3) for the inner region of a three-dimensional sphere S can be written as a sum of two contributions, namely

$$G^{\varepsilon'}_{S;\text{in}}(x, y) = G^{1}_{S;\text{in}}(x, y) + G^{2;\varepsilon'}_{S;\text{in}}(x, y) \tag{4.18}$$

where

$$\begin{aligned} G^{1}_{S;\text{in}}(x, y) &= \frac{\exp(\kappa |x-y|)}{|x-y|} \\ &= \sum_{l \geqslant 0} \frac{2l+1}{(|x|\,|y|)^{1/2}} I_{l+1/2}(s_<)\, K_{l+1/2}(s_>)\, P_l(\cos\alpha) \\ &\quad (s_0,\ s < Z;\ l \in N) \end{aligned} \tag{4.19}$$

is the well-known DH solution for a three-dimensional infinite medium and where

$$\begin{aligned} G^{2;\varepsilon'}_{S;\text{in}}(x, y) &= -\sum_{l \geqslant 0} \frac{2l+1}{(|x|\,|y|)^{1/2}} C^{l}_{S;\text{in}} I_{l+1/2}(s_0)\, I_{l+1/2}(s)\, P_l(\cos\alpha) \\ &\quad (s_0,\ s < Z;\ l \in N) \end{aligned} \tag{4.20}$$

The $P_l(\cos\alpha)$ are the Legendre polynomials of degree l and α is the angle between x and y.

On the other hand, $G^{\varepsilon'}_{S;\text{out}}(x, y)$ is given by

$$\begin{aligned} G^{\varepsilon'}_{S;\text{out}}(x, y) &= \sum_{l \geqslant 0} \frac{2l+1}{(|x|\,|y|)^{1/2}} C^{l}_{S;\text{out}} I_{l+1/2}(s_0)\, F_{l+1/2}(s)\, P_l(\cos\alpha) \\ &\quad (s_0 < Z < s;\ l \in N) \end{aligned} \tag{4.21}$$

where [notice the occurrence of the parameter $\xi_S = (\kappa L - Z)/Z$]

$$\begin{aligned} s^{-1/2} F_{l+1/2}(s) &= s^{-1} + \frac{\xi_S}{Z} \qquad \text{if} \quad l = 0 \\ s^{-1/2} F_{l+1/2}(s) &= s^{-(l+1)} \qquad \text{if} \quad l \neq 0 \end{aligned} \tag{4.22}$$

The coefficients $C^{l}_{S;\text{in}}$ and $C^{l}_{S;\text{out}}$ are obtained with the help of the

continuity conditions just as in the two-dimensional case. One finds, respectively,

$$C^l_{S;\text{in}} = \frac{\varepsilon' K_\mu(Z) F_\mu(Z) - 2\varepsilon' Z K_\mu(Z)\, F'_\mu(Z) + 2Z K'_\mu(Z)\, F_\mu(Z) - K'_\mu(Z)\, F_\mu(Z)}{\varepsilon' I_\mu(Z) F_\mu(Z) - 2\varepsilon' Z I_\mu(Z)\, F'_\mu(Z) + 2Z I'_\mu(Z)\, F_\mu(Z) - I'_\mu(Z)\, F_\mu(Z)} \tag{4.23}$$

and

$$C^l_{S;\text{out}} = \left[-Z\left(\varepsilon' I_\mu(Z)\, F'_\mu(Z) - I'_\mu(Z)\, F_\mu(Z) + \frac{1-\varepsilon'}{2Z} I_\mu(Z)\, F_\mu(Z) \right) \right]^{-1} \tag{4.24}$$

where we set $\mu = l + 1/2$ for convenience.

Now we apply to $C^l_{S;\text{in}}$ the same decomposition used in Section 4.1 [Eq. (4.9)]. Here we find

$$\begin{aligned} C^l_{S;\text{in}} &= C^{l;0}_{S;\text{in}} + C^{l;\Delta}_{S;\text{in}} \\ &= \frac{2ZK'_\mu(Z) - K_\mu(Z)}{2ZI'_\mu(Z) - I_\mu(Z)} \\ &\quad + \frac{\varepsilon'(\overline{2\mu+1})}{2Z^2}\left[I'^2_\mu(Z) + \frac{\beta-1}{2Z} I_\mu(Z)\, I'_\mu(Z) - \frac{\beta}{4Z^2} I^2_\mu(Z) \right]^{-1} \\ &\quad (l \geqslant 0;\ \varepsilon' \geqslant 0) \end{aligned} \tag{4.25}$$

where $\beta = (\overline{2\mu+1})\varepsilon' - 1$ and where

$$\begin{aligned} \overline{2\mu+1} &= \frac{2}{\xi_S + 1} \qquad \text{if} \quad l = 0 \\ \overline{2\mu+1} &= 2\mu + 1 \qquad \text{if} \quad l \neq 0 \end{aligned} \tag{4.26}$$

Equation (4.25) permits us to rewrite $G^{\varepsilon'}_{S;\text{in}}(x, y)$ as

$$\begin{aligned} G^{\varepsilon'}_{S;\text{in}}(x, y) &= G^1_{S;\text{in}}(x, y) + G^{2;0}_{S;\text{in}}(x, y) + G^{2;\Delta}_{S;\text{in}}(x, y) \\ &= \sum_{l \geqslant 0} \frac{2l+1}{(|x|\,|y|)^{1/2}} I_\mu(s_<)\, K_\mu(s_>)\, P_l(\cos\alpha) \\ &\quad - \sum_{l \geqslant 0} \frac{2l+1}{(|x|\,|y|)^{1/2}} \frac{2ZK'_\mu(Z) - K_\mu(Z)}{2ZI'_\mu(Z) - I_\mu(Z)} I_\mu(s_0)\, I_\mu(s)\, P_l(\cos\alpha) \\ &\quad - \frac{\varepsilon'}{2Z^2} \sum_{l \geqslant 0} \frac{2l+1}{(|x|\,|y|)^{1/2}} \left[I'^2_\mu(Z) + \frac{\beta-1}{2Z} I_\mu(Z)\, I'_\mu(Z) - \frac{\beta}{4Z^2} I^2_\mu(Z) \right]^{-1} \\ &\quad \times I_\mu(s_0)\, I_\mu(s)(\overline{2\mu+1})\, P_l(\cos\alpha) \end{aligned} \tag{4.27}$$

Here the long-range surface behavior of the ε'-dependent term of Eq. (4.27) is obtained using the asymptotic representations of the Bessel functions [Eqs. (4.13) and (4.14)] plus the following identities:

$$\sum_{l\geqslant 0}(2l+1)(\overline{2\mu+1})\,P_l(\cos\alpha)=\sum_{l\geqslant 0}(2l+1)^2\,P_l(\cos\alpha)-2+\frac{2}{\xi_S+1}$$

$$=-\left(\frac{1}{2\sin^3(\alpha/2)}+2\right)+\frac{2}{\xi_S+1} \tag{4.28}$$

where the last equality has been established using the generating function of the Legendre polynomials

$$y(t,z)=\sum_{l=0}^{\infty}t^l P_l(\cos\alpha)=(1-2tz+t^2)^{-1/2} \tag{4.29}$$

as well as its first and second derivatives with respect to t, evaluated at $t=1$.

Thus we have, for $\xi_S>0$ and $0<\varepsilon'<\infty$,

$$\kappa^{-1}G^{2;\mathrm{J}}_{S;\mathrm{in}}\underset{Z\to\infty}{=}-\frac{\varepsilon'}{2Z^2}\left(-\frac{1}{2Z\sin^3(\alpha/2)}-\frac{2}{Z}+\frac{2}{Z(\xi_S+1)}\right)$$

$$\times\exp(-2Z)\exp(s_0+s)[1+O(Z^{-1})]$$

$$=\left(\frac{2\varepsilon'}{[2Z\sin(\alpha/2)]^3}+\frac{\varepsilon'}{Z^3}-\frac{\varepsilon'}{Z^3(\xi_S+1)}\right)$$

$$\times\exp(-2Z)\exp(s_0+s)[1+O(Z^{-1})] \tag{4.30}$$

The surface correlation functions of the sphere thus have also a long-range polynomial decay proportional to the inverse cube of the chord which separates two points on the surface plus two angular-independent contributions proportional to the inverse cube of the radius of the sphere. Whereas the second of these contributions vanishes in the canonical limit ($\xi_S\to\infty$), the first one will be needed to recover the SM susceptibility given in Eq. (3.20c). As in the disk case, we recover in the semi-infinite wall limit the behavior of the correlation functions along a wall described by Jancovici [ref. 11, Eq. (2.6)]. However, this behavior does not fit with the law conjectured by Kennedy and Federbush (ref. 5, pp. 368–369, 415), which is that the surface correlation function does not decay with the inverse cube of the chord, but with the inverse cube of the arc. Of course there is a question of amplitude which is needed to compare these two results. The problem is that, besides its definition (ref. 5, p. 364), nowhere in the paper quoted is any estimate of this amplitude given.

5. DIELECTRIC SUSCEPTIBILITY OF THE DISK AND OF THE SPHERE

On the basis of the results obtained in Section 4, we take up now the explicit calculation as well as the investigation of the size, λ_Λ, and ε' dependence of the PF susceptibility and of its various contributions.

With the conventions that $\lambda_\Lambda = \xi_D$ for the disk and $\lambda_\Lambda = \xi_S + 1$ for the sphere and that $\bar{n} = n + \frac{1}{2}(\nu - 2)$, all the results can be given in a compact form including both cases.

We assume throughout this section that ε' is chosen before λ_Λ. This involves in particular the grand canonical case described in Section 3.

For convenience, the SM, excess, and PF susceptibility are presented separately in Sections 5.1–5.3.

5.1. The SM Susceptibility

Following the decomposition introduced before for the DH kernels, namely

$$G^{\varepsilon'}_{\Lambda;\mathrm{in}}(x, y) = G^{1}_{\Lambda;\mathrm{in}}(x, y) + G^{2;0}_{\Lambda;\mathrm{in}}(x, y) + G^{2;\Lambda}_{\Lambda;\mathrm{in}}(x, y) \tag{5.1}$$

we do the same with the SM susceptibility and we set

$$\chi^{\varepsilon'}_{11;\Lambda}(\mathrm{SM}) = \chi^{1}_{11;\Lambda}(\mathrm{SM}) + \chi^{2;0}_{11;\Lambda}(\mathrm{SM}) + \chi^{2;\Lambda}_{11;\Lambda}(\mathrm{SM}) \tag{5.2}$$

where

$$\chi^{1}_{11;\Lambda}(\mathrm{SM}) = \frac{1}{2\nu}\frac{\Gamma^2\rho^2}{|\Lambda|}\int_\Lambda d^\nu x\, d^\nu y\, |x-y|^2\, G^{1}_{\Lambda;\mathrm{in}}(x, y) \tag{5.3}$$

and

$$\chi^{2;0;\Lambda}_{11;\Lambda}(\mathrm{SM}) = \frac{1}{2\nu}\frac{\Gamma^2\rho^2}{|\Lambda|}\int_\Lambda d^\nu x\, d^\nu y\, |x-y|^2\, G^{2;0;\Lambda}_{\Lambda;\mathrm{in}}(x, y) \tag{5.4}$$

In carrying out the angular integration, one notices that only the terms $n = 0, 1$ (disk) and $l = 0, 1$ (sphere) give a nonvanishing contribution to the rhs of Eqs. (5.3) and (5.4) and we find

$$\chi^{1}_{11;\Lambda}(\mathrm{SM}) = \frac{1}{2\pi(\nu-1)} + \frac{Z^2}{2\pi(\nu-1)}\Big[K_2(Z)\, I_2(Z) - K_{\bar{1}}(Z)\, I_{\bar{1}}(Z) + \frac{1}{Z}K_{\bar{1}}(Z)\, I_2(Z) - \frac{1}{Z}K_2(Z)\, I_{\bar{1}}(Z)\Big] \tag{5.5}$$

and

$$\chi_{11;\Lambda}^{2;0;\Delta}(\mathrm{SM}) = \frac{Z^2}{2\pi(\nu-1)}\left[C_{\Lambda;\mathrm{in}}^{1;0;\Delta} I_2^2(Z) + C_{\Lambda;\mathrm{in}}^{0;0,\Delta}\left(\frac{2}{Z} I_{\bar{1}}(Z)\, I_2(Z) - I_{\bar{1}}^2(Z)\right)\right] \quad (5.6)$$

where the $C_{\Lambda;\mathrm{in}}^{m;0;\Delta}$ ($m = n$ or l) are defined by Eqs. (4.10) and (4.25).

We proceed now with the size-, λ_Λ-, and ε'-dependence analysis of Eqs. (5.5) and (5.6).

Since $\chi_{11;\Lambda}^{1}(\mathrm{SM})$ and $\chi_{11;\Lambda}^{2;0}(\mathrm{SM})$ are λ_Λ and ε' independent, the asymptotic behavior of these two terms can be taken up without having to distinguish several cases according to the values of λ_Λ and ε'. Using the asymptotic representations of the Bessel functions given in Eqs. (4.13) and (4.14), we thus find

$$\chi_{11;\Lambda}^{1}(\mathrm{SM}) = \frac{1}{2\pi(\nu-1)} + O(Z^{-1}) \quad (5.7)$$

and

$$\chi_{11;\Lambda}^{2;0}(\mathrm{SM}) = O(Z^{-1}) \quad (5.8)$$

In contrast, the analysis of $\chi_{11;\Lambda}^{2;\Delta}(\mathrm{SM})$ depends upon the values of λ_Λ and ε' and we are led to distinguish several cases, we summarize as follows:

$$\chi_{11;\Lambda}^{2;\Delta}(\mathrm{SM}) = \frac{\varepsilon'}{2\pi}\left[1 - \frac{1}{\lambda_\Lambda(\nu-1)} + O\left(\frac{1}{\lambda_\Lambda Z}\right)\right] + O(Z^{-1}), \quad \lambda_\Lambda > 0;\ 0 < \varepsilon' < \infty \quad (5.9)$$

$$\chi_{11;\Lambda}^{2;\Delta}(\mathrm{SM}) = -\frac{Z}{2\pi(\nu-1)} + \frac{\nu+3}{4\pi(\nu-1)} + \frac{\varepsilon'}{2\pi} + O(Z^{-1}), \quad \lambda_\Lambda = 0;\ 0 < \varepsilon' < \infty \quad (5.10)$$

$$\chi_{11;\Lambda}^{2;\Delta}(\mathrm{SM}) = O(Z^{-1}), \quad \lambda_\Lambda \geqslant 0;\ \varepsilon' = \infty \quad (5.11)$$

$$\chi_{11;\Lambda}^{2;\Delta}(\mathrm{SM}) \equiv 0, \quad \lambda_\Lambda \geqslant 0;\ \varepsilon' = 0 \quad (5.12)$$

The set of Eqs. (5.7)–(5.12) leads to the following behavior for the total SM susceptibility:

$$\chi_{11;\Lambda}^{\varepsilon'}(\mathrm{SM}) = \frac{1}{2\pi(\nu-1)} + \frac{\varepsilon'}{2\pi}\left[1 - \frac{1}{\lambda_\Lambda(\nu-1)} + O\left(\frac{1}{\lambda_\Lambda Z}\right)\right] + O(Z^{-1})$$
$$(\lambda_\Lambda > 0;\ 0 < \varepsilon' < \infty) \quad (5.13)$$

$$\chi_{11;\Lambda}^{\varepsilon'}(\mathrm{SM}) = -\frac{Z}{2\pi(\nu-1)} + \frac{\nu+3}{4\pi(\nu-1)} + \frac{1}{2\pi(\nu-1)} + \frac{\varepsilon'}{2\pi} + O(Z^{-1})$$

$$(\lambda_\Lambda = 0;\ 0 < \varepsilon' < \infty) \tag{5.14}$$

$$\chi_{11;\Lambda}^{\varepsilon'}(\mathrm{SM}) = \frac{1}{2\pi(\nu-1)} + O(Z^{-1})$$

$$(\lambda_\Lambda \geqslant 0;\ \varepsilon' = 0, \infty) \tag{5.15}$$

We notice here that the SM susceptibility assumes the SL value for both Neumann and Dirichlet boundary conditions. In the Neumann case it can correctly be concluded that the system would be in the plasma state, since $\chi_{11;\Lambda}^{\varepsilon'=0}(\mathrm{PF}) = \chi_{11;\Lambda}^{\varepsilon'=0}(\mathrm{SM})$ [Eq. (3.18c)], whereas in the second case this conclusion, although often drawn, does not hold, since $\chi_{11;\Lambda}^{\varepsilon'=\infty}(\mathrm{PF})$ diverges according to Eq. (3.19a).

Another comment concerns the surface contribution $\chi_{11;\Lambda}^{2;\Lambda}(\mathrm{SM})$ to the SM susceptibility: It can be shown that this quantity is, as expected, exactly reproduced by the second moment of the asymptotic surface behavior of $G_{\Lambda;\mathrm{in}}^{2;\Lambda}(x, y)$ given by Eqs. (4.17) and (4.30). The latter permits us also to obtain the three-dimensional analogue of the "arcsine law" found for the surface part of the partial susceptibility of the disk [II, Eq. (3.28)]. The derivation of this law is facilitated by the fact that

$$d^3x\, d^3y = 2\pi |x|\, d|x|\, |y|\, d|y|\, d^3|r|/|r|$$

and we find

$$\chi_{11;\Lambda}^{2;\Lambda}(|r|) = \frac{\varepsilon'}{4\pi}\left\{\frac{|r|}{2R} + \frac{\xi_S}{\xi_S+1}\left(\frac{|r|}{2R}\right)^4\right\}[1 + O(Z^{-1})]; \qquad |r| \in [0, 2R] \tag{5.16}$$

We emphasize that for $|r| = 2R$, $\chi_{11;\Lambda}^{2;\Lambda}(2R) \equiv \chi_{11;\Lambda}^{2;\Lambda}(\mathrm{SM})$ given by Eq. (5.9).

5.2. The Excess Susceptibility

Following again Eq. (5.1), we split the excess susceptibility

$$\Delta\chi_{11;\Lambda}^{\varepsilon'} = \frac{\Gamma\rho}{|\Lambda|}\int_\Lambda d^\nu y\ y_1^2\, p_\Lambda^{\varepsilon'}(y)$$

into three contributions:

$$\Delta\chi_{11;\Lambda}^{\varepsilon'} = \Delta\chi_{11;\Lambda}^{1} + \Delta\chi_{11;\Lambda}^{2;0} + \Delta\chi_{11;\Lambda}^{2;\Lambda} \tag{5.17}$$

where

$$\Delta\chi^{1}_{11;\Lambda} = \frac{\Gamma\rho}{|\Lambda|}\int_{\Lambda} d^{\nu}y\; y_1^2\left[1 - \Gamma\rho\int_{\Lambda} d^{\nu}x\, G^{1}_{\Lambda;\mathrm{in}}(x, y)\right] \tag{5.18}$$

and

$$\Delta\chi^{2;0;\Delta}_{11;\Lambda} = -\frac{\Gamma^2\rho^2}{|\Lambda|}\int_{\Lambda} d^{\nu}y\; y_1^2\int_{\Lambda} d^{\nu}x\, G^{2;0;\Delta}_{\Lambda;\mathrm{in}}(x, y) \tag{5.19}$$

since the excess density $p^{\varepsilon'}_{\Lambda}(y)$ is now given by

$$p^{\varepsilon'}_{\Lambda}(y) = 1 - \Gamma\rho\int_{\Lambda} d^{\nu}x\,[G^{1}_{\Lambda;\mathrm{in}}(x, y) + G^{2;0}_{\Lambda;\mathrm{in}}(x, y) + G^{2;\Delta}_{\Lambda;\mathrm{in}}(x, y)] \tag{5.20}$$

Since only the components $n=0$ (disk) and $l=0$ (sphere) give a non-vanishing contribution to the angular integration over x, Eqs. (5.18) and (5.20) can be performed easily and we find

$$\Delta\chi^{1}_{11;\Lambda} = -\Delta\chi^{2;0}_{11;\Lambda} = \frac{Z^2}{2\pi(\nu-1)}\left[K_{\bar{1}}(Z)\, I_{\bar{1}}(Z) - \frac{2}{Z}K_{\bar{1}}(Z)\, I_2(Z)\right] \tag{5.21}$$

$$\Delta\chi^{2;\Delta}_{11;\Lambda} = \frac{Z^2}{2\pi(\nu-1)}\, C^{0;\Delta}_{\Lambda;\mathrm{in}}\left[I^2_{\bar{1}}(Z) - \frac{2}{Z}I_{\bar{1}}(Z)\, I_2(Z)\right] \tag{5.22}$$

and

$$p^{\varepsilon'}_{\Lambda}(y) = C^{0;\Delta}_{\Lambda;\mathrm{in}}\, Z^{\bar{1}} I_{\bar{1}}(Z)\,\frac{I_{\bar{0}}(\kappa|y|)}{(\kappa|y|)^{\bar{0}}} \tag{5.23}$$

Equation (5.21) implies in particular that $\Delta\chi^{\varepsilon'}_{11;\Lambda} \equiv \Delta\chi^{2;\Delta}_{11;\Lambda}$. This means that the size-, λ_Λ-, and ε'-dependence analysis of the total excess susceptibility $\Delta\chi^{\varepsilon'}_{11;\Lambda}$ is entirely determined by that of $\Delta\chi^{2;\Delta}_{11;\Lambda}$. According to the values of λ_Λ and ε' and using Eqs. (4.13) and (4.14), we thus find

$$\Delta\chi^{\varepsilon'}_{11;\Lambda} = \frac{\varepsilon'}{2\pi}\left[\frac{1}{\lambda_\Lambda(\nu-1)} + O\left(\frac{1}{\lambda_\Lambda Z}\right)\right]; \qquad \lambda_\Lambda > 0;\quad 0 < \varepsilon' < \infty \tag{5.24}$$

$$\Delta\chi^{\varepsilon'}_{11;\Lambda} = \frac{Z}{2\pi(\nu-1)} - \frac{\nu+3}{4\pi(\nu-1)} + O(Z^{-1}); \qquad \lambda_\Lambda = 0;\quad 0 < \varepsilon' < \infty \tag{5.25}$$

$$\Delta\chi^{\varepsilon'}_{11;\Lambda} = \frac{Z}{2\pi(\nu-1)} - \frac{\nu+3}{4\pi(\nu-1)} + O(Z^{-1}); \qquad \lambda_\Lambda \geqslant 0;\quad \varepsilon' = \infty \tag{5.26}$$

$$\Delta\chi^{\varepsilon'}_{11;\Lambda} \equiv 0; \qquad \lambda_\Lambda \geqslant 0;\quad \varepsilon' = 0 \tag{5.27}$$

We notice that the equivalence between Eqs. (5.25) and (5.26) follows directly from the identity

$$C^{0;A}_{A;\mathrm{in}}(\lambda_A = 0; 0 < \varepsilon' < \infty) \equiv C^{0;A}_{A;\mathrm{in}}(\lambda_A \geqslant 0; \varepsilon' = \infty) = \frac{1}{ZI_{\bar{0}}(Z)\, I_{\bar{1}}(Z)} \tag{5.28}$$

and the result of Eq. (5.27) from the fact that

$$C^{0;A}_{A;\mathrm{in}}(\lambda_A \geqslant 0; \varepsilon' = 0) \equiv 0 \tag{5.29}$$

These two relations are also directly useful for examining the behavior of the excess density $p^{\varepsilon'}_A(y)$ given by Eq. (5.23), according to the values of ε' and λ_A. The results are the following:

$$p^{\varepsilon'}_A(y) = \left(\frac{Z}{\kappa\,|y|}\right)^{\bar{0}} \frac{\varepsilon' I_{\bar{0}}(\kappa\,|y|)}{\lambda_A Z I_{\bar{0}}(Z) + \varepsilon' I_{\bar{0}}(Z)}; \qquad \lambda_A > 0; \quad 0 < \varepsilon' < \infty \tag{5.30}$$

$$p^{\varepsilon'}_A(y) = \left(\frac{Z}{\kappa\,|y|}\right)^{\bar{0}} \frac{I_{\bar{0}}(\kappa\,|y|)}{I_{\bar{0}}(Z)}; \qquad \lambda_A = 0; \quad 0 < \varepsilon' < \infty \tag{5.31}$$

$$p^{\varepsilon'}_A(y) = \left(\frac{Z}{\kappa\,|y|}\right)^{\bar{0}} \frac{I_{\bar{0}}(\kappa\,|y|)}{I_{\bar{0}}(Z)}; \qquad \lambda_A \geqslant 0; \quad \varepsilon' = \infty \tag{5.32}$$

and

$$p^{\varepsilon'}_A(y) \equiv 0; \qquad \lambda_A \geqslant 0; \quad \varepsilon' = 0 \tag{5.33}$$

We observe that the excess densities are concentrated in a thin surface layer since they take their largest values ($\varepsilon'/Z\lambda_A$, 1, 1, and 0, respectively) on the edge and since they decrease exponentially within a Debye length toward the interior.

5.3. The PF Susceptibility

With Eqs. (5.5), (5.6), (5.21), and (5.22), the PF susceptibility is found to be given by

$$\chi^{\varepsilon'}_{11;A}(\mathrm{PF}) = \frac{Z^2}{2\pi(\nu - 1)} \left[K_{\bar{2}}(Z)\, I_{\bar{2}}(Z) + (C^{1;0}_{A;\mathrm{in}} + C^{1;A}_{A;\mathrm{in}})\, I^2_{\bar{2}}(Z)\right] \tag{5.34}$$

We emphasize that, as expected, $\chi^{\varepsilon'}_{11;A}(\mathrm{PF})$ does not depend upon λ_A, since the coefficient $C^0_{A;\mathrm{in}}$ does not appear in Eq. (5.34).

The size and ε' dependences of the PF susceptibility are obtained by gathering Eqs. (5.13)–(5.15) and Eqs. (5.24)–(5.27) or by direct expansion of Eq. (5.34). We find

$$\chi^{\varepsilon'}_{11;A}(\mathrm{PF}) = \frac{1}{2\pi(\nu - 1)} + \frac{\varepsilon'}{2\pi} + O(Z^{-1}); \qquad 0 \leqslant \varepsilon' < \infty \tag{5.35}$$

and

$$\chi_{11;\Lambda}^{\varepsilon'}(\mathrm{PF}) = \frac{Z}{2\pi(\nu-1)} - \frac{\nu+1}{4\pi(\nu-1)} + O(Z^{-1}); \qquad \varepsilon' = \infty \tag{5.36}$$

Equation (5.35) shows that the DH approximation is capable of reproducing in the thermodynamic limit the results of classical electrostatics [Eq. (2.9)]. Notice in particular that Eq. (5.35) assumes the SL value only with Neumann boundary conditions. Furthermore, Eq. (5.36) shows that in Dirichlet boundary conditions the PF susceptibility diverges like the radius of the system. This divergence is due to the excess susceptibility.

We are left now with the investigation of the "canonical case" ($\varepsilon' \to \infty$, $\lambda_\Lambda \to \infty$, $\varepsilon'/\lambda_\Lambda \to 0$). The latter is discussed in detail in the next section. We show that the PF susceptibility still diverges like the radius of the system, but it does so now through the divergence of the SM susceptibility instead of the excess susceptibility.

6. DH SOLUTION FOR $\epsilon' = \infty$

In Section 4 we studied the solution of the DH equation and in particular the surface correlations for $0 \leqslant \varepsilon' < \infty$, excluding carefully the case $\varepsilon' = \infty$. In Section 5 we computed in particular the dielectric susceptibility for $\varepsilon' = \infty$ (grand canonical limit) and observed a divergence of the susceptibility because of charge fluctuations. In this section we investigate the other limit, i.e., the canonical limit, which has not been examined up to now. We recall that in the canonical limit, only the SM susceptibility contributes to the PF susceptibility.

We show in this section that the divergence of the susceptibility (required by electrostatics) can be explained by the existence of long-range radial surface correlations.

We first mention that the two previous limits correspond respectively to the following physical situations:

(a) The system is subjected to Dirichlet boundary conditions and can exchange particles with the conducting wall. A physical realization of this situation would be an OCP separated by a permeable wall from another OCP with practically vanishing Debye length.

(b) The system is subjected to Dirichlet boundary conditions but cannot exchange particles, since the wall is supposed to be impermeable. This implies that the system must satisfy the charge conservation condition $\langle N^2 \rangle - \langle N \rangle^2 = 0$. A physical realization of this situation is an OCP within

another separated by an impermeable wall of zero thickness. We note (and show hereafter) that even a slight violation of the charge conservation condition transforms system (b) into system (a).

When we apply the DH approximation to a closed system with $\varepsilon' = \infty$, we cannot simultaneously satisfy the monopole sum rule of canonical systems and the Dirichlet boundary conditions, which require the DH kernel interpreted as a potential to be zero on the boundary. It is, however, consistent with the idea of a metallic environment to require the potential to be constant on the boundary. The value $V_0(s_0)$ of this constant is defined by the condition that the excess charge must vanish ($\xi_D = \infty$) and it depends explicitly on the position s_0 of the source. If one prefers to set the potential to zero on the boundary in order to satisfy to the strict Dirichlet boundary conditions (which is done, for instance, in a numerical simulation with the microscopic kernel of the Coulomb interaction), one could simply redefine the potential by subtracting from it the constant $V_0(s_0)$. While the kernel as a correlation function remains unchanged and symmetric, a potential constructed in this way would no longer be symmetric.

We want to investigate now the asymptotic surface behavior of the correlation functions for the disk in the canonical limit. The kernel is defined by

$$G_{\text{in}}(s, s_0) = \sum_{n \geqslant 0} \mu_n \cos n\theta [I_n(s_<) K_n(s_>) - C_{\text{in};n} I_n(s) I_n(s_0)]$$

where, according to Eq. (4.7),

$$C_{\text{in};n} = \frac{\varepsilon' K_n(Z) F_n'(Z) - K_n'(Z) F_n(Z)}{\varepsilon' I_n(Z) F_n'(Z) - I_n'(Z) F_n(Z)}$$

and

$$F_0(Z) = \xi_D, \qquad F_0'(Z) = -\frac{1}{Z}, \qquad F_{n \geqslant 1}(Z) = Z^{-n}, \qquad F_{n \geqslant 1}'(Z) = -\frac{n}{Z^{n+1}}$$

In the limit of $\varepsilon' \to \infty$, the coefficients are

$$\text{for } n \geqslant 1: \qquad C_{\text{in};n;\text{gcan}} = C_{\text{in};n;\text{can}} = \frac{K_n(Z)}{I_n(Z)}$$

$$\text{for } n = 0: \qquad C_{\text{in};0.\text{gcan}} = \frac{K_0(Z)}{I_0(Z)}; \qquad \frac{\xi_D}{\varepsilon'} \to 0$$

$$C_{\text{in};0;\text{can}} = -\frac{K_1(Z)}{I_1(Z)}; \qquad \frac{\xi_D}{\varepsilon'} \to \infty$$

One can obtain the canonical solution from the grand canonical one with the simple relation

$$G_{\text{in,can}}(s, s_0, \theta) = G_{\text{in;gcan}}(s, s_0, \theta) + I_0(s)\, I_0(s_0) \left(\frac{K_0(Z)}{I_0(Z)} + \frac{K_1(Z)}{I_1(Z)} \right)$$

$$= G_{\text{in;gcan}}(s, s_0, \theta) + \frac{1}{Z} \frac{I_0(s)\, I_0(s_0)}{I_0(Z)\, I_1(Z)} \tag{6.1}$$

If the observation point is on the boundary, i.e., $s = Z$, we obtain

$$G_{\text{in;can}}(Z, s_0) = \frac{1}{Z} \frac{I_0(s_0)}{I_1(Z)} \tag{6.2}$$

and for the surface potential

$$V_0(s_0) = G_{\text{in;can}}(Z, s_0) = \frac{1}{Z} \frac{I_0(s_0)}{I_1(Z)} \approx \frac{1}{Z} e^{-(Z - s_0)} \qquad \text{for large } Z \tag{6.3}$$

This relation indicates clearly that the surface potential is vanishing when the distance between the source and the edge is larger than a few Debye lengths.

In particular, if both arguments are on the boundary, we find

$$G_{\text{in;can}}(Z, Z) = I_0(Z)\, I_0(Z) \left(\frac{K_0(Z)}{I_0(Z)} + \frac{K_1(Z)}{I_1(Z)} \right) = \frac{1}{Z} \frac{I_0(Z)}{I_1(Z)} \approx \frac{1}{Z} \qquad \text{for large } Z \tag{6.4}$$

This indicates that the correlation function *on* the surface does not vanish as in the grand canonical case, but is proportional to $1/Z$.

For a complete analysis we need to know the decay of the kernel when the two arguments s and s_0 are close to Z. Although the complete kernel in the grand canonical limit is of short range,[3] it is easier to use the decomposition of Eq. (4.12), which contains two short-range parts and a surface part.[4] This last sum can be explicitly written, depending on the limits,

$$G_{\text{surf;gcan}}(\mathbf{x}, \mathbf{y}) = -\frac{1}{Z} \frac{I_0(s)\, I_0(s_0)}{I_0(Z)\, I_0'(Z)} - \frac{1}{Z} \sum_{n \geqslant 1} \mu_n \cos n\theta \, \frac{I_n(s)\, I_n(s_0)}{I_n(Z)\, I_n'(Z)}$$

$$G_{\text{surf;can}}(\mathbf{x}, \mathbf{y}) = -\frac{\varepsilon'}{\xi_D Z} \frac{I_0(s)\, I_0(s_0)}{I_0'^2(Z)} - \frac{1}{Z} \sum_{n \geqslant 1} \mu_n \cos n\theta \, \frac{I_n(s)\, I_n(s_0)}{I_n(Z)\, I_n'(Z)}$$

[3] In fact one can prove that $0 < G_{\text{in;gcan}}(\mathbf{x}, \mathbf{y}) < K_0(|\mathbf{x} - \mathbf{y}|)$ in Dirichlet boundary conditions.
[4] The surface part is long ranged for $\varepsilon' < \infty$ but becomes also short ranged for $\varepsilon' = \infty$.

Since the angular average ($n=0$) of the canonical surface kernel vanishes in the limit of $\xi_D/\varepsilon' \to \infty$, one has

$$G_{\text{surf;can}}(\mathbf{x}, \mathbf{y}) = G_{\text{surf;gcan}}(\mathbf{x}, \mathbf{y}) + \frac{1}{Z} \frac{I_0(s)\, I_0(s_0)}{I_0(Z)\, I_0'(Z)} \tag{6.5}$$

One can show that $G^{\varepsilon'=\infty}_{\text{surf;gcan}}(\mathbf{x}, \mathbf{y})$ is a periodically replicated K_0 (see Appendix A) and therefore is short ranged. The remaining angular-independent term can be expanded for large Z and reads

$$G_{\text{surf;can}}(\mathbf{x}, \mathbf{y}) \approx \frac{1}{Z} e^{-(Z-s)} e^{-(Z-s_0)} \tag{6.6}$$

This demonstrates that a finite canonical system indeed has long-range surface correlations in the case of Dirichlet boundary conditions. These correlations do not depend on the separation between the two points but on the distance from the wall only and lead to a divergence of the susceptibility which is linear with the size of the system. We note that the amplitude of this divergence is the same as the one we found in the grand canonical limit [Eq. (5.36)]. Indeed, we have with Eq. (6.6)

$$\chi_{11;\Lambda}(\text{SM}) = \frac{\Gamma^2 \rho^2}{2|\Lambda|} \int_\Lambda (\mathbf{x}-\mathbf{y})^2\, G_{\text{surf;can}}(\mathbf{x}, \mathbf{y})\, d^2x\, d^2y \approx \frac{Z}{2\pi} \tag{6.7}$$

Since the radial correlations are of order $1/Z$, they vanish in a system which is infinite at least in one direction. This shows that in order to explain the divergence of the susceptibility in a canonical system in Dirichlet boundary conditions in the thermodynamic limit one has to compute first the susceptibility and only *afterward* take the limit $Z = \kappa R \to \infty$.

As the last point of this section we want to discuss briefly the crossover from the $\varepsilon' < \infty$ to the $\varepsilon' = \infty$ regime. An infinite system has the somewhat puzzling property that the surface correlations increase linearly with ε' but completely vanish for $\varepsilon' = \infty$. A finite system, on the other hand, exhibits, as we show hereafter, a continuous transition from a dielectric to a metallic environment.

The surface part of the kernel given by Eq. (4.12) can be written

$$-\frac{1}{Z} \sum_{n \geqslant 0} \mu_n \left(\frac{I_n(s_0)\, I_n(s)}{I_n'^2(Z) + (\varepsilon' \hat{n}/Z)\, I_n(Z)\, I_n'(Z)} \right) \frac{\varepsilon' \hat{n}}{Z} \cos n\theta$$

The results of Section 5 assume that $\varepsilon'/Z \to 0$ (ε' fixed and $Z \to \infty$) or $\varepsilon' = \infty$ (metallic boundary conditions). For convenience we call the first case the dielectric regime and the second the metallic regime. The crossover takes place at $\varepsilon'/Z \approx 1$.

How do the correlation functions switch from the dielectric regime behavior to the metallic one? If we increase ε', only the small-n terms of the sum remain proportional to n. The large-n terms on the contrary decrease. This means that the amplitude of the surface correlations decrease at short distances and increase linearly with ε' for long distances only. The distance at which the ε'/r^2 behavior becomes valid is itself a function of ε'/Z and also increases with ε'/Z. If now ε'/Z increases beyond one, this distance becomes larger than the size of the disk and the correlation function cannot reach its asymptotic ε'/r^2 behavior. The surface correlations behave as in a conducting environment.

As an illustration we have plotted the DH susceptibility as a function of Z (see Fig. 1). We observe that for $Z \ll \varepsilon'$, the susceptibility increases linearly with the size of the system as in a conducting environment, but saturates at a value

$$\chi = \frac{1}{2\pi} + \frac{\varepsilon'}{2\pi} \tag{6.8}$$

if Z becomes larger than ε'.

7. NUMERICAL RESULTS: MONTE CARLO SIMULATIONS OF THE OCP

The purpose of this section is to confront the results obtained with the DH approximation with a "real" system. For simplicity we have chosen an

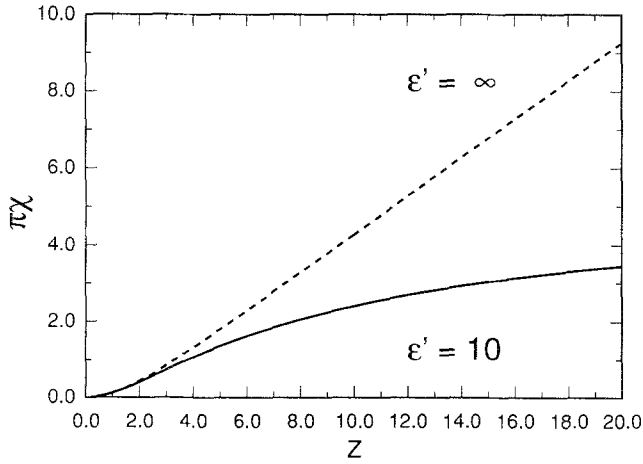

Fig. 1. The PF susceptibility of a disk-shaped system in DH approximation as a function of the size and for $\varepsilon' = 10$ and $\varepsilon' = \infty$.

OCP subjected to different boundary conditions and in either a canonical or grand ensemble. The boundary conditions are now put directly in the microscopic kernel and the number of particles is allowed to fluctuate or not, depending on the ensemble. We shall see that the problem of the canonical or grand canonical limit is here completely removed for $\varepsilon' = \infty$, but not for $\varepsilon' < \infty$.

The pairwise interaction between two point particles is given by

$$\psi(\mathbf{r}_1, \mathbf{r}_2) = -\frac{1}{2\varepsilon_1} \log \frac{(\mathbf{r}_1 - \mathbf{r}_2)^2}{L^2} - \frac{\Delta}{2\varepsilon_1} \log \left(\frac{R^2}{L^2} - 2 \frac{\mathbf{r}_1 \mathbf{r}_2}{L^2} + \frac{\mathbf{r}_1^2 \mathbf{r}_2^2}{R^2 L^2} \right)$$

where

$$\Delta = \frac{\varepsilon_1 - \varepsilon_2}{\varepsilon_1 + \varepsilon_2}$$

and R is the radius of the disk.

The first term is the direct interaction between the particles, the second the interaction between a particle and the image of the other (or vice versa). For simplicity we set $\varepsilon_1 = 1$ and $\varepsilon_2 = \varepsilon'$.

We can extract the terms which depend on the scale length of the logarithmic potential and obtain

$$\psi(\mathbf{r}_1, \mathbf{r}_2) = -\frac{1}{2} \log \frac{(\mathbf{r}_1 - \mathbf{r}_2)^2}{L^2} - \frac{\Delta}{2} \log \left(1 - 2 \frac{\mathbf{r}_1 \mathbf{r}_2}{R^2} + \frac{\mathbf{r}_1^2 \mathbf{r}_2^2}{R^4} \right) - \frac{1}{2} \log \left(\frac{R^2}{L^2} \right) (1 + \Delta) \tag{7.1}$$

Note that in the case of metallic boundary conditions ($\Delta = -1$), the kernel becomes independent of the scale length L. The kernel with $L = R$ is also given in ref. 12.

For numerical reasons, we use the following representation of the kernel:

$$\psi(\mathbf{r}_1, \mathbf{r}_2) = -\frac{1}{2} \log \frac{(\mathbf{r}_1 - \mathbf{r}_2)^2}{R^2} - \frac{1}{2} \log \left(\frac{R^2}{L^2} \right) - \frac{\Delta}{2} \log \left(\frac{(\mathbf{r}_1 - \mathbf{r}_2)^2}{R^2} + \frac{R^2 - \mathbf{r}_1^2}{R^2} \frac{R^2 - \mathbf{r}_2^2}{R^2} \right) - \frac{\Delta}{2} \log \left(\frac{R^2}{L^2} \right) \tag{7.2}$$

We need also the self-interaction. Removing the divergent term from the kernel, we find

$$\psi_s(\mathbf{r}) = -\frac{\Delta}{2} \log \left(\frac{(R^2 - \mathbf{r}_1^2)^2}{R^4} \right) - \frac{\Delta}{2} \log \left(\frac{R^2}{L^2} \right)$$

The reader may note that in the limit case of $\varepsilon' = \infty$ the kernel in Eq. (7.2) reproduces well the Dirichlet boundary conditions, i.e., the potential is zero on the boundary. In the opposite limit case, namely $\varepsilon' = 0$, the kernel in Eq. (7.2) does not reproduce the strict Neumann conditions (which implies that the field is zero on the boundary). By Gauss law, it is indeed impossible to satisfy the Neumann boundary conditions if the potential is produced by a single charged particle. A neutral assembly of charged particles, however, does produce a field that vanishes on the boundary. For that reason, it does not make sense in the case of $\varepsilon' = 0$ to perform a grand canonical simulation that would allow charge fluctuations.

The interaction between the particles and the background is obtained by integrating the kernel of Eq. (7.1) over the disk. One finds

$$\psi_{\text{p.b.}}(\mathbf{r}) = \frac{N_0}{2R^2}\mathbf{r}^2 - \frac{N_0}{2} + N_0 \log\left(\frac{L}{R}\right)(1+\Delta)$$

where $N_0 e$ is the total charge of the disk and e is the unit charge.

The energy of the background is given by

$$V_{\text{bb}} = \frac{N_0^2}{8} - \frac{N_0^2}{2}\log\left(\frac{R}{L}\right)(1+\Delta)$$

The total potential energy is now

$$V(\{\mathbf{r}_i\}) = e^2\left\{\sum_{i<j}\psi(\mathbf{r}_i, \mathbf{r}_j) + \frac{1}{2}\sum_i \psi_s(\mathbf{r}_i) + \sum_i \psi_{\text{pb}}(\mathbf{r}_i) + V_{\text{bb}}\right\} \tag{7.3}$$

It is interesting to analyze separately the scale-dependent part of the potential energy:

$$V_{\text{scale}} = -\frac{1}{2}\log\left(\frac{R}{L}\right)\{(N-N_0)^2(1+\Delta) - N(1-\Delta)\}$$

In the CMC simulations, this energy drops out in the observables, but the situation is very different in the grand ensemble. We have to consider two cases:

(a) $\varepsilon' = \infty$: Since $\Delta = -1$, the quadratic term $(N-N_0)^2$ in V_{scale} vanishes and we can absorb the linear term simply in the chemical potential, which has to be chosen such that the mean number of particles $\langle N \rangle$ is equal to N_0.

(b) $\varepsilon' < \infty$: The quadratic term does not vanish (except if $L = R$) in this case and we obtain fluctuations which depend now explicitly on

$\log(L/R) = \xi_D$. If $L/R \to \infty$, all fluctuations are suppressed (as in the DH theory) and the grand ensemble behaves like the canonical ensemble. One may ask if the grand ensemble has a physical meaning if the observables depend on the (usually) arbitrary scale length of the Coulomb logarithmic potential. In fact, one can even argue that the property of the grand ensemble, i.e., that it can exchange charges with the environment, is in contradiction with the hypothesis that the environment is a dielectric without any charges. Nevertheless, we present the MC results even for that situation in order to have a comparison with the DH results. The three-dimensional case is analoguous.

In the CMC simulations, we use the standard Metropolis algorithm. It may be noted that rejected moves resulting from a collision of an electron with the (infinite) wall surrounding the system *must* be counted in the averaging.

The GCMC simulations are based on the work of Adams[13,14] and a short review about the different methods is given in ref. 15. The main difference between the GCMC and the CMC simulations is that we have, besides the usual moves, attempts to add or remove a particle. The probability of acceptance of a particle insertion or removal is

$$P_{\text{acc}}(N+1, N) = \min(1, R_{N+1;N})$$
$$P_{\text{acc}}(N-1, N) = \min(1, R_{N-1;N})$$

where

$$R_{N+1;N} = e^{\beta(\mu_{\text{ex}} - \Delta U)} \frac{\langle N \rangle}{N+1}$$

$$R_{N-1;N} = e^{\beta(\mu_{\text{ex}} + \Delta U)} \frac{N}{\langle N \rangle}$$

The symbol μ_{ex} denotes the excess chemical potential with respect to a perfect gas. The ratio $\langle N \rangle/(N+1)$, respectively $N/\langle N \rangle$, accounts for the factor $1/n!$ in the grand partition function.

While in most GCMC simulations of multicomponent Coulomb systems[16–18] only neutral pairs of particles have been added or removed, we cannot (and do not want to) have this restriction in an OCP. The reason why particles are usually inserted by pairs is based on the fact that charge fluctuations in a normal Coulomb system are very small. This is not true in the case of penetrable metallic boundary conditions, where the charge fluctuations are proportional to the surface of the system. Such a system has been solved in the grand ensemble by Forrester,[19] who com-

puted the charge fluctuations of an OCP on a strip. The advantage of the grand ensemble is that the truncated pair correlation function does not have to obey the sum rule valid for a canonical ensemble

$$\frac{1}{\Lambda}\int_{\Lambda} d\mathbf{x}\, d\mathbf{y}\, \rho_2^{T;\mathrm{can}}(\mathbf{x}, \mathbf{y}) = -\frac{N}{|\Lambda|}$$

We therefore may expect a different behavior of the correlation function in the two ensembles.

We focus our attention on the three following aspects:

1. The Debye–Hückel theory predicts two different regimes of the polarization fluctuations, depending on the parameter

$$\frac{z}{\varepsilon'} = \frac{\kappa R}{\varepsilon'} = \frac{(2\Gamma N)^{1/2}}{\varepsilon'}$$

For a given ε', we expect a linear increase of the polarization fluctuations as a function of $N^{1/2}$ in the range $0 < (2\Gamma N)^{1/2} < \varepsilon'$. For higher values of $(2\Gamma N)^{1/2}$, we expect a saturation.

2. Electrostatics gives the following relation connecting ε, χ, and ε':

$$\varepsilon = \frac{1 + \varepsilon' + 2\pi\varepsilon'\chi}{1 + \varepsilon' - 2\pi\chi}$$

where

$$\chi = \frac{\beta}{2}\frac{\langle \mathbf{P}^2 \rangle}{|\Lambda|}$$

depends of course on the number of particles and on the boundary conditions. We compare systems of different sizes and of different ε'.

3. The Debye–Hückel theory produces a result which depends on the parameter ξ_D. If ξ_D is much larger than ε', the system has very small charge fluctuations and the Debye–Hückel solution is expected to mimic a system in the canonical ensemble. For ξ_D close to 1, the Debye–Hückel approximation allows charge fluctuations similarly to a grand ensemble. The total polarization fluctuation $\chi(\mathrm{PF})$, which is the sum of the second moment $\chi(\mathrm{SM})$ and of $\Delta\chi$, is expected to be independent of ξ_D. The purpose of these simulations is to check the validity of these analytical results.

7.1. Special Numerical Techniques

The generation of configurations in the grand ensemble is straightforward and barely more complicated than in a canonical ensemble. The excess chemical potential is obtained on a short preliminary run, which adjusts the chemical potential until the average number of particles is close to the intended N. The precise calculation of the truncated pair correlation function is difficult, because one cannot simply subtract from the pair correlation function the square of the densities, which is possible in a translationally invariant system (for example, a system in periodic boundary conditions). The calculation of the truncated pair correlation requires two steps: in a first run, we compute the pair correlation function and the density. The pair correlation, which is naturally obtained in a computer simulation, is defined in terms of the two-body correlation functions through the following relation (for the notations cf. II):

$$\hat{\rho}_{2;\mathrm{disk}}(|\mathbf{r}|) = \int_0^{2\pi} d\theta\, |\mathbf{r}|\, \bar{\rho}_{2;\mathrm{disk}}(|\mathbf{r}|, \theta)$$

$$\bar{\rho}_{2;\mathrm{disk}}(|\mathbf{r}|, \theta) = \frac{1}{|A|} \int_{D_A(r)} d^2x\, \rho^T_{2;A}(\mathbf{x}, \mathbf{x} + \mathbf{r}(\theta))$$

The function $\hat{\rho}_{2;\mathrm{disk}}(|\mathbf{r}|)$ represents the average of the two-body correlation function over all different origins and angles, and $\mathbf{x}$ and $\mathbf{r}$ represent two-dimensional vectors.

In a second run, we compute the average over all origins and angles of the product $\rho_1(\mathbf{x})\,\rho_1(\mathbf{x}+\mathbf{r}(\theta))$. This function must then be subtracted from the pair correlation function in order to give the truncated pair correlation function. The computation of the average of the product of the densities is most conveniently done with a "Monte Carlo simulation of independent particles." N particles are randomly distributed on the disk with a probability density corresponding to the density measured in the first run. The "product of the densities" is now computed in the same way as in the previous real simulation. In the case of a GCMC simulation, this function must be scaled with the factor $(\langle N\rangle/N)^2$, because the average number of particles $\langle N\rangle$ is not exactly equal to N.

A last comment about the sampling. Since the density in a finite system may vary over several magnitudes (especially for $\varepsilon' = \infty$, where the electrons build up a surface layer), the rejection method in the computation of the product of the densities is inefficient. We use a mapping technique based on the following idea. Define

$$y = f(x), \qquad y \in [0; R] \qquad \text{with} \quad f(x) = c \int_0^x \rho(x')\, 2\pi x'\, dx'$$

If y is uniformly distributed on the interval $[f(0), f(R)]$, $x = f^{-1}(y)$ has a distribution according to the weight factor $2\pi\rho(x)$. Since $\rho(x)$ is not known analytically, the function $f^{-1}(y)$ is replaced by a numerical table combined with a linear interpolation scheme.

7.2. Results

We show in Table I–VII the results of the Monte Carlo simulations in the canonical ensemble and in the grand ensemble. The dielectric constant ε' takes the values 0, 1, 10, ∞. The number N of particles ranges from 5 to 220 and $\Gamma = 0.5$.

The error bars $\Delta\chi$ for the polarization fluctuations and $\Delta\varepsilon$ for the dielectric constant are estimated in the following way: ten subaverages of χ during a run of 40,000 moves per particle are computed. The error $\Delta\chi$ is defined as

$$\Delta\chi = 2\left[\frac{\text{Variance}(\chi)}{10}\right]^{1/2}$$

and $\Delta\varepsilon$ is defined as

$$\Delta\varepsilon = \tfrac{1}{2}\{\varepsilon(\chi + \Delta\chi) - \varepsilon(\chi - \Delta\chi)\}$$

The symbol $\langle N; N\rangle$ in the tables stands for $\langle N^2\rangle - \langle N\rangle^2$.

We note that the polarization fluctuations χ(PF) and the dielectric constant ε do not depend (within the error bars) on the ensemble. The values of χ and ε increase with the number of particles. The dielectric constant ε seems to be a little larger for large ε' than for small ε'. The accuracy of χ decreases for large ε', but the accuracy of ε increases resulting from a less nonlinear relation between ε and χ. A puzzling observation is that the

Table I. $\epsilon' = \infty$, Canonical Ensemble

N	$\chi\pi$	$\Delta\chi\pi$	ε	$\Delta\varepsilon$
5	0.581	0.078	2.163	0.156
10	0.973	0.821	2.946	1.641
20	2.223	1.080	5.446	2.167
40	2.724	0.181	6.446	0.361
80	3.849	0.262	8.698	0.361
120	5.674	0.707	12.344	1.414
220	7.183	0.456	15.366	0.921

Table II. $\epsilon' = 10$, Canonical Ensemble

N	$\chi\pi$	$\Delta\chi\pi$	ε	$\Delta\varepsilon$
5	0.526	0.068	2.16	0.17
10	1.386	0.652	4.7	0.39
20	2.163	1.545	8.13	10.68
40	1.772	0.143	6.23	0.62
80	2.361	0.242	9.28	1.49
120	2.558	0.103	10.56	0.72
220	3.063	0.080	14.83	0.89

Table III. $\epsilon' = 1$, Canonical Ensemble

N	$\chi\pi$	$\Delta\chi\pi$	ε	$\Delta\varepsilon$
5	0.376	0.039	2.20	0.20
10	0.202	0.063	1.50	0.20
20	0.602	0.301	4.02	17.78
40	0.925	0.199	25.53	—
80	0.783	0.041	8.23	1.81
120	0.803	0.017	9.19	0.91
220	0.880	0.010	15.72	1.49

Table IV. $\epsilon' = 0$, Canonical Ensemble

N	$\chi\pi$	$\Delta\chi\pi$	ε	$\Delta\varepsilon$
5	0.251	0.031	2.01	2.57
10	0.219	0.060	1.78	0.51
20	0.263	0.129	2.11	1.03
40	0.390	0.077	4.55	6.24
80	0.449	0.050	9.76	205.8
120	0.456	0.014	11.45	4.19
220	0.469	0.004	16.15	2.03

Table V. $\epsilon' = \infty$, Grand Ensemble

N	$\chi\pi$	$\Delta\chi\pi$	ε	$\Delta\varepsilon$	$\langle N; N \rangle$
5	0.628	0.062	2.26	0.12	3.52
10	0.981	0.149	2.96	0.30	5.66
20	1.726	0.182	4.45	0.36	9.65
40	2.904	0.221	6.81	0.44	12.94
80	3.885	0.299	8.77	0.60	16.75
120	5.004	0.261	11.01	0.52	22.85
220	7.589	0.228	16.18	0.45	31.62

Table VI. $\epsilon' = 10$, Grand Ensemble

N	$\chi\pi$	$\Delta\chi\pi$	ε	$\Delta\varepsilon$	$\langle N; N \rangle$
5	0.507	0.045	2.12	0.11	2.86
10	0.731	0.091	2.69	0.24	3.95
20	1.260	0.200	4.27	0.67	5.40
40	1.892	0.115	6.77	0.53	6.91
80	2.398	0.088	9.51	0.55	8.99
120	2.623	0.086	11.03	0.62	9.79
220	3.077	0.131	14.97	1.36	11.13

Table VII. $\epsilon' = 1$, Grand Ensemble

N	$\chi\pi$	$\Delta\chi\pi$	ε	$\Delta\varepsilon$	$\langle N; N \rangle$
5	0.363	0.050	2.14	0.25	1.63
10	0.470	0.114	2.78	0.85	1.96
20	0.556	0.146	3.51	1.66	2.17
40	0.757	0.077	7.24	2.90	2.37
80	0.809	0.019	9.45	1.04	2.42
120	0.839	0.024	11.44	1.93	2.58
220	0.886	0.018	16.60	2.83	2.65

error bars are particularly high for canonical systems having 20–80 particles. This problem seems to be absent in the grand ensemble.

The polarization fluctuation displays two behaviors. At $\varepsilon' = \infty$ the fluctuations are roughly proportional to $\sqrt{N}$. For smaller ε' (for instance, $\varepsilon' = 10$), they saturate more or less quickly at the value predicted by electrostatics. This is in agreement with the Debye–Hückel approximation, which also predicted the two regimes with a crossover at $kR = (2\Gamma N)^{1/2} = \varepsilon'$.

The charge fluctuations $\langle N; N \rangle$ in the grand ensemble are roughly proportional to $\sqrt{N}$, i.e., to the surface for $\varepsilon' = \infty$, and much smaller for other values of ε'. Figures 2–7 and 11–13 show the radial density, the truncated radial pair distribution function (TRPDF), and the partial second moment of the TRPDF for different ensembles and ε'.

The partial second moment is defined as

$$\chi_{11;A}(r) = -\frac{\Gamma}{2}\int_0^r d^2r'\, r'^2 \bar{\rho}^T(|\mathbf{r}'|)$$

It shows the contribution to the total second moment $[=\chi_{11;A}(2R)]$ of pairs of particles with increasing separation.

Figures 2–4 show an OCP at $\varepsilon' = 0$ in the canonical ensemble. Since the number of particles is fixed ($N = 40$), the second moment is identical with the polarization fluctuations. There are no long-range correlations near the wall and the value of the polarization fluctuations is the bulk value $(1/2\pi)$.

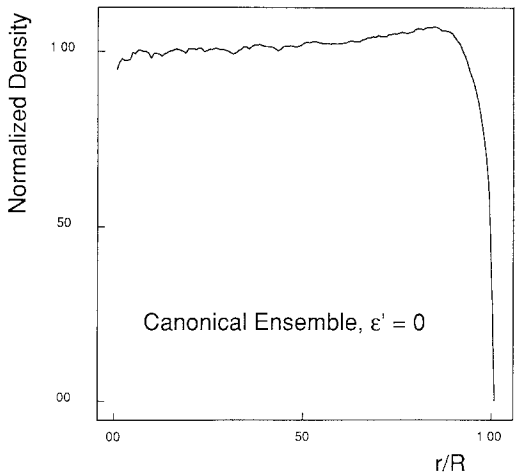

Fig. 2. Normalized density obtained by a canonical MC simulation with Neumann boundary conditions. The system is an OCP (40 particles) on a disk at $\Gamma = 0.5$.

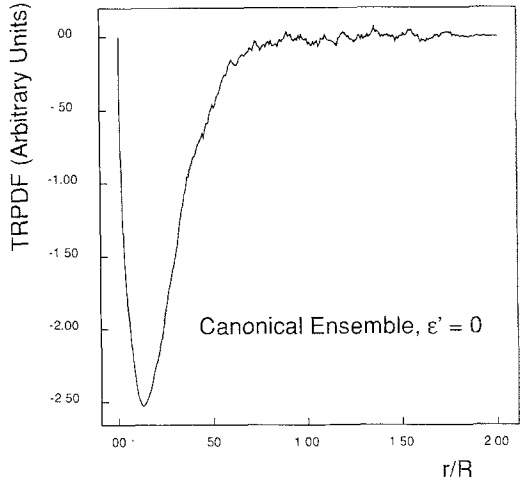

Fig. 3. Truncated radial pair distribution function (TRPDF) corresponding to the situation of Fig. 2.

Figures 5–7 show an OCP at $\varepsilon' = \infty$ in the canonical ensemble. The density profile reflects the attraction of the particles by their images on the other side of the wall. Figure 6 is particularly interesting, since it reveals the existence of a depression in the TRPDF for large separations between the particles. As shown in Appendix B, such a behavior can be reproduced with the DH approximation in the canonical limit. The behaviors we obtain for

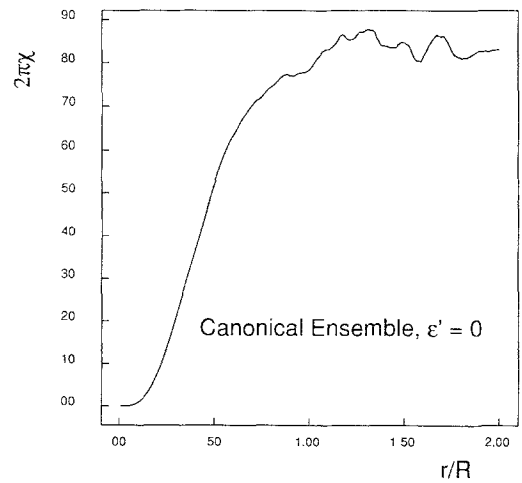

Fig. 4. Partial second moment obtained from the TRPDF of Fig. 3.

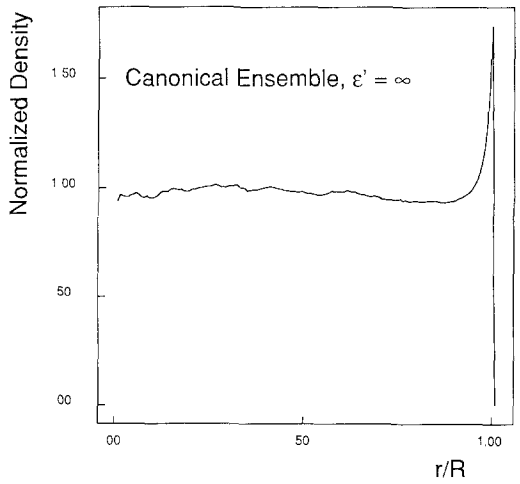

Fig. 5. Normalized density obtained by a canonical MC simulation with Dirichlet boundary conditions and for the system of Fig. 2.

the disk and for the sphere are respectively given in Figs. 8 and 9. Qualitatively, one can understand the behavior of the TRPDF by considering the sketch given in Fig. 10: For very small separations, the contribution to the TRPDF is essentially given by the bulk part. Now let us consider a point A close to the surface. For intermediate and large separations (say r), the TRPDF is made up only of surface contributions which are propor-

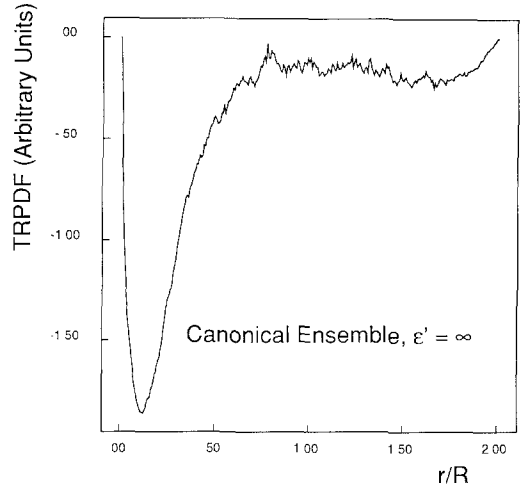

Fig. 6. TRPDF corresponding to the situation of Fig. 5.

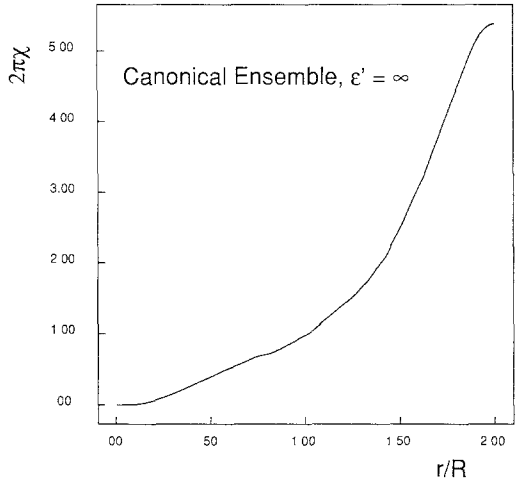

Fig. 7. Partial second moment obtained from the TRPDF of Fig. 6.

tional to the intersection of a circle (centered on A) of radius r with the surface layer. Thus, it can easily be understood that the TRPDF increases from $r \cong r_2$ up to a maximum near $r \cong r_1$ and then rapidly decays to zero.

Figures 11–13 show the same system in the grand ensemble. The pair correlation function now decays very quickly and there are no long-range surface correlations. The partial second moment does not converge exactly to $1/2\pi$, as predicted by the Stillinger–Lovett sum rule, but to a value

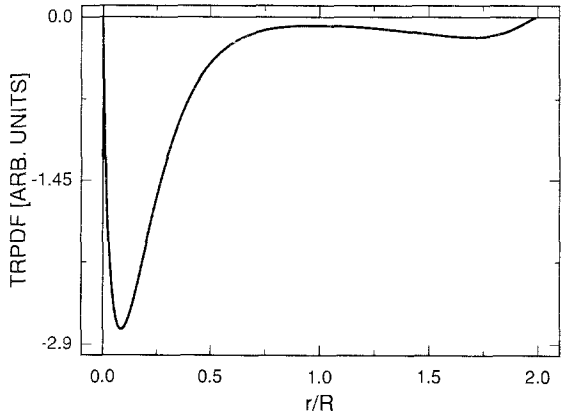

Fig. 8. The TRPDF for a disk in DH approximation and canonical limit at $Z = (2\Gamma N)^{1/2} = (2 \times 0.5 \times 40)^{1/2} \cong 6.36$.

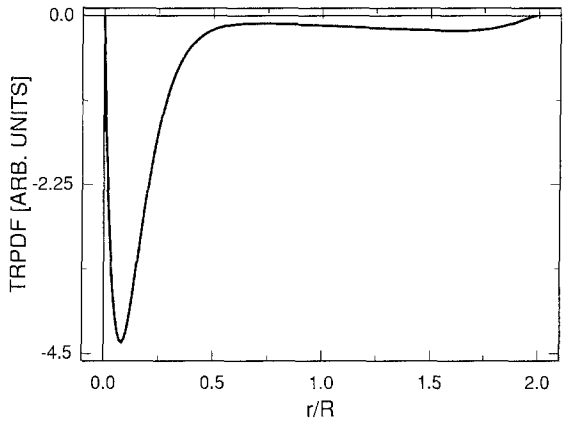

Fig. 9. TRPDF for a sphere in DH approximation and canonical limit at $Z = 12$.

which is substantially lower. This can be explained by the fact that the particles near the wall include in their screening cloud also "image charges" which are of course not counted in the second moment. The polarization fluctuation as the sum of the second moment and $\Delta\chi$, however, is much larger than $1/\pi$ and has about the same value as the polarization fluctuations (alone) in the canonical ensemble.

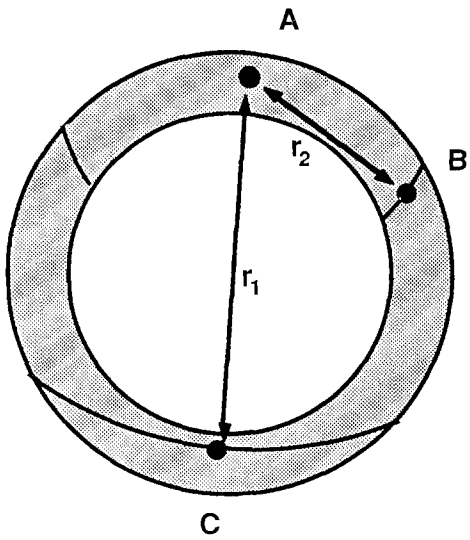

Fig. 10. Qualitative description of the depression of the TRPDF in the canonical ensemble and in Dirichlet boundary conditions

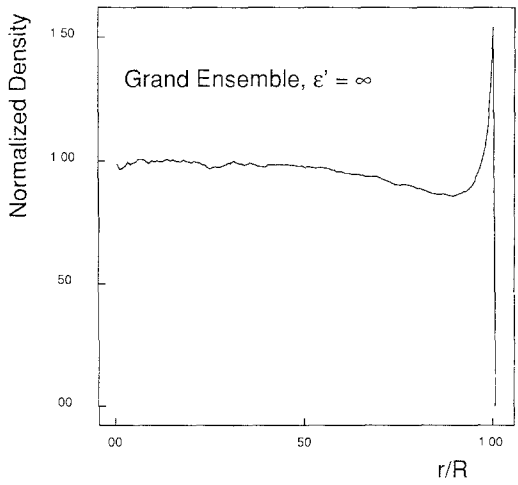

Fig. 11. Normalized density obtained by a grand canonical MC simulation with Dirichlet boundary conditions and for the system of Fig. 2.

8. ELLIPSE IN DH APPROXIMATION

Here we deal with the elliptic geometry and therefore we shall use elliptical coordinates τ and σ defined by

$$x = r\left(\frac{\pi}{|A|}\right)^{1/2} = \frac{1}{(\mathrm{sh}\,\tau_0\,\mathrm{ch}\,\tau_0)^{1/2}}\,(\mathrm{ch}\,\tau\cos\sigma;\ \mathrm{sh}\,\tau\sin\sigma) \tag{8.1}$$

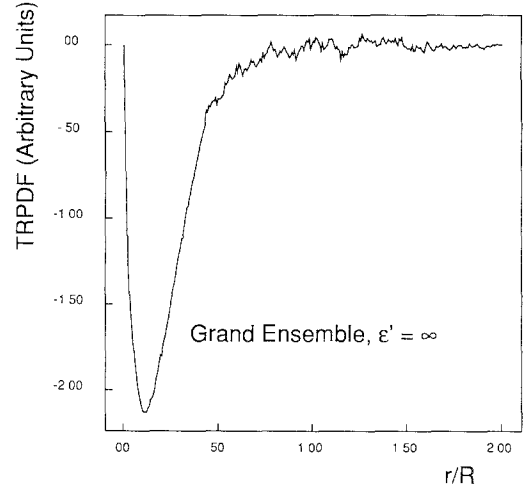

Fig. 12. TRPDF corresponding to the situation of Fig. 11.

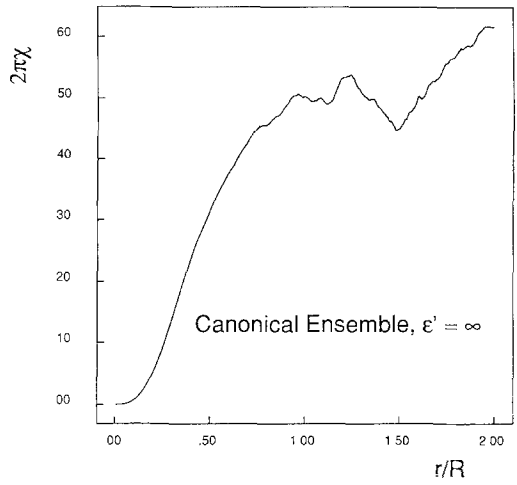

Fig. 13. Partial second moment obtained from the TRPDF of Fig. 12.

with $\tau \in [0, \infty]$ and $\sigma \in [0, 2\pi]$. Here $\tau = \tau_0$ defines the elliptical boundary of Λ. The ratio of the two axes of the ellipse is $b/a = \text{th}\, \tau_0$. In this section, all the distances are expressed in units of $(|\Lambda|/\pi)^{1/2}$. The length of an infinitesimal vector dx is given by

$$dx^2 = h^2(\tau, \sigma)(d\tau^2 + d\sigma^2); \qquad h(\tau, \sigma) = \left(\frac{\text{sh}^2\, \tau + \sin^2 \sigma}{\text{sh}\, \tau_0\, \text{ch}\, \tau_0}\right)^{1/2} \tag{8.2}$$

In the limit $\tau_0 \to \infty$, the ellipse becomes a circle and $h(\tau, \sigma) \underset{\tau \to \infty}{\approx} 1$.

We introduce the dimensionless parameter

$$q^2 = 2\pi\Gamma\rho\,|\Lambda|/\pi = 2\Gamma\rho\,|\Lambda| = \kappa^2\,|\Lambda|/\pi \tag{8.3}$$

In order to simplify the writing, $G^{\varepsilon'}_{\Lambda}(x, x_1)$ will be called $\varphi(x)$ in this part, where x and x_1 are, respectively, associated with (τ, σ) and (τ_1, σ_1). With the definitions

$$\begin{aligned} \lambda^{\text{in}}(\sigma) &= \lim_{\tau \to \tau_0^-} \varphi(\tau, \sigma) & \lambda^{\text{out}}(\sigma) &= \lim_{\tau \to \tau_0^+} \varphi(\tau, \sigma) \\ \mu^{\text{in}}(\sigma) &= \lim_{\tau \to \tau_0^-} \partial_\tau \varphi(\tau, \sigma) & \mu^{\text{out}}(\sigma) &= \lim_{\tau \to \tau_0^+} \partial_\tau \varphi(\tau, \sigma) \end{aligned} \tag{8.4}$$

the boundary conditions for $\varphi(x)$ are

$$\lambda^{\text{in}}(\sigma) = \lambda^{\text{out}}(\sigma) = \lambda(\sigma), \qquad \mu^{\text{in}}(\sigma) = \varepsilon' \mu^{\text{out}}(\sigma) \tag{8.5}$$

Whereas the disk can be solved exactly by using Bessel functions, Mathieu functions, which occur in the elliptic case, make the situation

much more difficult. Nevertheless, we are not concerned with the exact full solution, but only with the asymptotic behavior of $\varphi(x)$ far away from x_1. As q is very large compared to one, because the system is assumed to be macroscopic, we shall be able to solve approximately the problem in this limit.

We proceed in the following way. We first look for the relations between λ and μ outside and inside the boundary (the differential equations are of elliptic kind). Then, by using the continuity conditions [Eq. (8.5)], we obtain the three functions λ, μ^{in}, and μ^{out}. Finally, φ in A will result from Green's identity.

8.1. Outside the Ellipse

As $\varphi(x)$ is harmonic in this domain, we expand φ as a function of σ in a Fourier series:

$$\varphi(\tau, \sigma) = \sum_n \varphi_n(\tau)\, g_n(\sigma); \qquad g_n(\sigma) = \frac{1}{(2\pi)^{1/2}} e^{in\sigma} \tag{8.6}$$

Writing the Laplacian in the (τ, σ) coordinates, we deduce the following differential equation for the $\varphi_n(\tau)$:

$$\left(\frac{d^2}{d\tau^2} - n^2\right) \varphi_n(\tau) = 0 \tag{8.7}$$

For $n \neq 0$, the nondiverging solution in the limit $\tau \to \infty$ is

$$\varphi_n(\tau) = A_n e^{-|n|(\tau - \tau_0)}; \qquad \lambda_n = A_n; \qquad \mu_n^{\text{out}} = -|n| A^n \tag{8.8}$$

from which follows the expected relation between λ and μ^{out}:

$$\mu_n^{\text{out}} = -|n| \lambda_n; \qquad n \neq 0 \tag{8.9}$$

For $n = 0$, both solutions of Eq. (8.7) have to be kept

$$\varphi_0(\tau) = A_0(\tau - \tau^*); \qquad \lambda_0 = A_0(\tau_0 - \tau^*); \qquad \mu_0^{\text{out}} = A_0 \tag{8.10}$$

τ^* is the aforementioned arbitrary constant, which controls the total charge of the conductor. This leads to the relation

$$\mu_0^{\text{out}} = \frac{\lambda_0}{\tau_0 - \tau^*} \tag{8.11}$$

8.2. Inside the Ellipse

It is somewhat more complicated to get the relation between λ and μ^{in}. We start from Green's identity, which follows from Eqs. (3.2) and (3.3),

$$\varphi(x) = K_0(q|x - x_1|) + \frac{1}{2\pi}\oint [h(\tau_0, \sigma')\,\lambda(\sigma')\,q\cos\alpha K_1(qD) + \mu^{\text{in}}(\sigma')\,K_0(qD)]\,d\sigma' \quad (8.12)$$

where K_0 and K_1 are the modified Bessel functions of order 0 and 1, D is the distance between x and the integration point $x' = (\tau_0, \sigma')$, and α is the angle between the straight line xx' and the normal line to the ellipse at the point x' (cf. Fig. 14),

Let d be the shortest distance from x to the ellipse at the point P. Some care has to be taken in the limit $d \to 0$, because in that case D may vanish and this causes $K_1(qD)$ to diverge. In Appendix C we show the following limit for the integral I:

$$I = \frac{1}{2\pi}\oint d\sigma'\, h(\tau_0, \sigma')\,\lambda(\sigma')q\cos\alpha K_1(qD) \xrightarrow[d\to 0]{} \frac{1}{2}\lambda(\sigma) + \frac{1}{2\pi}\oint d\sigma'\, h(\tau_0, \sigma')\,\lambda(\sigma')q \lim_{d\to 0}\{\cos\alpha K_1(qD)\} \quad (8.13)$$

As $\varphi(x)$ tends to $\lambda(\sigma)$, we deduce for $d = 0$

$$\lambda(\sigma) = 2\lambda^{\infty}(\sigma) + \frac{1}{\pi}\oint [h(\tau_0, \sigma')\,\lambda(\sigma')q\cos\alpha K_1(qD) + \mu^{\text{in}}(\sigma')\,K_0(qD)]\,d\sigma' \quad (8.14)$$

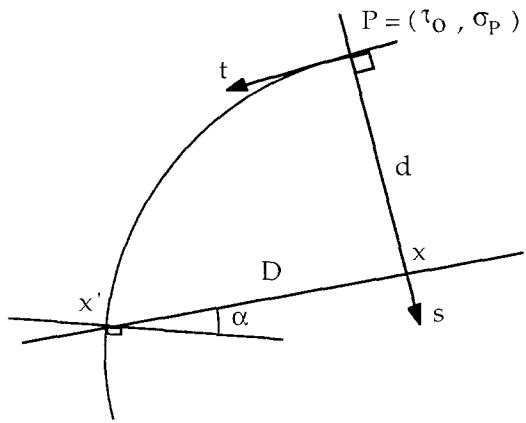

Fig. 14.

where $\lambda^{\infty}(\sigma)$ indicates the value of φ on the ellipse for the infinite DH problem

$$\lambda^{\infty}(\sigma) = K_0(q|x - x_1|) \qquad \text{for} \quad x = (\tau_0, \sigma) \tag{8.15}$$

In this form, the relation between λ and μ^{in} is not very useful. At this point we shall take into account that q is large compared to one. In this limit $q \gg 1$, the integrals with $K_0(qD)$ and $K_1(qD)$ can be expanded when the factors of these functions are slowly varying. So we shall get a relation between the low-frequency Fourier coefficients ($|n| \ll q$) of λ and μ^{in}. By using the expansions (C.12) and (C.15) of Appendix C, we are led to

$$\lambda_n = 2\lambda^{\infty}(\sigma) + \frac{1}{q}\left(\frac{\mu^{\text{in}}}{h}\right)_n + \frac{1}{q^2}\left(\frac{\lambda}{h^2}\right)_n + O\left(\frac{\mu^{\text{in}}}{q^3}; \frac{\lambda}{q^4}\right); \qquad |n| \ll q \tag{8.16}$$

The contribution of these coefficients to the sum of the Fourier series is

$$\lambda(\sigma) = 2\lambda^{\infty}(\sigma) + \frac{1}{q}\left(\frac{\mu^{\text{in}}(\sigma)}{h(\tau_0, \sigma)}\right) + \frac{1}{q^2}\left(\frac{\lambda(\sigma)}{h^2(\tau_0, \sigma)}\right) + \cdots; \qquad |n| \ll q \tag{8.17}$$

We have recalled $|n| \ll q$ in order to point out that the integrals in Eq. (8.14) are only accurately evaluated in the "low"-frequency limit.

8.3. Solution for λ and μ

It follows from Eq. (8.5), (8.9), and (8.11) that

$$\mu_n^{\text{in}} = -\varepsilon' |n| \lambda_n \quad (n \neq 0), \qquad \mu_{n=0}^{\text{in}} = \varepsilon' \frac{\lambda_0}{\tau_0 - \tau^*} \tag{8.18}$$

The leading term of λ_n is $2\lambda_n^{\infty}$ [Eq. (8.16)]. Then the leading term of μ_n^{in} is

$$\mu_n^{\text{in}} \cong -2\varepsilon' |n| \lambda_n^{\infty} \quad (n \neq 0, |n| \ll q); \qquad \mu_{n=0}^{\text{in}} \cong 2\varepsilon' \frac{\lambda_0^{\infty}}{\tau_0 - \tau^*} \tag{8.19}$$

For $\lambda(\sigma)$, we have to keep the second term of Eq. (8.17) because $\lambda^{\infty}(\sigma)$ is exponentially decreasing over a distance of the order of q^{-1},

$$\lambda(\sigma) \cong 2\lambda^{\infty}(\sigma) + \frac{1}{q}\left(\frac{\mu^{\text{in}}(\sigma)}{h(\tau_0, \sigma)}\right); \qquad |n| \ll q \tag{8.20}$$

Now it remains to calculate λ_n^{∞}, always for $|n| \ll q$. For that we use the expansion [Eq. (C.12)] based on the Appendix C,

$$\lambda_n^{\infty} = \oint d\sigma' \frac{e^{-in\sigma'}}{(2\pi)^{1/2}} K_0(qD_1) = g_n^*(\sigma_{1P}) \oint d\sigma' \frac{e^{-in(\sigma'-\sigma_{1P})}}{h(\tau_0, \sigma')} K_0(qD_1)$$

$$\cong \frac{\pi e^{-qd_1}}{qh_{1P}(1-d_1 h_{1P}^{-3})^{1/2}} g_n^*(\sigma_{1P}); \qquad |n| \ll q \tag{8.21}$$

where d_1 (cf. Fig. 15) is the distance from x_1 to the ellipse [at the point (τ_0, σ_{1P})] and h_{1P} is

$$h_{1P} = h(\tau_0, \sigma_{1P}) \tag{8.22}$$

The sum of the "low"-frequency contributions to $\mu^{\text{in}}(\sigma)$ is carried out with a convergence factor $e^{-\alpha|n|}$. The constant α is chosen according to

$$q^{-1} \ll \alpha \ll 1 \tag{8.23}$$

Taking into account

$$\sum_n |n| e^{in\theta - \alpha|n|} = \frac{\operatorname{ch}\alpha \cos\theta - 1}{(\operatorname{ch}\alpha - \cos\theta)^2} \underset{\substack{\alpha \ll 1 \\ \alpha \ll \theta}}{\cong} -\frac{1}{2\sin^2(\theta/2)} \tag{8.24}$$

we obtain $\mu^{\text{in}}(\sigma)$,

$$\mu^{\text{in}}(\sigma) \cong \left(\frac{\varepsilon'}{q}\right) \frac{e^{-qd_1}}{h_{1P}(1-d_1 h_{1P}^{-3})^{1/2}} \left\{\frac{1}{\tau_0 - \tau^*} + \frac{1}{2\sin^2((\sigma-\sigma_{1P})/2)}\right\}$$

$$(|n| \ll q, \ \alpha \ll |\sigma - \sigma_{1P}|) \tag{8.25}$$

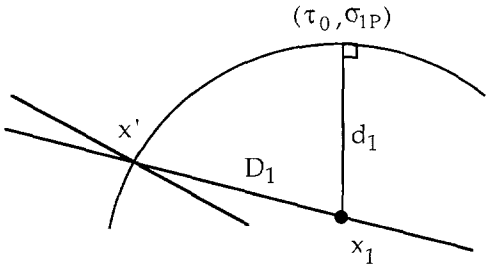

Fig. 15.

For $\lambda(\sigma)$, the first term of Eq. (8.20) is negligible ($q^{-1} \ll |\sigma - \sigma_{1P}|$) and then we have

$$\lambda(\sigma) \cong \left(\frac{\varepsilon'}{q^2 h(\tau_0, \sigma)}\right) \frac{e^{-qd_1}}{h_{1P}(1 - d_1 h_{1P}^{-3})^{1/2}} \left\{\frac{1}{\tau_0 - \tau^*} + \frac{1}{2\sin^2((\sigma - \sigma_{1P})/2)}\right\}$$
$$(|n| \ll q,\ \alpha \ll |\sigma - \sigma_{1P}|) \tag{8.26}$$

8.4. $\varphi(x)$ in the Ellipse

Since we know λ and μ^{in} on the boundary, it is not difficult to get φ inside the ellipse with the help of the Green's identity [Eq. (8.12)]. Assuming that $q|x - x_1| \gg 1$, we can neglect the first term. In the integrals with K_0 and K_1, the leading contributions come from the neighborhood of the point on the ellipse (τ_0, σ_P) which is nearest from x. As the functions λ and μ^{in} are slowly varying (compared to K_0 and K_1), the "high-q" expansions (C.12) and (C.15) can be used. It follows that

$$\varphi(x) = G_{\Lambda}^{\varepsilon'}(x, x_1)$$
$$\cong \left(\lambda(\sigma_P) + \frac{\mu^{\text{in}}(\sigma_P)}{qh_P}\right) \frac{e^{-qd}}{2(1 - dh_P^{-3})^{1/2}}$$
$$\cong \frac{\varepsilon' e^{-q(d+d_1)}}{q^2 h_P h_{1P}(1 - dh_P^{-3})^{1/2}(1 - dh_{1P}^{-3})^{1/2}} \left\{\frac{1}{\tau_0 - \tau^*} + \frac{1}{2\sin^2((\sigma_P - \sigma_{1P})/2)}\right\}$$
$$(|n| \ll q,\ \alpha \ll |\sigma_P - \sigma_{1P}|) \tag{8.27}$$

where d is the distance from x to the ellipse [at the point (τ_0, σ_P)] and h_P is

$$h_P = h(\tau_0, \sigma_P) \tag{8.28}$$

Equation (8.27) gives the leading term of $\varphi(x) = G_{\Lambda}^{\varepsilon'}(x, x_1)$ for $q \gg 1$. When $\tau_0 \to \infty$, the Green's function of the circular domain [Eq. (4.17)] is recovered because h_P and h_{1P} are then equal to 1, $\sigma_P - \sigma_{1P}$ becomes the angle between x and x_1, and the roots in the denominator represent unsizable corrective contributions. For finite τ_0, $G_{\Lambda}^{\varepsilon'}(x, x_1)$ also decreases exponentially in directions perpendicular to the boundary and exhibits long-range correlation along this boundary, with a new law which generalizes that of the circular case. The qualitative new effect is the dependence of $G_{\Lambda}^{\varepsilon'}(x, x_1)$ on the curvatures of the boundary near x and x_1, which comes from the factors h_P and h_{1P} in the denominator of Eq. (8.27). This results from a "needle effect" on the conductor, as been mentioned in introduction. It follows that the points $\tau = \tau_0$, $\sigma = 0$ and π are more

correlated than the points $\tau = \tau_0$, $\sigma = \pi/2$ and $3\pi/2$, although the distance is larger in the first case. An easy calculation shows that

$$\frac{G_{\Lambda}^{\varepsilon'}[(\tau_0; 0); (\tau_0; \pi)]}{G_{\Lambda}^{\varepsilon'}[(\tau_0; \pi/2); (\tau_0; 3\pi/2)]} = \frac{1}{\text{th}^2 \tau_0} = \frac{a^2}{b^2} > 1 \tag{8.29}$$

We also point out that this effect agrees with the results obtained in the case of the strip geometry,[20] where long-range correlations are only observed in the direction of the straight lines. Finally, the term $(\tau_0 - \tau^*)^{-1}$ in Eq. (8.27), where τ^* is an arbitrary constant, is the outcome of the total charge of the conductor in the meaning of classical electrostatics.

8.5. Dielectric Susceptibility

We start from the definition of the tensor $\chi_{\alpha\beta}$ and use the equation satisfied by $G_{\Lambda}^{\varepsilon'}(x, x_1)$ [Eqs. (3.2) and (3.3)] to transform one of the integrals over Λ to an integral over the boundary. It follows that

$$\chi_{\alpha\beta} = -\frac{q^2}{4\pi^3} \int_{\Lambda} dx_1 \, x_{1\beta} \oint d\sigma \, h(\tau_0, \sigma) \left[x_\alpha \frac{\mu^{\text{in}}(\sigma)}{h(\tau_0, \sigma)} - \hat{n}_\gamma \lambda(\sigma) \right] \tag{8.30}$$

where $\hat{n}$ is the unit vector perpendicular to the boundary at the point $x = (\tau_0, \sigma)$.

A straightforward calculation leads to

$$\chi_{1\beta} = -\frac{q^2}{4\pi^3} \int_{\Lambda} dx_1 \, x_{1\beta} (2\pi)^{1/2} \left[\frac{\text{Re}\, \mu_1^{\text{in}}}{(\text{th}\, \tau_0)^{1/2}} - (\text{th}\, \tau_0)^{1/2} \, \text{Re}\, \lambda_1 \right] \tag{8.31}$$

$$\chi_{2\beta} = -\frac{q^2}{4\pi^3} \int_{\Lambda} dx_1 \, x_{1\beta} (2\pi)^{1/2} \left[-(\text{th}\, \tau_0)^{1/2} \, \text{Im}\, \mu_1^{\text{in}} + \frac{1}{(\text{th}\, \tau_0)^{1/2}} \, \text{Im}\, \lambda_1 \right] \tag{8.32}$$

In the limit $q \gg 1$, we take for μ_1^{in} and λ_1 [Eqs. (8.19) and (8.20)]

$$\mu_1^{\text{in}} = -2\varepsilon' \lambda_1^{\infty}; \qquad \lambda_1 = 2\lambda_1^{\infty} \tag{8.33}$$

with λ_1^{∞} given by Eq. (8.21). The integration over x_1 is performed by integrating first over d_1 from zero to infinity and then over σ_{1P} from 0 to 2π. This approximation is valid for $q \gg 1$ because of the factor e^{-qd_1}. More precisely, we have for a function $f(\tau, \sigma)$ which does not depend on q

$$\int_{\Lambda} dx_1 \, f(\tau_1, \sigma_1) e^{-qd_1} \underset{q \gg 1}{\cong} \frac{1}{q} \oint d\sigma_{1P} \, h(\tau_0, \sigma_{1P}) f(\tau_0, \sigma_{1P}) \tag{8.34}$$

We are then led to

$$\lim_{q\to 0} \chi_{12} = \lim_{q\to 0} \chi_{21} = 0$$

$$\lim_{q\to 0} \chi_{11} = \frac{1}{2\pi}\left(\frac{\varepsilon'}{\text{th}\,\tau_0} + 1\right) \tag{8.35}$$

$$\lim_{q\to 0} \chi_{22} = \frac{1}{2\pi}(\varepsilon' \,\text{th}\,\tau_0 + 1)$$

This result agrees with the dielectric susceptibility of an ellipse in classical electrostatics (cf. II). Therefore, the DH approximation is able to recover the values given by electrostatics as for the other geometries.

9. GENERAL FORMULATION FOR THE SOLUTION OF THE DEBYE–HÜCKEL KERNEL NEAR THE SURFACE

The potential created by a point charge in a weakly coupled plasma obeys in the DH approximation the differential equation

$$\begin{aligned} -\Delta_{\mathbf{r}_2} G_\Lambda(\mathbf{r}_1, \mathbf{r}_2) &= s_v\, \delta(\mathbf{r}_1 - \mathbf{r}_2) - s_v \Gamma \rho G_\Lambda(\mathbf{r}_1, \mathbf{r}_2) \\ &= s_v\, \delta(\mathbf{r}_1 - \mathbf{r}_2) - \kappa^2 G_\Lambda(\mathbf{r}_1, \mathbf{r}_2); \qquad \mathbf{r}_2 \in \Lambda \\ &= 0; \qquad\qquad\qquad\qquad\qquad\quad \mathbf{r}_2 \notin \Lambda \end{aligned}$$

We are interested in the case where a charged particle and the point of the measurement of the potential are close to the surface. One can write $\mathbf{r}_1 = \hat{\mathbf{r}}_1 - s_1 \mathbf{n}_1$ and $\mathbf{r}_2 = \hat{\mathbf{r}}_2 - s_2 \mathbf{n}_2$, where $\hat{\mathbf{r}}$ is located on the surface and $\mathbf{n}$ is a unit vector perpendicular to the surface at the point $\hat{\mathbf{r}}$ (cf. Fig. 16). If the

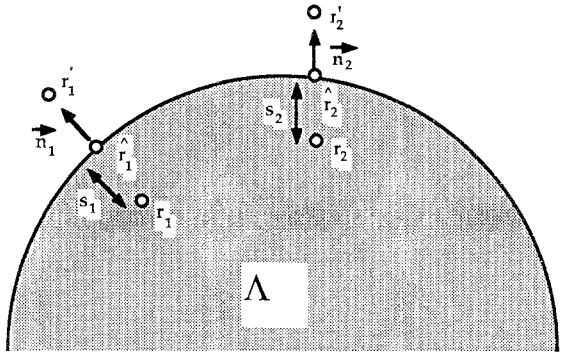

Fig. 16.

two points are widely separated, the potential $G_A(\mathbf{r}_1, \mathbf{r}_2)$ can only "propagate" through the vacuum outside the system because the screening property of the plasma leads to an exponential decay of the potential inside the system. Let us consider the potential created by a source at $\mathbf{r}_1$ and evaluated at the point $\mathbf{r}_2$ far away from $\mathbf{r}_1$. The variations of this potential along the surface in the vacuum are much smaller than the variations perpendicular to the surface in the plasma and we can neglect them locally in a first approximation. We can therefore assumed that, for sufficiently smooth surfaces (i.e., curvatures larger than a Debye length), the potential in the neighborhood of the point $\mathbf{r}_2$ is a function of the distance to the boundary only

$$G_A(\mathbf{r}_1, \mathbf{r}_2) \approx G_A(\mathbf{r}_1, \hat{\mathbf{r}}_2, s_2); \qquad \kappa s_2 \lesssim 1$$

and

$$-\Delta_{\mathbf{r}_2} G_A(\mathbf{r}_1, \mathbf{r}_2) \approx -\frac{d^2}{ds_2^2} G_A(\mathbf{r}_1, \hat{\mathbf{r}}_2, s_2) = -\kappa^2 G_A(\mathbf{r}_1, \hat{\mathbf{r}}_2, s_2)$$

This immediately leads to the well-known exponential decay in the plasma

$$G_A(\mathbf{r}_1, \mathbf{r}_2) = G_A(\mathbf{r}_1, \hat{\mathbf{r}}_2) e^{-\kappa s_2}$$

For the next step we have to use the property that the kernel is symmetric, i.e., that the potential $G_A(\mathbf{r}_1, \mathbf{r}_2)$ at the point $\mathbf{r}_2$ produced by the point charge at $\mathbf{r}_1$ is the same as the potential at the point $\mathbf{r}_1$ produced by the point charge at $\mathbf{r}_2$. It follows that

$$G_A(\mathbf{r}_1, \mathbf{r}_2) = G_A(\hat{\mathbf{r}}_1, \mathbf{r}_2) e^{-\kappa s_1} = G_A(\hat{\mathbf{r}}_1, \hat{\mathbf{r}}_2) e^{-\kappa(s_1 + s_2)} \tag{9.1}$$

The obvious advantage of this "assumption" is that we can simplify the problem in the sense that we now only need to compute the kernel with both arguments *on* the boundary. In the next step we define a kernel $G_{\text{ext}}(\mathbf{r}_1', \mathbf{r}_2')$ that corresponds to a potential produced by a unit charge *outside* the system and evaluated at a point *outside* the system. This potential satisfies

$$-\Delta G_{\text{ext}}(\mathbf{r}_1', \mathbf{r}_2') = s_v \, \delta(\mathbf{r}_1' - \mathbf{r}_2')$$

and, because it takes into account the presence of the plasma, matches at the boundary with $G_A(\mathbf{r}_1, \mathbf{r}_2)$. This means that the value of the kernel as well as the normal derivative with respect to one or to two arguments must be the same as for $G_A(\mathbf{r}_1, \mathbf{r}_2)$ if $\mathbf{r}_1 = \mathbf{r}_1' = \hat{\mathbf{r}}_1$ and $\mathbf{r}_2 = \mathbf{r}_2' = \hat{\mathbf{r}}_2$:

$$G_{\text{ext}}(\hat{\mathbf{r}}_1, \hat{\mathbf{r}}_2) = G_A(\hat{\mathbf{r}}_1, \hat{\mathbf{r}}_2) \tag{9.2}$$

$$\left.\frac{dG_{\text{ext}}(\hat{\mathbf{r}}_1 + s_1\mathbf{n}, \hat{\mathbf{r}}_2)}{ds_1}\right|_{s_1=0} = -\left.\frac{dG_A(\hat{\mathbf{r}}_1 - s_1\mathbf{n}, \hat{\mathbf{r}}_2)}{ds_1}\right|_{s_1=0} \tag{9.3}$$

$$\left.\frac{d^2G_{\text{ext}}(\hat{\mathbf{r}}_1 + s_1\mathbf{n}, \hat{\mathbf{r}}_2 + s_2\mathbf{n})}{ds_1\, ds_2}\right|_{s_1=s_2=0} = \left.\frac{d^2G_A(\hat{\mathbf{r}}_1 - s_1\mathbf{n}, \hat{\mathbf{r}}_2 - s_2\mathbf{n})}{ds_1\, ds_2}\right|_{s_1=s_2=0} \tag{9.4}$$

To proceed with the development of the kernel outside the plasma, we note that in the limit of $\kappa \to \infty$, the plasma can be assimilated to a perfect conductor with a dielectric constant $\varepsilon = \infty$. The matching conditions for G_{ext} at the interface are transformed into simple Dirichlet boundary conditions and $G_{\text{ext}}(\mathbf{r}_1', \mathbf{r}_2')$ can be replaced by $G_A^D(\mathbf{r}_1', \mathbf{r}_2')$. In order to relate the kernel inside the system to the (known) Dirichlet kernel outside the system, we use one of Eqs. (9.2)–(9.4), assuming that we can replace in the expressions G_{ext} by G_A^D even for finite κ. We note that Eqs. (9.2) and (9.3) are useless because the Dirichlet kernel and even the gradient with respect to one argument is identically zero if both arguments are on the boundary. There remains the bigradient of Eq. (9.4), which takes a finite value and which we will use for the evaluation of G_A. We must (and can) assume that the (perpendicular) field near a conductor is not much altered if the conductor is not perfect in the sense that the potential does not exactly vanish on the boundary ($\kappa = \infty$) but can penetrate in a finite but small layer inside the conductor (κ large).

Using Eq. (9.1), we have a relation between the bigradient of G_A and G_A itself;

$$\left.\frac{d^2G_A(\hat{\mathbf{r}}_1 - s_1\mathbf{n}, \hat{\mathbf{r}}_2 - s_2\mathbf{n})}{ds_1\, ds_2}\right|_{s_1=s_2=0} = \kappa^2 G_A(\hat{\mathbf{r}}_1, \hat{\mathbf{r}}_2)$$

and we can write

$$G_A(\hat{\mathbf{r}}_1, \hat{\mathbf{r}}_2) = \frac{1}{\kappa^2}\left.\frac{d^2G_A^D(\hat{\mathbf{r}}_1 + s_1\mathbf{n}, \hat{\mathbf{r}}_2 + s_2\mathbf{n})}{ds_1\, ds_2}\right|_{s_1=s_2=0}$$

The final solution valid at any point close to the surface and at large separation is

$$G_A(\mathbf{r}_1, \mathbf{r}_2) = (\mathbf{n}_1\nabla_{\hat{\mathbf{r}}_1})(\mathbf{n}_2\nabla_{\hat{\mathbf{r}}_2})\, G_A^D(\hat{\mathbf{r}}_1, \hat{\mathbf{r}}_2)\frac{1}{\kappa^2}e^{-\kappa(s_1+s_2)} \tag{9.5}$$

This equation is proved for the disk in Appendix D. The advantage of this formulation is that the problem of solving the long-range surface part of the Debye–Hückel kernel amounts to finding the kernel outside the system which satisfies the Dirichlet boundary conditions. Although not trivial in complicated geometry, it is nevertheless easier than the original

problem, as we show hereafter. We should point out that the asymptotic behavior of the surface correlation functions of the disk, the sphere, and the ellipse established in the previous sections are recovered in the following examples.

9.1. The Disk

The kernel of the Poisson equation satisfying the Dirichlet boundary conditions is most easily constructed with the method of images.[21,22] If a is the radius of the disk, r_1 and r_2 the distances from the center of the disk, and ϕ the angle between $\mathbf{r}_1$ and $\mathbf{r}_2$, the kernel is written

$$G^D_{\text{disk}}(r_1, r_2, \phi) = \frac{1}{2}\left\{\log\left[\left(\frac{r_2}{a}\right)^2 + \left(\frac{a}{r_1}\right)^2 - 2\frac{r_2}{r_1}\cos\phi\right] - \log\left[1 + \left(\frac{r_2}{r_1}\right)^2 - 2\frac{r_2}{r_1}\cos\phi\right]\right\} \tag{9.6}$$

The image charge, as can easily been seen from the kernel, is put at a distance a^2/r_1.

The first derivative with respect to r_2 and evaluated on the surface corresponds to the induced surface charge density at the point $\mathbf{r}_2$ by a unit charge at the point $\mathbf{r}_1$:

$$\sigma(r_2 = a, \phi) = -\frac{1}{2\pi}\frac{d}{dr_2} G^D_{\text{disk}}(r_1, r_2, \phi)\Big|_{r_2 = a} = -\frac{1}{2\pi a}\left(\frac{1 - (a/r_1)^2}{1 + (a/r_1)^2 - 2(a/r_1)\cos\phi}\right) \tag{9.7}$$

The derivative of $G^D_{\text{disk}}(r_1, r_2, \phi)$ with respect to both arguments and evaluated on the surface is

$$\frac{d^2}{dr_1\, dr_2} G^D_{\text{disk}}(r_1, r_2, \phi)\Big|_{r_1 = r_2 = a} = \frac{1}{2a^2 \sin^2(\phi/2)}$$

The surface Debye–Hückel kernel is therefore given by

$$G_{\text{disk}}(r_1, r_2, \phi) = \frac{1}{2a^2 \sin^2(\phi/2)}\frac{1}{\kappa^2} e^{-\kappa(s_1 + s_2)} \tag{9.8}$$

where s is again the distance between a point and the surface.

It is worth noting that the integral of the charge density $\sigma(r_1, r_2 = a, \phi)$ over ϕ is exactly -1 for any $\mathbf{r}_1$. A point charge is therefore always compensated by opposite surface charges on a grounded conductor. The situation is similar in the case of the Debye–Hückel approximation, but not exactly the same.

If the source is located at a distance αR ($\alpha > 1$) from the center of the disk, one can show that charge compensation occurs if (a) at fixed R, $\kappa \to \infty$ and the scale length of the Coulomb logarithmic potential $L \to \infty$ or $L \to 0$, (b) at fixed κ and L, $R \to \infty$.

9.2. The Sphere

As in the case of the disk in two dimensions, the Dirichlet kernel is constructed by putting an image with the charge $q' = -qa/r_1$ at a distance $r' = a^2/r_1$ from the center,

$$G^D_{\text{disk}}(r_1, r_2, \phi) = \frac{1}{(r_1^2 + r_2^2 - 2r_1 r_2 \cos\phi)^{1/2}} - \frac{a}{r_1[r_2^2 + (a^2/r_1)^2 - 2r_2(a^2/r_1)\cos\phi]^{1/2}} \tag{9.9}$$

The surface charge $\sigma(r_2 = a, \phi)$ is given by

$$\sigma(r_2 = a, \phi) = -\frac{1}{4\pi}\frac{d}{dr_2} G^D_{\text{sphere}}(r_1, r_2, \phi)\Big|_{r_2 = a} = -\frac{1}{4\pi}\frac{1}{a^2}\left(\frac{a}{r_1}\right)\frac{(1 - a^2/r_1^2)}{[1 + a^2/r_1^2 - 2(a/r_1)\cos\phi]^{3/2}} \tag{9.10}$$

The integral of the surface charge density is not equal to -1, but $-a/r_1$, which is the value of the image charge. The second derivative is

$$\frac{d^2}{dr_1\, dr_2} G^D_{\text{sphere}}(r_1, r_2, \phi)\Big|_{r_1 = r_2 = a} = \frac{1}{4a^3 \sin^3(\phi/2)}$$

and the surface Debye–Hückel kernel is

$$G_{\text{sphere}}(r_1, r_2, \phi) = \frac{1}{4a^3 \sin^3(\phi/2)}\frac{1}{\kappa^2} e^{-\kappa(s_1 + s_2)} \tag{9.11}$$

9.3. The Ellipse

The Green's kernel in elliptic coordinates is given by (ref. 21, p. 1202)

$$G_1(\mu, \theta, \mu_0, \theta_0) = -\left(\mu_0 + \log\frac{a}{4}\right) + \frac{1}{2}\sum_{n=1}^{\infty}\frac{4}{n} e^{-n\mu_0}[\cosh(n\mu)\cos(n\theta)\cos(n\theta_0) + \sinh(n\mu)\sin(n\theta)\sin(n\theta_0)]; \qquad \mu < \mu_0 \tag{9.12}$$

where the relation $z = x + iy = \frac{1}{2}a\cosh(\mu + i\theta)$ defines the mapping from Cartesian to elliptic coordinates.

One can easily see that the kernel diverges if $\mu = \mu_0$ because the product $\cosh(n\mu)e^{-n\mu_0}$ goes to 1 as n increases. For the construction of the Dirichlet kernel we must subtract a function $G_2(\mu, \theta, \mu_0, \theta_0)$, which contains terms with respectively $\cos(n\theta)e^{-n\mu}$ and $\sin(n\theta)e^{-n\mu}$ because the singularities at $\mu = \mu_0$ are avoided and the function has an acceptable asymptotic behavior at large μ. On the boundary of the elliptic domain ($\mu = b$), one has the matching condition

$$\begin{aligned} \cosh(n\mu)e^{-n\mu_0} &= e^{-n\mu} f_1(\mu_0) \\ \sinh(n\mu)e^{-n\mu_0} &= e^{-n\mu} f_2(\mu_0) \end{aligned} \tag{9.13}$$

which defines the amplitudes in G_1

$$f_1(\mu_0) = e^{-n\mu_0}\cosh(nb)e^{nb}$$

$$f_2(\mu_0) = e^{-n\mu_0}\sinh(nb)e^{nb}$$

The complete Dirichlet kernel is

$$\begin{aligned} &G^D_{\text{ell}}(\mu, \theta, \mu_0, \theta_0) \\ &\quad = \frac{1}{2}\sum_{n=1}^{\infty}\frac{4}{n}\{\cos(n\theta)\cos(n\theta_0)\,[e^{-n\mu_0}\cosh(n\mu) \\ &\qquad - e^{-n\mu}e^{-n\mu_0}\cosh(nb)\,e^{nb}] \\ &\qquad + \sin(n\theta)\sin(n\theta_0)\,[e^{-n\mu_0}\sinh(n\mu) \\ &\qquad - e^{-n\mu}e^{-n\mu_0}\sinh(nb)\,e^{nb}]\} \end{aligned} \tag{9.14}$$

The first derivative evaluated at $\mu = b$ is

$$\begin{aligned} &\frac{d}{d\mu}G^D_{\text{ell}}(\mu, \theta, \mu_0, \theta_0)\bigg|_{\mu=b} \\ &\quad = \frac{1}{2}\sum_{n=1}^{\infty}\{4\cos(n\theta)\cos(n\theta_0)\,[e^{-n\mu_0}\sinh(nb) + e^{-n\mu_0}\cosh(nb)] \\ &\qquad + 4\sin(n\theta)\sin(n\theta_0)[e^{-n\mu_0}\cosh(nb) + e^{-n\mu_0}\sinh(nb)]\} \end{aligned}$$

The second derivative is

$$\frac{d^2}{d\mu\, d\mu_0} G^D_{\text{ell}}(\mu, \theta, \mu_0, \theta_0)\bigg|_{\mu=\mu_0=b}$$

$$= \frac{1}{2} \sum_{n=1}^{\infty} \{4\cos(n\theta)\cos(n\theta_0)(-n) + 4\sin(n\theta)\sin(n\theta_0)(-n)\}$$

$$= -2 \sum_{n=1}^{\infty} n \cos n(\theta - \theta_0) = \frac{1}{2\sin^2((\theta-\theta_0)/2)}$$

To complete the demonstration, we have to take into account that the component of the gradient that is perpendicular to the surface, i.e., parallel to $\mathbf{e}_\mu$, is given by the relation

$$\mathbf{n}\nabla G^D_{\text{ell}} = \frac{1}{h_\mu} \frac{dG^D_{\text{ell}}}{d\mu}$$

where $h_\mu(\mu, \theta) = \frac{1}{2}a(\sinh^2\mu + \sin^2\theta)^{1/2}$.

The surface Debye–Hückel kernel now reads

$$G_{\text{ell}}(\mu, \theta, \mu_0, \theta_0) = \frac{1}{h_\mu(b, \theta)\, h_\mu(b, \theta_0)} \frac{1}{2\sin^2((\theta-\theta_0)/2)} \frac{1}{\kappa^2} e^{-\kappa(s_0+s)} \tag{9.15}$$

9.4. The Cylinder

The kernel of the Coulomb potential in cylindrical coordinates is given by (ref. 22, p. 118)

$$\frac{1}{|x-x'|} = \frac{2}{\pi} \sum_{m=-\infty}^{\infty} \int_0^\infty dk\, e^{im(\phi-\phi')} \cos k(z-z')\, I_m(k\rho_<)\, K_m(k\rho_>) \tag{9.16}$$

In order to generate Dirichlet boundary conditions, one has to subtract a potential G_2 which is homogeneous outside the cylinder, which decays to zero at large distances, and which takes the same value as the Coulomb kernel on the surface $\rho = R$:

$$G_2(x; x') = \frac{2}{\pi} \sum_{m=-\infty}^{\infty} \int_0^\infty dk\, e^{im(\phi-\phi')} \cos k(z-z')\, A_m K_m(k\rho)\, K_m(\kappa\rho')$$

with

$$A_m = I_m(kR)/K_m(kR)$$

Therefore the Dirichlet kernel is

$$G^D(\rho;\phi;\rho';\phi') = \frac{2}{\pi}\sum_{m=-\infty}^{\infty}\int_0^{\infty} dk\, e^{im(\phi-\phi')}\cos k(z-z') \times\left\{I_m(k\rho_<)\,K_m(k\rho_>) - \frac{I_m(kR)}{K_m(kR)}K_m(k\rho)\,K_m(k\rho')\right\}$$

The first derivative evaluated at $\rho = R$ is

$$\left.\frac{d}{d\rho}G^D(\rho;\phi;\rho';\phi')\right|_{\rho=R} = \frac{2}{\pi}\sum_{m=-\infty}^{\infty}\int_0^{\infty} dk\, e^{im(\phi-\phi')}\cos k(z-z') \times k\left\{I'_m(kR)\,K_m(k\rho') - \frac{I_m(kR)}{K_m(kR)}K'_m(kR)\,K_m(k\rho')\right\} \tag{9.17}$$

It is interesting to note that the integral of the charge density given by

$$\sigma(R;\phi;\rho';\phi') = -\frac{1}{4\pi}\left.\frac{d}{d\rho}G(\rho;\phi;\rho';\phi')\right|_{\rho=R}$$

exactly compensates the external charge for any ρ'. Indeed, if one substitutes the asymptotic behavior of the Bessel functions for small k in the term with $m = 0$ in the bracket of Eq. (9.17), the value in the bracket multiplied with k is 1 in the limit of $k \to 0$.

The second derivative is

$$\left.\frac{d^2}{d\rho\,d\rho'}G^D(\rho;\phi;\rho';\phi';z-z')\right|_{\rho=\rho'=R} = \frac{2}{\pi}\sum_{m=-\infty}^{\infty}\int_0^{\infty} dk\, e^{im(\phi-\phi')}\cos k(z-z') \times k^2\left\{I'_m(kR)\,K'_m(kR) - \frac{I_m(kR)}{K_m(kR)}K'_m(kR)\,K'_m(kR)\right\}$$

which, by using the Wronskian $W\{I_\nu(z);\,K_\nu(z)\} = -1/z$, can be simplified to

$$= \frac{2}{\pi}\sum_{m=-\infty}^{\infty}\int_0^{\infty} dk\, e^{im(\phi-\phi')}\cos k(z-z')\,\frac{k}{R}\,\frac{K'_m(kR)}{K_m(kR)} \tag{9.18}$$

We analyze the term with $m=0$ in the bracket by using the following asymptotic behaviors for small k: $K_0(kR) \approx -\log(kR)$ and $K_0'(kR) \approx -(kR)^{-1}$. It follows that Eq. (9.18) presents a singularity $\propto 1/\log(k)$. This means that the function $G(z-z')$ behaves like $1/[|z-z'| \log^2(R^{-1}|z-z'|)]$ for large $|z-z'|$.[9]

9.5. The Wedge in Three Dimensions

We first derive the Dirichlet kernel for a wedge with an opening angle θ. The Poisson equation in cylindrical coordinates is given by

$$\nabla_x^2 G(x=(\rho, \phi, z); x'=(\rho'; \phi'; z')) = \frac{\partial^2}{\partial \rho^2} G + \frac{1}{\rho}\frac{\partial G}{\partial \rho} + \frac{1}{\rho^2}\frac{\partial^2}{\partial \phi^2} G + \frac{\partial^2}{\partial z^2} G$$

$$= -\frac{4\pi}{\rho} \delta(\rho-\rho')\,\delta(\phi-\phi')\,\delta(z-z')$$

One can write the solution as a linear combination of products of functions $R_\nu(\rho, \rho')$, $Q_m(\phi, \phi')$, and $Z_k(z-z')$, the last two functions being solutions of the equations

$$\frac{d^2}{d\phi^2} Q_m + \nu_m^2 Q_m = 0$$

and

$$\frac{d^2}{dz^2} Z_k + k^2 Z_k = 0$$

Since we impose Dirichlet boundary conditions on $\phi=0$ and $\phi=\theta$, a natural choice for Q_m is

$$Q_m(\phi, \phi') = \frac{2}{\theta} \sin\left(\frac{m\pi\phi}{\theta}\right) \sin\left(\frac{m\pi\phi'}{\theta}\right)$$

The adequate solution for Z_k is

$$Z_k = \frac{1}{2\pi} e^{ik(z-z')}$$

We may write the Dirichlet kernel in the following way and determine the unknown function g_m with the help of the Poisson equation:

$$G(x, x') = \frac{1}{2\pi}\frac{2}{\theta}\sum_{m=1}^{\infty} \sin\left(\frac{m\pi\phi}{\theta}\right)\sin\left(\frac{m\pi\phi'}{\theta}\right)\int_{-\infty}^{\infty} dk\, e^{ik(z-z')}\, g_m(\rho, \rho', k)$$

$$\Delta G(x, x') = \frac{1}{2\pi}\frac{2}{\theta}\sum_{m=1}^{\infty} \sin\left(\frac{m\pi\phi}{\theta}\right)\sin\left(\frac{m\pi\phi'}{\theta}\right)\int_{-\infty}^{+\infty} dk\, e^{ik(z-z')}$$
$$\times\left\{g_m(\rho, \rho', k)\left[-\frac{(m\pi/\theta)^2}{\rho^2} - k^2\right] + \frac{d^2}{d\rho^2} g_m(\rho, \rho', k)\right.$$
$$\left. + \frac{1}{\rho}\frac{d}{d\rho} g_m(\rho, \rho', k)\right\}$$

The term in $\{\cdot\}$ must vanish if $\rho \neq \rho'$ and it must be $-(4\pi/\rho)\,\delta(\rho-\rho')$ for $\rho = \rho'$. The solutions of a differential equation of the type $g'' + (1/\rho)\,g' - (\nu^2/\rho^2 + k^2)\,g = 0$ are the modified Bessel functions $K_\nu(k\rho)$ and $I_\nu(k\rho)$. The solution, which depends on the arguments ρ and ρ' and which has a discontinuity of $-4\pi/\rho'$ in the first derivative at $\rho = \rho'$, is given by $g_m(\rho, \rho', k) = 4\pi I_\nu(k\rho_<)\, K_\nu(k\rho_>)$, where $\nu = m\pi/\theta$, $\rho_< = \min(\rho, \rho')$, and $\rho_> = \max(\rho, \rho')$. The Dirichlet kernel now reads

$$G(x, x') = \frac{8}{\theta}\sum_{m=1}^{\infty}\int_0^{\infty} dk \cos[k(z-z')]$$
$$\times \sin\left(\frac{m\pi\phi}{\theta}\right)\sin\left(\frac{m\pi\phi'}{\theta}\right) I_{m\pi/\theta}(k\rho_<)\, K_{m\pi/\theta}(k\rho_>) \quad (9.19)$$

The second derivative which one needs for the surface correlations is

$$\frac{d^2}{d\phi\, d\phi'} G^D(\rho, \phi, z, \rho', \phi', z')\Big|_{\phi=\phi'=0}$$
$$= \frac{8\pi^2}{\theta^3}\int_0^{\infty} dk \cos[k(z-z')]$$
$$\times \sum_{m=1}^{\infty} m^2 I_{m\pi/\theta}(k\rho_<)\, K_{m\pi/\theta}(k\rho_>) \quad (9.20)$$

Using the integral representation (ref. 10, p. 140)

$$I_\nu(u)\, K_\nu(v) = \frac{1}{2}\int_{\log(v/u)}^{\infty} J_0([4uv\sinh^2(t/2) - (u-v)^2]^{1/2}) e^{-\nu t}\, dt$$
$$(u > 0,\ v > 0,\ \mathrm{Re}(\nu) > -1/4)$$

and introducing the symbols F for the second derivative, x for $\rho_<$, y for $\rho_>$, α for π/θ, and z for $|z-z'|$, we obtain

$$F=\frac{4\alpha^2}{\theta}\int_0^\infty dk\cos(kz)\int_{\log(y/x)}^\infty J_0(k[4xy\sinh^2(t/2)-(x-y)^2]^{1/2})$$
$$\times\left\{\sum_{m=1}^\infty m^2 e^{-m\alpha t}\right\}dt$$

The series in the curly brackets can be summed up and after interchange of the integration we obtain

$$F=\frac{\alpha^2}{\theta}\int_{\log(y/x)}^\infty dt\frac{\cosh(\alpha t/2)}{\sinh^3(\alpha t/2)}\int_0^\infty dk\cos(kz)$$
$$\times J_0(k[4xy\sinh^2(t/2)-(x-y)^2]^{1/2})$$

The integral over k is given by (ref. 23, p. 731)

$$=\frac{1}{(xy)^{1/2}}\frac{1}{[4\sinh^2(t/2)-b^2]^{1/2}};\qquad 4\sinh^2\left(\frac{t}{2}\right)>b^2>0$$
$$=\infty;\qquad 4\sinh^2\left(\frac{t}{2}\right)=b^2$$
$$=0;\qquad 0<4\sinh^2\left(\frac{t}{2}\right)<b^2$$

where b is defined by

$$b^2=\frac{z^2+(x-y)^2}{xy}$$

The change of variable

$$4\sinh^2(t/2)=b^2(1+s^2)$$

thus leads to[5]

$$F=\frac{\alpha^2}{(xy)^{1/2}}\frac{1}{\theta}\int_0^\infty\frac{\cosh(\alpha t(s)/2)}{\sinh^3(\alpha t(s)/2)}\frac{1}{(1+s^2)^{1/2}}\frac{1}{[1+(b/2)^2(1+s^2)]^{1/2}}ds$$

Since we are interested in the behavior of F at large distance along the edge, i.e., $b\gg 1$, we may write

$$\frac{\cosh(\alpha t(s)/2)}{\sinh^3(\alpha t(s)/2)}\approx\frac{4^{1-\alpha}}{(b/2)^{2\alpha}(1+s^2)^\alpha}$$

[5] Note that the divergence of the Fourier transform of J_0 is integrable, since $b>0$.

and obtain

$$F \approx \frac{\alpha^3}{\pi} (xy)^{-1/2} \left(\frac{2}{b}\right)^{1+2\alpha} 4^{1-\alpha} \int_0^\infty \frac{ds}{(1+s^2)^{1+\alpha}}$$

The integral over s can be computed and gives (ref. 23, p. 245)

$$\int_0^\infty \frac{ds}{(1+s^2)^{1+\alpha}} = \frac{1}{2} \frac{\Gamma(1/2)\,\Gamma(1/2+\alpha)}{\Gamma(1+\alpha)}; \qquad \mathrm{Re}\left(\frac{1}{2}-\alpha\right) < 1$$

The final solution (in the old coordinates) is given by

$$(\mathbf{n}_1 \nabla_{\mathbf{r}_1})(\mathbf{n}_2 \nabla_{\mathbf{r}_2})\, G_A^D(\hat{\mathbf{r}}_1, \hat{\mathbf{r}}_2) = \frac{F}{\rho\rho'}$$

$$= \frac{4\alpha^3}{\pi} (\rho\rho')^{\alpha-1} \frac{1}{|z-z'|^{1+2\alpha}} \frac{\Gamma(1/2)\,\Gamma(1/2+\alpha)}{\Gamma(1+\alpha)} \tag{9.21}$$

It is worth noting that the result of Eq. (9.21) differs from the conjecture based on the *Carnie and Chan* sum rule proposed in ref. 6. However, the analysis presented above deserves the following comments: The wedge is qualitatively different from all the other geometries considered so far. The angle at $\rho = 0$ represents a singularity of the surface where the assumptions made in the derivation at the beginning of this section break down. First, in the region close to the edge, the (locally integrable) divergence of the kernel (9.21) for an angle θ larger than π is clearly unphysical. Second, it is obvious that close to the edge of the wedge the potential does not penetrate from one side of the wedge only, but from both sides. It remains to determine whether the singularity at the edge produces only a minor correction to the long-range behavior of the correlation function or if it affects the overall solution in the sense of a possible nonalgebraic decay confined to a small region close to the edge as proposed by Jancovici *et al.*[6]

9.6. Illustration for Particular Angles of the Wedge

The Dirichlet kernel can be constructed with the image method for angles θ which are fractions of π ($\theta = \pi$, $\pi/2$, $\pi/3$,... or $\alpha = 1, 2, 3, \ldots$). It is a direct check of the general solution given by Eq. (9.21) and also provides a simple physical explanation for the dependence of the power of the decay upon the angle of the wedge, a few Debye lengths away from its edge.

In the simplest case of a plane wall ($\alpha = 1$) with the boundary on the plane $x = 0$, the kernel is

$$G^D_{\text{p.w.}}(\mathbf{r}; \mathbf{r}') = \Phi(x, y, z, x', y', z') - \Phi(x, y, z, -x', y', z')$$

where $\Phi(\mathbf{r}, \mathbf{r}')$ is the Coulomb potential in free boundary conditions $[\Phi(\mathbf{r}, \mathbf{r}') = 1/|\mathbf{r} - \mathbf{r}'|]$.

The derivatives with respect to x and x' can be expanded at large $|z - z'|$ and one obtains

$$\frac{d^2}{dx\,dx'} G^D_{\text{p.w.}}(x, y, z, x', y', z')\bigg|_{x=x'=0} \approx \frac{2}{|z - z'|^3}$$

which is the result given by Eq. (9.21) for $\alpha = 1$.

In the case of an angle of $\pi/2$ we have to sum over the direct interaction in the first quadrant and the three images in the other three quadrants. If we evaluate the derivatives on the y–z plane we can use the previous plane wall result and obtain

$$\begin{aligned}\frac{d^2}{dx\,dx'} G^D_{\alpha=2}(x, y, z, x', y', z')\bigg|_{x=x'=0} &= \frac{d^2}{dx\,dx'} G^D_{\text{p.w.}}(x, y, z, x', y', z')\bigg|_{x=x'=0} \\ &\quad - \frac{d^2}{dx\,dx'} G^D_{\text{p.w.}}(x, y, z, x', -y', z')\bigg|_{x=x'=0}\end{aligned}$$

An expansion for large $|z - z'|$ leads to

$$\frac{d^2}{dx\,dx'} G^D_{\alpha=2}(x, y, z, x', y', z')\bigg|_{x=x'=0} \approx \frac{12yy'}{|z - z'|^5}$$

which is the solution given by Eq. (9.21) for $\alpha = 2$.

The solutions for higher values of α are constructed in a similar way and correspond to "multipole–dipole" interactions, which are known to decrease with powers of z^{-3}, z^{-5}, z^{-7}, etc. The solution for noninteger values of α cannot be constructed with the method of images, since the power of the decay does not correspond to a "multipole–dipole" interaction.

APPENDIX A

The purpose of this Appendix is to show how the DH kernel of the disk given by Eq. (4.12) goes over to the DH kernel of the semi-infinite

plane given by Jancovici (ref. 4, p. 55) and why the surface part of $G^{\varepsilon'=\infty}_{D;\text{gcan}}$ is of short range, as mentioned under Eq. (6.5). To this end, it is convenient to start from the expansion constructed on the basis of Eqs. (4.1), (4.2), and (4.7), namely

$$G^{\varepsilon'}_{D;\text{in}}(s, s_0, \theta, \xi_D) \equiv \sum_{n\geqslant 0} \left\{ I_n(s_<)\, K_n(s_>) - \frac{K_n'(Z) + \varepsilon'(\hat{n}/Z)\, K_n(Z)}{I_n'(Z) + \varepsilon'(\hat{n}/Z)\, I_n(Z)} I_n(s_0)\, I_n(s) \right\} \mu_n \cos n\theta \tag{A.1}$$

where we recall that $|x| = s$, $|y| = s_0$, $s_< = \min(s_0, s)$, $s_> = \max(s_0, s)$, and $\hat{n} = \xi_D^{-1}\delta_{n;0} + (1-\delta_{n;0})n$, with $\xi_D = \ln(L/R)$ according to Eq. (4.11).

At this point we introduce a new independent variable $p = n/Z$ and since Z is very large, we look for a large-n and large-Z expansion of $I_n'(Z)$, of $K_n'(Z)$, and also of $I_n(Z)\, K_n(Z)$ with n/Z finite. From Eqs. (9.7.7)–(9.7.10) of ref. 24 we have [cf. Remark below (A.13)]

$$I_n'(Z) = \left[1 + \left(\frac{n}{Z}\right)^2\right]^{1/2} I_n(Z) \left[1 + O\left(\frac{1}{n}\right)\right] \tag{A.2}$$

$$K_n'(Z) = -\left[1 + \left(\frac{n}{Z}\right)^2\right]^{1/2} K_n(Z) \left[1 + O\left(\frac{1}{n}\right)\right] \tag{A.3}$$

and from Eq. (9.7.5) of ref. 24 we can extract the series

$$\begin{aligned} I_n(Z)\, K_n(Z) &\cong \frac{1}{2Z}\left[1 - \frac{1}{2}\left(\frac{n}{Z}\right)^2 + \frac{1}{2}\frac{3}{4}\left(\frac{n}{Z}\right)^4 \cdots\right]\left[1 + O\left(\frac{1}{Z^2}\right)\right] \\ &= \frac{1}{2Z}\frac{1}{[1 + (n/Z)^2]^{1/2}}\left[1 + O\left(\frac{1}{Z^2}\right)\right] \end{aligned} \tag{A.4}$$

With the help of Eqs. (A.2) and (A.3), we can approximate $I_n(s)$ and $K_n(s)$ for s close to Z by

$$\ln I_n(s) \cong \ln I_n(Z) + (s - Z)\, I_n'(Z)/I_n(Z) \tag{A.5}$$

$$\ln K_n(s) \cong \ln K_n(Z) + (s - Z)\, K_n'(Z)/K_n(Z) \tag{A.6}$$

Next we take the canonical limit $\xi_D \to \infty$ for $\varepsilon' < \infty$, and in defining

$$G^{\varepsilon'}_{D;\text{can}}(s, s_0, \theta) \equiv \frac{1}{Z} \sum_{n\geqslant 0} \mu_n \hat{G}^{\varepsilon'}_D(s, s_0, n) \cos n\theta \tag{A.7}$$

we obtain, since $s_< - s_> = -|s - s_0|$,

$$\hat{G}_D^{\varepsilon'}(s, s_0, p) \cong \frac{1}{2(1+p^2)^{1/2}} \left\{ \exp[-(1+p^2)^{1/2}|s-s_0|] + \frac{(1+p^2)^{1/2} - \varepsilon' p}{(1+p^2)^{1/2} + \varepsilon' p} \exp[(1+p^2)^{1/2}(s+s_0-2Z)] \right\} \tag{A.8}$$

With the substitutions $Z - s_0 = \kappa x_1$, $Z - s = \kappa x_2$, $p = \kappa^{-1} l$, $\varepsilon' = 1$, $Z \to \infty$, we find that $\hat{G}_D^1(s, s_0, p)$ becomes exactly $\kappa^{-1} \rho \hat{h}(x_1, x_2, l)$ given by Eq. (3.12) of ref. 4. This result means that, given some knowledge about the Fourier transform $h(x_1, x_2, y)$ of $\hat{h}(x_1, x_2, l)$, a very good approximation to the surface behavior of the DH kernel of the disk can be constructed in term of the Poisson sum of the function $h((Z-s)/\kappa, (Z-s_0)/\kappa, Z(\theta - 2n\pi))$. For example, the bulk part of the DH kernel on the surface of the disk, i.e., the function $K_0(2Z \sin \theta/2)$, turns out to be approximated by the sum of $K_0(Z(\theta - 2n\pi))$. Another example is given by the θ-dependent long-range surface part $(2Z \sin \theta/2)^{-2}$ of $G_{D;\text{in}}$ given in Eq. (4.17) and which turns out to be exactly the periodized version of the function y^{-2}, i.e., the long-range surface correlation discussed in ref. 4.

As a further example, let us consider the Dirichlet limit $\varepsilon' \to \infty$ of Eq. (A.1). In order for the ratio $\hat{n}/\hat{n}$ to be meaningfull for $n \geqslant 0$, we need $\xi_D < \infty$, which corresponds to the "grand canonical" DH kernel. We find, accordingly,

$$G_{\text{in;gcan}}^{\varepsilon' = \infty}(s, s_0, \theta, \xi_D) = \sum_{n \geqslant 0} \mu_n \left\{ I_n(s_<) K_n(s_>) - \frac{K_n(Z)}{I_n(Z)} I_n(s_0) I_n(s) \right\} \cos n\theta \tag{A.9}$$

and we obtain, with the approximations (A.2)–(A.4) and for s and s_0 close to the edge,

$$G^{\varepsilon' = \infty} \cong \frac{1}{Z} \sum_{n \geqslant 0} \mu_n \cos n\theta \frac{1}{2(1+p^2)^{1/2}} \times \{\exp[-(1+p^2)^{1/2}|s-s_0|] - \exp[(1+p^2)^{1/2}(s+s_0-2Z)]\} \tag{A.10}$$

It is now possible to find the function $h(Z-s, Z-s_0, Z\theta)$ such that $G_{\text{in;gcan}}^{\varepsilon' = \infty}(s, s_0, \theta, \xi_D)$ becomes its periodized realization. With the help of Eq. (3.914) of ref. 23 and after some manipulations, we find

$$\int_0^\infty dp \frac{1}{(1+p^2)^{1/2}} \exp[-(1+p^2)^{1/2}|s-s_0|] \cos px = K_0([|s-s_0|^2 + (Z\theta)^2]^{1/2}) \tag{A.11}$$

and thus

$$G^{\varepsilon'=\infty} \cong \sum_m \{K_0([|s-s_0|^2 + Z^2(\theta - 2\pi m)^2]^{1/2}) - K_0([(s+s_0-2Z)^2 + Z^2(\theta-2\pi m)^2]^{1/2})\} \tag{A.12}$$

which is indeed a short-ranged correlation function. We remark lastly that the Neumann limit $\varepsilon' \to 0$ of Eq. (A.1) becomes, for $\xi_D > 0$, i.e., for both canonical and grand canonical DH kernels,

$$G^{\varepsilon'=0}_{\text{in;gcan}}(s, s_0, \theta, \xi_D > 0) = \sum_{n \geqslant 0} \mu_n \left\{ I_n(s_<) K_n(s_>) - \frac{K_n'(Z)}{I_n'(Z)} I_n(s_0) I_n(s) \right\} \cos n\theta \tag{A.13}$$

For s and s_0 close to the edge of the disk and with the approximations (A.2) and (A.3), we find that $G^{\varepsilon'=0}_{D;\text{surf}}$ is given by Eq. (A.12) with a plus sign.

Remark. A simple derivation of (A.2) and (A.3) can be obtained by considering the integral representations of $K_n(Z)$ and $I_n(Z)$ for large n and Z with $n/Z = p$ fixed as a "partition function" and to evaluate $K_n'(Z)$ and $I_n'(Z)$ in a mean field type of approximation. From Eq. (9.6.23) of ref. 24 we have, for example,

$$K_n(Z) = \frac{(Z)^n}{(2n-1)!!} \int_0^\infty e^{-Z \operatorname{ch} t} \operatorname{sh}^{2n}(t)\, dt$$

$$K_n'(Z) = \frac{n}{Z} K_n(Z) - \langle \operatorname{ch} t \rangle K_n(Z)$$

where $\langle \operatorname{ch} t \rangle$ is the expectation value of $\operatorname{ch} t$ over the probability distribution $[(Z)^n/(2n-1)!!] e^{Z \operatorname{ch} t} \operatorname{sh}^{2n}(t)/K_n(Z)$. Since the distribution is "thermodynamically" peaked at $Z \operatorname{sh} \hat{t} = 2n \operatorname{ch} \hat{t}/\operatorname{sh} \hat{t}$ or $2p = \operatorname{sh}^2 \hat{t}/\operatorname{ch} \hat{t} = (\operatorname{ch}^2 \hat{t} - 1)/\operatorname{ch} \hat{t}$, i.e., $\operatorname{ch} \hat{t} = p + (1+p^2)^{1/2}$, we notice that in approximating $\langle \operatorname{ch} t \rangle$ by its mean-field value $\operatorname{ch} \hat{t}$ we obtain

$$K_n'(Z) = pK_n(Z) - [p + (1-p^2)^{1/2}] K_n(Z) = -(1+p^2)^{1/2} K_n(Z)$$

which is precisely Eq. (A.5). Similarly, with Eq. (9.6.18) of [ref. 24], namely

$$I_n(Z) = \frac{(Z)^n}{(2n-1)!!} \frac{1}{\pi} \int_0^\pi e^{-Z \cos\theta} \sin^{2n}(\theta)\, d\theta$$

we have

$$I_n'(Z) = \frac{n}{Z} I_n(Z) - \langle \cos\theta \rangle I_n(Z) \cong pI_n(Z) + \cos\hat{\theta}\, I_n(Z)$$

and since $2p = (1 - \cos^2\hat{\theta})/\cos\hat{\theta}$, i.e., $\cos\hat{\theta} = -p + (1+p^2)^{1/2}$, we find $I_n'(Z) \cong (1+p^2)^{1/2} I_n(Z)$, which is Eq. (A.2).

APPENDIX B

The purpose of this Appendix is to show that the behavior of the truncated radial pair distribution function (TRPDF) which we observed for the disk in CMC simulation (cf. Section 7) can be reproduced with the DH approximation in the canonical limit.

Using the notation of II and the results of Section 4.1 and Section 6, we have

$$\hat{\rho}^{\text{can}}_{2;\text{disk}}(|\mathbf{r}|) = 2\pi|\mathbf{r}| \frac{1}{\pi R^2} \int_{D(|\mathbf{r}|)} d^2x\, \rho^{T;\text{can}}_{2;\text{disk}}(\mathbf{x}, \mathbf{x}+\mathbf{r})$$

$$= 2\pi|\mathbf{r}| \frac{1}{\pi R^2} (-\beta q^2 \rho^2) \int_{D(|\mathbf{r}|)} d^2x\, G^{\text{can}}_{\text{disk;in}}(\mathbf{x}, \mathbf{x}+\mathbf{r}) \qquad \text{(B.1)}$$

with

$$G^{\text{can}}_{\text{disk;in}}(\mathbf{x}, \mathbf{x}+\mathbf{r}) = G^{\text{gcan}}_{\text{disk;in}}(\mathbf{x}, \mathbf{x}+\mathbf{r}) + \frac{1}{z} \frac{I_0(\kappa|\mathbf{x}|)\, I_0(\kappa|\mathbf{x}+\mathbf{r}|)}{I_0(Z)\, I_1(Z)} \qquad \text{(B.2)}$$

Since we know (cf. Section 6) $G^{\text{gcan}}_{\text{disk;in}}(\mathbf{x}, \mathbf{x}+\mathbf{r})$ to be of short range, it is obvious that the surface contribution of $G^{\text{gcan}}_{\text{disk;in}}(\mathbf{x}, \mathbf{x}+\mathbf{r})$ to the TRPDF is much smaller than the bulk one. Therefore we can neglect this surface term and write {using Eq. (3.6) of II for $D(|\mathbf{r}|)$ and setting $s = |\mathbf{r}|/R$, $s \in [0; 2]$}

$$\hat{\rho}^{\text{can}}_{2;\text{disk}}(s) \cong -\frac{\kappa\rho}{2\pi}(2\pi Z s) \left\{ \frac{2}{\pi} \left\{ \arccos\left(\frac{s}{2}\right) - \left(\frac{s}{2}\right) \left[1 - \left(\frac{s}{2}\right)^2 \right]^{1/2} \right\} K_0(Zs) \right.$$

$$\left. + \frac{1}{Z} \frac{\kappa^2}{\pi Z^2} \int_{D(|\mathbf{r}|)} d^2x \frac{I_0(\kappa|\mathbf{x}|)\, I_0(\kappa|\mathbf{x}+\mathbf{r}|)}{I_0(Z)\, I_1(Z)} \right\} \qquad \text{(B.3)}$$

We are left to examine the last term of Eq. (B.3). Since it is a surface contribution, it is sufficient to consider the case where the two particles are close to the edge of the disk. For this purpose we introduce the two new dimensionless variables u and v ($u, v \ll 1$) defined by $\kappa|\mathbf{x}| = Z(1-u)$ and $\kappa|\mathbf{x}+\mathbf{r}| = Z(1-v)$, which represent the distances from the surface.

In terms of these new variables we have

$$\frac{I_0(\kappa|\mathbf{x}|)\, I_0(\kappa|\mathbf{x}+\mathbf{r}|)}{I_0(Z)\, I_1(Z)} \underset{Z\gg 1}{\approx} \frac{1}{(1-u)^{1/2}} \frac{1}{(1-v)^{1/2}} e^{-Z(u+v)} \tag{B.4}$$

and

$$\begin{aligned} d^2x = 2x\, dx\, d|\theta| &= \frac{2x\, dx\, y\, dy}{xr \sin|\theta|} = \frac{2x\, dx\, y\, dy}{xr[(1-\cos\theta)(1+\cos\theta)]^{1/2}} \\ &= \frac{4x\, dx\, y\, dy}{[(y-x+r)(y+x-r)(x+r-y)(x+r+y)]^{1/2}} \\ &= \frac{4z^2}{\kappa^2} \frac{(1-u)(1-v)\, du\, dv}{[(s+u-v)(s-u+v)(2-s-u-v)(2+s-u-v)]^{1/2}} \end{aligned} \tag{B.5}$$

As for the domain of integration $D(|\mathbf{r}|)$, it is defined in terms of these variables as in II, pp. 608–609.

Therefore, with Eqs. (B.4) and (B.5) and for large separation ($s \cong 2$) we obtain [with $u = \frac{1}{2}(u' + v')$ and $v = \frac{1}{2}(u' - v')$]

$$\begin{aligned} &\frac{1}{Z}\frac{\kappa^2}{\pi Z^2}\int_{D(|\mathbf{r}|)} d^2x \frac{I_0(\kappa|\mathbf{x}|)\, I_0(\kappa|\mathbf{x}+\mathbf{r}|)}{I_0(Z)\, I_1(Z)} \\ &\quad \cong \frac{2}{\pi Z}\int_0^{2-s} du' \frac{e^{-Zu'}}{[(2-u')^2 - s^2]^{1/2}} \int_0^{u'} dv' \left[\frac{(2-u')^2 - v'^2}{s^2 - v'^2}\right]^{1/2} \\ &\quad \cong \frac{2}{\pi Z}\int_0^{2-s} du' \frac{u' e^{-Zu'}}{[(2-u')^2 - s^2]^{1/2}} \cong \frac{1}{\pi Z}\int_0^{2-s} du' \frac{u' e^{-Zu'}}{(2-s-u')^{1/2}} \end{aligned}$$

Finally, after the two successive changes of variables $u' = (2-s)\, y$ and $y = 1 - x^2$, we find for $s \cong 2$

$$\begin{aligned} &\frac{1}{Z}\frac{\kappa^2}{\pi Z^2}\int_{D(|\mathbf{r}|)} d^2x \frac{I_0(\kappa|\mathbf{x}|)\, I_0(\kappa|\mathbf{x}+\mathbf{r}|)}{I_0(Z)\, I_1(Z)} \\ &\quad \cong \frac{2}{\pi Z}(2-s)^{3/2}\int_0^1 dx\ (1-x^2) e^{-Z(2-s)(1-x^2)} \end{aligned} \tag{B.6}$$

The last relation is suited for a numerical calculation since the integrand is now regular for all $x \in [0; 1]$. We note that for small separations ($s \ll 1$) the contribution to the TRPDF of the term in the lhs of Eq. (B.6) can be neglected. Indeed, it is easy to see that this contribution

is much smaller than the bulk contribution. In conclusion we can approximate with quite good accuracy the TRPDF by[6]

$$\hat{\rho}^{\text{can}}_{2;\text{disk}}(s) \cong -\frac{\kappa\rho}{2\pi}(4s)\left(ZK_0(Zs)\left\{\arccos\left(\frac{s}{2}\right)-\left(\frac{s}{2}\right)\left[1-\left(\frac{s}{2}\right)^2\right]^{1/2}\right\}\right.$$
$$\left.+(2-s)^{3/2}\int_0^1 dx\,(1-x^2)e^{-Z(2-s)(1-x^2)}\right) \tag{B.7}$$

A numerical check of Eq. (B.7) is shown in Fig. 8 of Section 7. By comparison with Fig. 6, we see that the DH approximation is capable of reproducing the results obtained by CMC simulation on an OCP even at Γ as high as 1/2!

The case of the sphere can be treated in exactly the same way. The calculations are, however, much easier than in the two-dimensional case, since the volume element d^3x is now simply given by

$$d^3x = \frac{2\pi}{r}x\,dx\,y\,dy = \frac{2\pi Z^3}{s\kappa^3}(1-u)(1-v)\,du\,dv \tag{B.8}$$

As for the domain $D(|\mathbf{r}|)$, it is now given by

$$D(|\mathbf{r}|) = \frac{4\pi R^3}{3}\left[1-\frac{3}{2}\left(\frac{r}{2R}\right)+\frac{1}{2}\left(\frac{r}{2R}\right)^3\right] \tag{B.9}$$

and we find

$$\hat{\rho}^{\text{can}}_{2;\text{sphere}}(s) \cong -\frac{\kappa\rho}{4\pi}(4\pi Zs)\left(e^{-Zs}\left(1-\frac{3s}{4}+\frac{s^3}{16}\right)\right.$$
$$\left.+\frac{3}{2Z^3}\{1-e^{-Z(2-s)}[1+Z(2-s)]\}\right) \tag{B.10}$$

The result is presented in Fig. 9 of Section 7. It shows that the TRPDF of the sphere manifests the same qualitative behavior as that observed for the disk.

APPENDIX C

Here we present some calculations which are necessary for the evaluation of the integrals in Eq. (8.12). Let P be the point of the ellipse which

[6] Although Eq. (B.6) is established assuming $s \gtrsim 2$, we extend its domain of validity to all s. This can be done since this contribution for small s is also quite negligible with respect to the bulk contribution.

is the nearest to the x point (see Fig. 14). We take a local Cartesian coordinate system (t, s) made up of the tangent and the normal to the curve. The equation of the curve in this coordinate system is $s(t)$, whose small-t expansion is

$$s(t) \underset{t \to 0}{\cong} \tfrac{1}{2} s_2 t^2 + \tfrac{1}{6} s_3 t^3 + \cdots \tag{C.1}$$

s_2 is the curvature radius of the point P. We consider a new variable u defined by

$$D^2 = d^2 + u^2; \qquad \operatorname{sgn}(u) = \operatorname{sgn}(t) \tag{C.2}$$

It is easily shown that

$$u = \operatorname{sgn}(t)\,[-2ds(t) + t^2 + s^2(t)]^{1/2} \underset{t \to 0}{\cong} t(1 - ds_2)^{1/2} \tag{C.3}$$

The element of arc length along this curve is

$$dl' = du \frac{[1 + s'^2(t)]^{1/2}}{du(t)/dt} \tag{C.4}$$

After a straightforward calculation, we obtain $\cos\alpha$ (see Fig. 14),

$$\cos\alpha = \frac{d}{(d^2 + u^2)^{1/2}} \frac{1}{[1 + s'^2(t)]^{1/2}} + \frac{u^2 c(u)}{(d^2 + u^2)^{1/2}} \tag{C.5}$$

where the function $c(u)$ is defined by

$$c(u) = \frac{ts'(t) - s(t)}{u^2[1 + s'^2(t)]^{1/2}} \underset{u \to 0}{\cong} \frac{1}{2} \frac{s_2}{1 - ds_2} \tag{C.6}$$

The first term of $\cos\alpha$ gives a contribution to the integral I [Eq. (8.13)]

$$I^{(1)} = \frac{q}{2\pi} \int_{u_1}^{u_2} du\, \lambda(u) \frac{dt(u)}{du} \left[\frac{d}{(d^2 + u^2)^{1/2}} K_1(q(d^2 + u^2)^{1/2}) \right] \tag{C.7}$$

with integration bounds ($u_1 < 0$, $u_2 > 0$) that it is not necessary to specify. As d goes to zero, we have to be careful with the term in square brackets, which behaves at small u as $d/q(d^2 + u^2)$ and then is proportional to a delta function $\delta(u)$ in the limit $d \to 0$. It follows that

$$\lim_{d \to 0} I^{(1)} = \frac{1}{2\pi} \lambda(u = 0) \frac{dt}{du}(u = 0, d = 0) \int_{-\infty}^{+\infty} du \frac{d}{d^2 + u^2} = \frac{1}{2} \lambda(\sigma) \tag{C.8}$$

The second term of $\cos\alpha$ [Eq. (C.5)] causes no problem because of the factor u^2 in the numerator. This gives Eq. (8.13).

Now we show how it is possible to calculate the integrals along the ellipse [Eq. (8.12)],

$$I[f]=\frac{1}{2\pi}\oint dl'\, f(x')\, K_0(qD)$$

$$J[g]=\frac{1}{2\pi}\oint dl'\, g(x')\cos\alpha\, K_1(qD) \tag{C.9}$$

when the functions f and g have slow variations over distances of the order of q^{-1} and have such behaviors that the leading contributions come from the neighborhood of the point P where D is minimum. As for the previous calculation, we use the variable u [Eq. (C.2)] and put together the contributions $u>0$ and $u<0$,

$$I[f]=\frac{1}{2\pi}\int_0^{u_2} du\, K_0(q(d^2+u^2)^{1/2})\frac{dl'(u)}{du}f(u)$$
$$+\frac{1}{2\pi}\int_0^{-u_1} du\, K_0(q(d^2+u^2)^{1/2})\frac{dl'(-u)}{du}f(-u) \tag{C.10}$$

We expand the function $[dl'(u)/du]\, f(u)$ in series of u and we extend the integration to infinity with an exponentially small error. Using the integral

$$\int_0^\infty du\, K_0(q(d^2+u^2)^{1/2})u^{2\nu+1}=I_\nu(q,d)=\frac{2^\nu\Gamma(\nu+1)}{q^{\nu+1}d^{-\nu-1}}K_{-\nu-1}(qd) \tag{C.11}$$

we obtain

$$I[f]=\frac{1}{\pi}\sum_{n\geqslant 0}\frac{1}{(2n)!}\left(\frac{dl'}{du}f\right)^{(2n)}(u=0)\, I_{n-1/2}(q,d) \tag{C.12}$$

with

$$\frac{dl'}{du}(u=0)=\frac{1}{(1-ds_2)^{1/2}},\qquad I_{-1/2}=\frac{\pi}{2q}e^{-qd} \tag{C.13}$$

In the same way, for $J[g]$, we use the integral

$$\int_0^\infty du\,\frac{d}{(d^2+u^2)^{1/2}}K_1(q(d^2+u^2)^{1/2})u^{2\nu+1}=J_\nu(q,d)=\frac{2^\nu\Gamma(\nu+1)}{q^{\nu+1}d^{-\nu-1}}K_{-\nu}(qd) \tag{C.14}$$

and we get

$$J[g]=\frac{1}{\pi}\sum_{n\geqslant 0}\frac{1}{(2n)!}\left[\left(\frac{dl'}{du}\frac{g}{(1+s'^2)^{1/2}}\right)^{(2n)}(u=0)\,J_{n-1/2}(q,d)\right.$$
$$\left.+\left(\frac{dl'}{du}gc\right)^{(2n)}(u=0)\,J_{n+1/2}(q,d)\frac{1}{d}\right] \tag{C.15}$$

[$c(u)$ is defined in Eq. (C.6)] with

$$\left(\frac{dl'}{du}\frac{1}{(1+s'^2)^{1/2}}\right)(u=0)=\frac{1}{(1-ds_2)^{1/2}},\qquad \left(\frac{dl'}{du}c\right)(u=0)=\frac{1}{2}\frac{s_2}{(1-ds_2)^{3/2}}$$
$$J_{-1/2}(q,d)=\frac{\pi}{2q}e^{-qd},\qquad J_{1/2}(q,d)=\frac{\pi d}{2q^2}e^{-qd} \tag{C.16}$$

Finally, it remains to give the coefficients $s_2, s_3,\ldots$ [Eq. (C.1)] for the ellipse. The only one we need is s_2. An easy calculation shows that the curvature radius s_2 at the point $P=(\tau_0,\sigma_P)$ is

$$s_2=[h(\tau_0;\sigma_P)]^{-3}=h_P^{-3} \tag{C.17}$$

APPENDIX D

The purpose of this Appendix is to prove, for the particular case of a disk, that in the canonical limit $\xi_D\to\infty$ the long-range surface part of $G_{D;\mathrm{in}}^{\varepsilon'=1}$ is indeed given by Eq. (9.5), i.e., by the bigradient of the Dirichlet kernel evaluated on the edge of the disk.

To this end we start from Eq. (4.10) for the coefficient $C_{D;\mathrm{in}}^{0}$ and from Eq. (4.7) for the coefficients $C_{D;\mathrm{in}}^{n\geqslant 1}$. Setting $\varepsilon'=1$, we have the expansion

$$G_{D;\mathrm{in}}^{\varepsilon'=1}=-\frac{1}{Z^2}\left(\frac{1}{\xi_D+I_0(Z)/ZI_1(Z)}\right)\frac{I_0(s_0)\,I_0(s)}{I_1(Z)\,I_1(Z)}$$
$$+\sum_{n\geqslant 0}\mu_n\cos n\theta\left[I_n(s_<)\,K_n(s_>)-\frac{K_n'(Z)+(n/Z)\,K_n(Z)}{I_n'(Z)+(n/Z)\,I_n(Z)}I_n(s_0)\,I_n(s)\right] \tag{D.1}$$

Next we construct the solution of the equation

$$-\Delta G_{D;\mathrm{out}}^{\varepsilon'=1}(x',y')=2\pi\delta(x'-y') \tag{D.2}$$

with both x' and y' outside the disk and we require that $G_{D;\mathrm{in}}^{\varepsilon'=1}$ and $G_{D;\mathrm{out}}^{\varepsilon'=1}$

match together with their normal derivative on $|x| = |x'| = |y| = |y'| = Z$. To this end, we write the expansion

$$G^{\varepsilon'=1}_{D;\text{out}} = F_0(s'_>) + \sum_{n\geqslant 1} \frac{1}{n}\left(\frac{s'_<}{s'_>}\right)^n \cos n\theta$$
$$- B_0 F_0(s'_0)\, F_0(s') - \sum_{n\geqslant 1} \frac{1}{n} B_n \left(\frac{Z^2}{s'_0 s'}\right)^n \cos n\theta \qquad \text{(D.3)}$$

where $F_0(s')$ is given by Eq. (4.6).

The matching conditions result in

$$B_0 = \frac{1}{\xi_D + I_0(Z)/ZI_1(Z)}$$
$$B_n = \frac{I'_n(Z) - (n/Z)\, I_n(Z)}{I'_n(Z) + (n/Z)\, I_n(Z)}; \qquad n > 0$$

Notice here that the same coefficients would have been found if we had required to match $G^{\varepsilon'=1}_{D;\text{out}}(x', y')$ with the solution of the *homogeneous* DH equation $G^{\varepsilon'=1}_{D;\text{in}}(x, y')$ with x inside the disk and the source y' outside. We have, therefore,

$$G^{\varepsilon'=1}_{D;\text{out}}(s'_0, s', \theta) = F_0(s'_>) - B_0\, F_0(s'_0)\, F_0(s')$$
$$+ \sum_{n\geqslant 1} \frac{1}{n}\left[\left(\frac{s'_<}{s'_>}\right)^n - \frac{I'_n(Z) - (n/Z)\, I_n(Z)}{I'_n(Z) + (n/Z)\, I_n(Z)}\left(\frac{Z^2}{s'_0 s'}\right)^n\right] \cos n\theta \qquad \text{(D.4)}$$

The problem is now to establish a relation between $G^{\varepsilon'=1}_{D;\text{in}}$ and $G^{\varepsilon'=1}_{D;\text{out}}$ in the sense of Eq. (9.5). We notice first that, from the interior of the disk, up to a typical distance of a Debye length, the plasma "sees" a vacuum in the exterior of the disk with a vanishing ratio of dielectric constants and second that, from the exterior of the disk, again up to a distance of the order of a Debye length, the vacuum "sees" the interior of the disk as a perfect conductor with an infinite ratio of dielectric constants. These observations suggest that we extract from $G^{\varepsilon'=1}_{D;\text{in}}$ a Neumann part and from $G^{\varepsilon'=1}_{D;\text{out}}$ a Dirichlet part. For $G^{\varepsilon'=1}_{D;\text{in}}$, we have with Eq. (A.13)

$$G^{\varepsilon'=1}_{D;\text{in}}(s_0, s; \theta)$$
$$= G^{\varepsilon'=0}_{D;\text{in}}(s_0, s, \theta) - \frac{1}{Z^2}\left(\frac{1}{\xi_D + I_0(Z)/ZI_1((Z)}\right)\frac{I_0(s_0)\, I_0(s)}{I_1(Z)\, I_1(Z)}$$
$$+ \sum_{n\geqslant 0} \mu_n \left[\frac{K'_n(Z)}{I'_n(Z)} - \frac{K'_n(Z) + (n/Z)\, K_n(Z)}{I'_n(Z) + (n/Z)\, I_n(Z)}\right] I_n(s_0)\, I_n(s) \cos n\theta$$

$$= G^{\varepsilon'=0}_{D;\text{in}}(s_0, s, \theta) - \frac{1}{Z^2}\left(\frac{1}{\xi_D + I_0(Z)/ZI_1(Z)}\right)\frac{I_0(s_0)\, I_0(s)}{I_1(Z)\, I_1(Z)}$$

$$- \sum_{n \geqslant 1} 2\left(\frac{n}{Z^2}\right)\left(\frac{1}{I_n'(Z)[I_n'(Z) + (n/Z)\, I_n(Z)]}\right) I_n(s_0)\, I_n(s) \cos n\theta$$

At this point we introduce the large-n and large-Z approximations given by Eqs. (A.2)–(A.6) and we find, multiplying the numerator and denominator by $(1+p^2)^{1/2} - p$ in order to simplify the latter,

$$G^{\varepsilon'=1}_{D;\text{in}}(s_0, s, \theta)) \cong G^{\varepsilon'=0}_{D;\text{in}}(s_0, s, \theta) - \frac{1}{Z^2}\left(\frac{1}{\xi_D + I_0(Z)/ZI_1(Z)}\right)\exp(s + s_0 - 2Z)$$

$$- \sum_{n \geqslant 1} 2\left(\frac{n}{Z^2}\right)\left(1 - \frac{n}{Z[1 + (n/Z)^2]^{1/2}}\right)$$

$$\times \exp\left\{\left[1 + \left(\frac{n}{Z}\right)^2\right]^{1/2}(s + s_0 - 2Z)\right\} \cos n\theta \tag{D.5}$$

The long-range θ-dependent surface part of Eq. (D.5) is consequently given by

$$G^{\varepsilon'=1}_{D;\text{in;surf}}(s_0, s, \theta) \cong - \sum_{n \geqslant 1} \frac{2n}{Z^2} \exp(s + s_0 - 2Z) \cos n\theta \tag{D.6}$$

Proceeding similarly with $G^{\varepsilon'=1}_{D;\text{out}}$, we extract a Dirichlet part [ref. 22, Eq. (10.1.19)], namely

$$G^{\varepsilon'=\infty}_{D;\text{out}}(s_0, s, \theta, \xi_D = 0)$$

$$= G_{\text{Dirichlet}}(s_0', s', \theta)$$

$$= -\ln\left(\frac{Z}{s'_<}\right) + \sum_{n \geqslant 1} \frac{1}{n}\left[\left(\frac{s'_<}{s'_>}\right)^n - \left(\frac{Z^2}{s_0' s'}\right)^n\right] \cos n\theta \tag{D.7}$$

we introduce the auxiliary function

$$C^0 = \ln\left(\frac{Z}{s'_<}\right) + F_0(s'_>) - B_0 F_0(s_0')\, F_0(s')$$

$$= \frac{1}{\xi_D + I_0(Z)/ZI_1(Z)}\left[\frac{I_0(Z)}{ZI_1(Z)} - \ln\left(\frac{Z}{s_0'}\right) - \ln\left(\frac{Z}{s'}\right) + \ln\left(\frac{Z}{s_0'}\right)\ln\left(\frac{Z}{s'}\right)\right] \tag{D.8}$$

which vanishes in the canonical limit and we obtain

$$
\begin{aligned}
G_{D;\mathrm{out}}^{\varepsilon'=1} &= G_{D;\mathrm{out}}^{\varepsilon'=\infty}(\xi_D=0) \\
&\quad + \sum_{n\geqslant 1}\frac{1}{n}\left(1-\frac{I_n'(Z)-(n/Z)\,I_n(Z)}{I_n'(Z)+(n/Z)\,I_n(Z)}\right)\left(\frac{Z^2}{s_0 s}\right)^n\cos n\theta + C^0 \\
&= G_{D;\mathrm{out}}^{\varepsilon'=\infty} + \sum_{n\geqslant 1}\frac{2}{Z}\frac{I_n(Z)}{I_n'(Z)+(n/Z)\,I_n(Z)}\left(\frac{Z^2}{s_0 s}\right)^n\cos n\theta + C^0 \\
&\cong G_{D;\mathrm{out}}^{\varepsilon'=\infty} + \sum_{n\geqslant 1}\frac{2}{Z}\left(\frac{1}{(1+p^2)^{1/2}+p}\right)\left(\frac{Z^2}{s_0 s}\right)^n\cos n\theta + C^0 \\
&= G_{D;\mathrm{out}}^{\varepsilon'=\infty} + \sum_{n\geqslant 1}\frac{2}{Z}\left(-p+\frac{1+p^2}{(1+p^2)^{1/2}}\right)\left(\frac{Z^2}{s_0 s}\right)^n\cos n\theta + C^0
\end{aligned}
$$

Again, the long-range θ-dependent surface part of $G_{D;\mathrm{out}}^{\varepsilon'=1}$ is given by

$$
G_{D;\mathrm{out;surf}}^{\varepsilon'=1} = \sum_{n\geqslant 1}\frac{-2n}{Z^2}\left(\frac{Z^2}{s_0 s}\right)^n\cos n\theta \tag{D.9}
$$

which matches exactly with Eq. (D.6) on the edge of the disk. The remarkable fact is now that we can construct the angular-dependent surface part of Eq. (D.6) as

$$
\begin{aligned}
&\sum_{n\geqslant 1}\frac{-2n}{Z^2}\cos n\theta \\
&\quad = \frac{d^2}{ds_0'\,ds'}\left\{-\ln\left(\frac{Z}{s'_<}\right)+\sum_{n\geqslant 1}\frac{1}{n}\left[\left(\frac{s'_<}{s'_>}\right)^n-\left(\frac{Z^2}{s_0' s'}\right)^n\right]\cos n\theta\right\} \\
&\quad \equiv \frac{d^2}{ds_0'\,ds'}\,G_{\mathrm{Dirichlet}}(s_0', s', \theta)\Big|_{s_0'=s'=Z}
\end{aligned}
\tag{D.10}
$$

We have lastly, for s_0 and s close to Z and $\xi_D\to\infty$,

$$
\begin{aligned}
&G_{D;\mathrm{in}}^{\varepsilon'=1}(s_0, s, \theta, \xi_D\to\infty) \\
&\quad \cong G_{D;\mathrm{in}}^{\varepsilon'=0}(s_0, s, \theta, \xi_D=0) \\
&\qquad + \frac{d^2}{ds_0'\,ds'}\,G_{\mathrm{Dirichlet}}(s_0', s', \theta)\Big|_{s_0'=s'=Z}\exp(s+s_0-2Z)
\end{aligned}
\tag{D.11}
$$

This result shows in particular that the first term of the rhs of Eq. (D.11) is of short range.

ACKNOWLEDGMENTS

We are very much indebted to B. Jancovici, J.-P. Hansen, B. Bernu, and P. A. Martin for careful reading of the manuscript and for their constructive criticisms. This work was supported in part by the Fonds National Suisse de la Recherche Scientifique under grant 2.433-0.87.

REFERENCES

1. Ph. Choquard, B. Piller, and R. Rentsch, *J. Stat. Phys.* **43**(1/2):197–205 (1985).
2. Ph. Choquard, B. Piller, and R. Rentsch, *J. Stat. Phys.* **46**(3/4):599–633 (1986).
3. Ph. A. Martin, *Sum rules in charged fluids*, *Rev. Mod. Phys.* **60**(4) (1988).
4. B. Jancovici, *J. Stat. Phys.* **28**(1):43–65 (1982).
5. P. Kennedy and T. Federbush, *Commun. Math. Phys.* **102**:361–423 (1985).
6. B. Jancovici, J. L. Lebowitz, and Ph. A. Martin, *J. Stat. Phys.* **41**(5/6):941–974 (1985).
7. C. J. F. Böttcher, *Theory of Electric Polarization*, Vol. 1 (Elsevier, 1973).
8. J. A. Stratton, *Théorie de l'Électromagnétisme* (Dunod, Paris, 1961).
9. B. Jancovici and X. Artru, *Mol. Phys.* **49**(2):487–497 (1983).
10. N. N. Lebedev, *Special Functions and Their Applications* (Prentice-Hall, 1965).
11. B. Jancovici, *J. Stat. Phys.* **29**(2):263–280 (1982).
12. E. R. Smith, *J. Phys. A: Math. Gen.* **15**:1271–1281 (1982).
13. D. J. Adams, *Mol. Phys.* **28**:1241–1252 (1974).
14. D. J. Adams, *Mol. Phys.* **29**:307–311 (1975).
15. D. Frenkel, in *Molecular Dynamics, Simulations of Statistical Mechanical Systems, Proceedings of the International School of Physics "Enrico Fermi"* (North-Holland, 1986).
16. J. P. Valleau and L. K. Cohen, *J. Chem. Phys.* **72**:5935–5941 (1980).
17. J. P. Valleau, L. K. Cohen, and D. N. Card, *J. Chem. Phys.* **72**:5942–5954 (1980).
18. W. von Megen and I. Snook, *J. Chem. Phys.* **73**:4656–4662 (1980).
19. P. J. Forrester, *J. Phys. A: Math. Gen.* **18**:1419–1434 (1985).
20. P. J. Forrester and E. R. Smith, *J. Phys. A: Math. Gen.* **15**:3861–3868 (1982).
21. P. M. Morse and H. Feshbach, *Methods of Theoretical Physics I and II* (McGraw-Hill, 1953).
22. J. D. Jackson, *Classical Electrodynamics* (Wiley, 1975).
23. I. S. Gradshteyn and I. M. Ryzhik, *Table of Integrals, Series and Products* (Academic Press, 1980).
24. M. Abramowitz and I. A. Stegun, *Handbook of Mathematical Functions* (Dover, New York, 1970).